2016

Data Analysis and Numerical Modeling of Seawater Intrusion Through Conduit Network in a Coastal Karst Aquifer

Zexuan Xu

FLORIDA STATE UNIVERSITY

COLLEGE OF ARTS AND SCIENCES

DATA ANALYSIS AND NUMERICAL MODELING OF SEAWATER INTRUSION THROUGH CONDUIT NETWORK IN A COASTAL KARST AQUIFER

By

ZEXUAN XU

A Dissertation submitted to the
Department of Earth, Ocean and Atmosphere Science
in partial fulfillment of the
requirements for the degree of
Doctor of Philosophy

2016

Zexuan Xu defended this dissertation on February 16, 2016.
The members of the supervisory committee were:

Bill Hu
Professor Directing Dissertation

Ming Ye
University Representative

Stephen Kish
Committee Member

Doron Nof
Committee Member

The Graduate School has verified and approved the above-named committee members, and certifies that the dissertation has been approved in accordance with university requirements.

This dissertation is dedicated to my family.

ACKNOWLEDGMENTS

I never thought all my PhD works could be finished within the amazing four years at Florida State University, and now I'm ready to unfold a brand new page of my life. Everything is like a dream and the dream comes true today. I'm happy to become an independent scientific researcher, and move on to meet more excited challenges in the future. Therefore, this is a great opportunity for me to acknowledge all the help and support I received in the past four years, which are extremely important for me to overcome all difficulties and problems.

First, I would like to express my deep gratitude to my major professor Dr. Bill Hu for giving me this opportunity to do my PhD at FSU. Dr. Hu guides me to the career path of numerical modeling and encourages me to grow as a critical thinker. I also want to say thank you to my committee members Dr. Stephen Kish, Dr. Ming Ye and Dr. Doron Nof for their guidance in the past four years. Dr. Ming Ye teaches me knowledge of numerical modeling and pushes me to think about the purpose of scientific research. Dr. Doron Nof's experience of fluid dynamic and karst helps me understand the science issues. Dr. Kish gains my understanding of the local karst environment setting and involves me in the laboratory experiments. And Thais, thanks for your company and I'm sorry for losing you in the last semester. You will be missed.

I appreciate Seth Bassett and Scott Dyer at Florida Geological Survey for providing the long-term field observation and working on the data analysis for Chapter Two of this dissertation. I would especially thank Seth Bassett for allowing my work at FGS as summer intern, writing a paper with me and becoming my dear friend. Hal Davis deserves a special appreciation for selflessly providing all the data and model files, and guiding me to get familiar with the hydrological models. The modeling developments cannot be done without a numbers of previous works by Hal Davis and Josue Gallegos. Many data used in this paper were collected and provided by my collaborators, including Kristopher Barrios, Kathleen Coates, Lewis Graham and Edward Chelette at NWFWMD (Northwest Florida Water Management District), Brien Katz and Zoe Kulakowaski at Florida DEP (Department of Environmental Protection). Dr. Paul Lee also came up many good ideas and suggested comments to my research. Thanks to the department chair Dr. James Tull for providing the teaching assistantship to financially support my study at

FSU and the graduate research grant for presenting my research on international conferences. Many professors at FSU provide significant helps in my study and research, including Dr. Yang Wang, Dr. Nicolas Wienders at Dept. of EOAS and Dr. Xiaoqiang Wang, Dr. Janet Peterson at Dept. of Scientific Computing, FSU.

During the four-year study, I received numerous assistances and patient suggestions with the code developers, Barclay Shoemaker at USGS Florida Water Science Center and Dr. Thomas Reimann at TU Dresden. The numerical methodology developments and coding cannot be done without their help. The former students in our group, including Luanjing Guo, Juxiu Tong, Xinya Li, Jonathan Faulkner and Xiaoying Zhang also significantly helped me in both the research and the career path. I would also like to express my gratitude to my mentor Dr. Hai Huang at Idaho National Laboratory for providing me the internship opportunity at INL. Without this experience, I don’t think I can get the job offer at Lawrence Berkeley National Laboratory after my graduation. Thanks also to my colleagues and friends during my internship at INL, Jing Zhou and Yidong Xia, for all your helps in that wonderful summer.

Last but not the least, I would like to express my appreciation to my immediate family, my father, mother and girlfriend, to whom this dissertation is dedicated to, for giving me enormous love and support all these years. I love you all, and wish you all stay on my side in the future.

TABLE OF CONTENTS

LIST OF TABLES

LIST OF FIGURES

ABSTRACT

The dissertation reports a series of hydrological studies that relates to seawater intrusion in a karst aquifer. In the Woodville Karst Plan (WKP), karst conduit system is well developed and directly open to the Gulf of Mexico that allows seawater intrudes into the aquifer. The Spring Creek Springs Complex and Wakulla Spring, located in a marine estuary and 11 miles inland, respectively, are the two major groundwater discharge spots and connected through subsurface conduit network in the Woodville Karst Plain (WKP), North Florida, USA. Investigation of seawater intrusion in the Woodville Karst Plain is the objective and motivation of this dissertation work.

Potential evidence of the longest documented seawater intrusion through conduit network in the Woodville Karst Plain (WKP) is found by the data analysis of electrical conductivity and chemical measurements. Five periods of increased electrical conductivity have been observed in the karst conduits supplying water at Wakulla Spring, one of Florida's largest first magnitude springs. A composite analysis of rainfall, electrical conductivity and geochemical data provides strong evidence that the increases in conductivity are directly tied to saltwater intrusion occurring at the Spring Creek Springs through the conduit network. This interpretation is supported by the conceptual model established by prior researchers, and represents the first and longest documented case of saltwater intrusion through conduit network in the WKP.

Several numerical models are able to simulate the density-dependent seawater intrusion issue. On the other hand, discrete-continuum numerical models are designed to simulate groundwater flow and solute transport in a dual-permeability karst aquifer. However, none of the pre-existed code or model is able to deal with the two issues together. Therefore, a hybrid discrete-continuum numerical model of Variable-Density Flow and Solute Transport - Conduit Flow Process (VDFST-CFP) is developed as a new modeling method that provides more accurate simulation of seawater intrusion in a coastal karst aquifer with conduit network. Darcy-Weisbach equation is applied to simulate non-laminar groundwater flow in the conduit system. Density-dependent groundwater flow with appropriate density terms in both the conduit and porous media systems are analytically derived, then coupled with transport equations and solved numerically using finite difference method with an implicit iteration procedure. Two synthetic two-dimensional cases are developed to validate the newly developed VDFST-CFP model by

comparing with other numerical models. The VDFST-CFP model improves simulations of density-dependent seawater/freshwater mixing processes and exchanges between the two domains. In comparison with the discrete-continuum models, Darcy equation of the continuum numerical models overestimates the flow rate but the VDFST-CFP is accurate under turbulent flow condition. The pros and cons of model uncertainties, assumptions, conceptual simplifications and numerical techniques of the VDFST-CFP are discussed.

Several studies of numerical modeling have been done as an important method to evaluate seawater intrusion in coastal karst aquifers with conduit network, since field observations are usually insufficient. A regional groundwater flow cycling numerical model is developed to provide a general understanding of the flow regime that controlled by seawater/freshwater interaction in the WKP, using a discrete-continuum CFPv2 model. Non-laminar flows in conduits and flow exchange between the two domains are coupled in the hybrid numerical model. The time-variable salinity and equivalent freshwater head at the submarine spring have significant impacts on seawater/freshwater interaction and discharges of springs. Simulated results match well to measurements with correlation coefficients 0.891 and 0.866 at Spring Creeks Springs and Wakulla Springs, respectively. The impacts of sea level rise on regional groundwater flow field and the relationship between the two springs are evaluated as well by the numerical model.

The controlling factors of seawater intrusion in a dual-permeability are evaluated by local and global parameter sensitivity analysis with a two-dimensional SEAWAT model, which also estimates the extents of seawater intrusion in the WKP. The local sensitivity study indicates the salinity at the submarine spring is the most parameter to simulations in both the conduit and porous medium, which are effective to all parameters near the mixing zone. The results of global sensitivity analysis exhibit similar pattern with the local study but are different for some parameters due to their non-linear relationship to the simulations. Simulations in the porous medium are sensitive to not only matrix parameters but also conduit conditions because of the conduit-matrix interaction. Dispersivity is important in a homogeneous porous medium model but is no longer significant in an advection-dominated karst system. The effects of the identified important parameters on the extents of seawater intrusion are quantitatively evaluated by examining the variation of salinity at the submarine spring with rainfall recharge, sea level rise and longer simulation time under an extended low rainfall period.

CHAPTER ONE

INTRODUCTIONS AND BACKGROUND

1.1 Dual-permeability Karst Aquifer

Karst aquifer systems underlie approximately 10-20% of the Earth's landmass and supply potable water to nearly 25% of the world's population (Ford and Williams, 1989). In the United States, karst carbonate aquifers supply almost 52% of all bedrock aquifer withdrawals on a yearly basis (Maupin and Barber, 2005; Covington et al., 2011). Karst aquifers are typically characterized by relatively large void spaces and loose porous media, which make the karst aquifers to be the most productive aquifer systems in the world, for example, the Floridan Aquifer in the USA (Bush and Johnson, 1988). The open and porous nature of karst aquifers, combined with the dissolution of joints and fractures within carbonates over time, generate complex subsurface conduit systems and dual-permeability flow regimes (Davis, 1996). Groundwater flow and solute transport processes in conduit networks are generally more rapid than that in the surrounding carbonate porous media due to significantly higher hydraulic conductivity and porosity in the conduit system (Ritter et al., 2002; Scanlon et al., 2003). As a result, the water and solute interchanges between the conduit and matrix are particularly important in a dual-permeability karst aquifer system. Karst aquifers are particularly vulnerable when one considers the problems of groundwater contamination or seawater intrusion (Kuniansky, 2008). During high-flow events, contaminants in the conduit system can be rapidly transported through the aquifer or actively pushed into the carbonate matrix when the water pressure is high in the conduit system. The process is reversed during low-flow events, and contaminants are slowly released from the surrounding matrix into the conduit system (Martin and Dean, 1999; Martin and Dean, 2001). Therefore, groundwater contamination and seawater intrusion in a karst aquifer can persist for a long time because of the retention and release effect between the conduits and matrix domains (Katz et al., 2004; Green et al., 2006).

Laboratory experiments using physical models with artificial gypsum or sandbox analog were taken to simulate karst groundwater flow and solute transport (Ford et al., 2000). Li (2004) evaluated the solute transport and retention in a karst aquifer using two categories of laboratory experiments. Faulkner et al. (2009) designed a sandbox laboratory experiment to simulate the interaction between conduit and porous medium domain. In addition to laboratory studies, many numerical models have been developed to study groundwater flow and solute transport in dual-permeability systems, as well as chemical reaction and carbonate dissolution in karst aquifers (Bakalowicz, 2005). For example, a limestone dissolution continuum model coupled with conduit flow was proposed to simulate groundwater flow and karst evolution (Dreybrodt, 1988). Lauritzen et al. (1992) coupled laminar flow and carbonate dissolution in two-dimensional pipe networks to study groundwater flow and karst development in a limestone aquifer. Groves and Howard (1994) used two-dimensional pipe networks to simulate conduit development processes under laminar flow conditions at field scales, and the simulation method was later extended to turbulent flow by Howard and Groves (1995). Kaufmann and Braun (2000) coupled a pipe network with a continuum system to study karst development, and their study results indicated that early karstification might be enhanced by the presence of a diffuse flow system.

The coupling of non-linear or turbulent flow within the conduit network and Darcian laminar flow in the porous medium is a challenging issue in numerical simulation of a dual-permeability karst aquifer (Davis, 1996; Shoemaker et al., 2008b; Gallegos et al., 2013). Darcy's Law and continuum groundwater flow equations are applicable for laminar flow in the porous medium that is linear to hydraulic gradient, but are not accurate for describing non-laminar or turbulent flow in the conduit. Some hybrid discrete-continuum numerical models were developed to couple Darcian flow in the porous medium with non-laminar channel flow in the conduit, such as CAVE (Carbonate Aquifer Void Evolution) (Clemens et al., 1996; Liedl et al., 2003), MODFLOW-CFPM1 (Shoemaker et al., 2008b) and CFPv2 (Reimann et al., 2013; Reimann et al., 2014). Those discrete-continuum models were also applied and evaluated in a number of studies (Hill et al., 2010; Gallegos et al., 2013; Saller et al., 2013; Xu et al., 2015a; Xu et al., 2015b). On the other hand, MODFLOW-CFPM2 calculates turbulent transmissivity and/or hydraulic conductivity in the preferential flow layer with an adjustment factor to simulate turbulent preferential groundwater flow in the highly permeable conduits (Shoemaker et al., 2008b). The MODFLOW-CFPM2 requires limited data and less computational efforts, however, is less physically based than CFPM1 (Shoemaker et al., 2008b). Recently, MODFLOW-CFPM2 has been modified by Reimann et al. (2012) and applied in many modeling studies as well (Shoemaker et al., 2008a; Reimann et al., 2011b).

The solute transport simulation in the discrete-continuum model involves the coupling of one-dimensional solute transport within the conduit network and the 2D/3D solute transport in the porous medium domain. MT3DMS is a widely used modular 3D model to simulate solute transport in a porous medium, which is based on the solution of groundwater flow from MODFLOW simulation (Zheng and Wang, 1999). Therefore, MT3DMS is only applicable for solute transport in porous medium aquifer (Zheng and Wang, 1999). Spiessl (2004) and Spiessl et al. (2007) modified the source code of MT3DMS and developed the reactive hybrid transport RUMT3D model. RUMT3D was coupled with CAVE to calculate groundwater flow in the conduits, and then solve solute transport equations in the conduit and porous medium domains of a karst aquifer. Reimann et al. (2011a) enabled MODFLOW-CFP simulation of unsaturated flow in conduits and water exchange between matrix and variably filled conduits. Furthermore, conduit associated drainable storage (CADS) was added in MODFLOW-CFPM1 as well as fixed head limited flow boundary condition in Reimann et al. (2014). Based on those studies, a research version of CFPv2 has been recently developed by Reimann et al. (2013) and used in Xu et al. (2015a) to simulate flow of laminar and non-laminar, as well as nitrate-N transport in conduits and matrix with an updated UMT3D. The CFPv2 and UMT3D model were combined to calculate solute advective exchange between conduit and medium, as well as transport process within a porous medium by advection and dispersion. However, the nitrate-N transport study of Xu et al. (2015a) is a part of my PhD study but not included in this dissertation, because it is not related to seawater intrusion in a karst aquifer.

1.2 Seawater Intrusion in Coastal Karst Aquifers

Seawater intrusion has become an important environmental research topic in recent years. The soil salinization, marine and estuarine ecological changes, and groundwater contamination by seawater are all significant problems in coastal regions (Bear, 1999). The groundwater salinization is the primary detrimental effect of seawater intrusion to groundwater resources since mixing with less than 1% of seawater (250 mg/L chloride) by volume can make freshwater non-potable (WHO, 2011). Singh (2006) pointed out that 40%~50% of the world’s population live within 100 km of the coastline with the highest rates of population growth as well, indicated significant increase of water supply demand in the coastal areas (Boesch et al., 2000). Owing to over-pumping, depression cones of groundwater level in coastal aquifers could reduce the freshwater hydraulic pressure resisting against seawater intrusion. In some coastal metropolitan areas such as New York in the USA and Shanghai in China, conditions of seawater intrusion are significantly severe than rural coastal areas due to great amount of groundwater withdrawal for industrial and public supplies (Konikow and Kendy, 2005; Chen and Jiao, 2007). Werner et al. (2013) concluded that climate variations, groundwater pumping and fluctuating sea levels are important factors in determining the distribution and inflow of seawater in a coastal aquifer. Custodio (1987) and Li et al. (2009) also summarized the controlling factors of seawater intrusion into a freshwater coastal aquifer, including the geologic and lithological heterogeneity, localized surface recharge, paleo-hydrogeological conditions and anthropogenic influences. Buoyancy force associated with density difference between freshwater and seawater is a major factor governing the movements of the two fluids in a coastal aquifer, which is described by the Ghyben-Herzberg equation and Hubbert relationship (Hubbert, 1940; Guo and Langevin, 2002; Fleury et al., 2007). Important factors that control seawater intrusion in a costal aquifer are evaluated in Chapter 4 of this study using a density-dependent numerical model, including advective forces resulting hydraulic gradient, effects of diffusion and dispersion, initial and boundary conditions, etc.

Sea level rise has been recognized as one of the most serious environmental threats to the world in this century (Voss and Souza, 1987; Bear, 1999; IPCC, 2007). The influence of sea level fluctuation on seawater intrusion can be complex under different conditions (Werner et al., 2013). Oude Essink et al. (2010) pointed out that sea level rise and the changes of rainfall and evaporation due to global climate changes are expected to exacerbate seawater intrusion. According to the Ghyben-Herzberg relationship, rising sea level is able to result in extended seawater intrusion in a coastal aquifer, and can significantly move the position of mixing interface further landward (Werner and Simmons, 2009). On the other hand, hurricane or tropical storm events have been found to affect the extent of seawater intrusion in a coastal aquifer due to the temporary high tidal stage (Moore and Wilson, 2005; Wilson et al., 2011). However, the effect of tide variation on mixing interface movement is generally negligible especially in a regional spatial scale and long-term temporal period (Inouchi et al., 1990). Davis and Verdi (2014) recently reported a groundwater flow cycling conceptual model in a coastal karst aquifer, and point out that sea level rise at the Gulf of Mexico in the past century could be a reason for the increasing discharge at an inland karst spring (Wakulla Springs) and decreasing discharge at a coastal spring (Spring Creek Springs) in the Woodville Karst Plain (WKP), Florida, which will be introduced in detail in Section 1.3.

Numerical simulation of seawater intrusion has been studied for several decades, which is a density-dependent problem that involves coupled groundwater flow and salt transport processes. In the variable-density numerical modeling, transport model is calculated based on the solution of groundwater velocity field from flow modeling, while the salinity also determines the groundwater density and affects the simulation of flow regime. As a result, the flow equation with additional density terms is required to coupled with transport equation, and then solved simultaneously by numerical methods (Werner et al., 2013). Many variable-density numerical codes have been developed, including SUTRA (Voss and Provost, 1984) in which finite element and finite difference hybrid methods are applied to solve the mathematical model, and FEFLOW (Diersch, 2002; Diersch, 2005) in which a finite element code solves both flow and transport equations. SEAWAT is one of the most popular codes for numerical simulation of variable-density seawater intrusion process, in which MODFLOW is used to solve flow field by finite difference method and MT3D is applied to solve solute transport by multiple numerical methods (Guo and Langevin, 2002; Langevin et al., 2003). Generally speaking, most coupled variable-density flow and transport systems are numerically complicated and computationally demanding (Werner et al., 2013).

Karst aquifers near the coast are particularly vulnerable to seawater intrusion due to high effective porosity and dissolution conduits. However, the interactions of seawater and freshwater in coastal karst aquifers remain poorly understood. The complex interchange between the conduit and matrix components is particularly important for seawater intrusion in karst aquifers (Kuniansky, 2008). Coastal karst coastal aquifers are known to have extensive conduit networks that terminate at submarine springs opening directly to the sea (Werner et al., 2013). Freshwater discharge and seawater intrusion through intermittent coastal springs and submarine caves largely depends on the hydraulic gradient between the local groundwater level and the sea (Fleury et al., 2007). The flow pattern at a submarine spring typically exhibits a strong seasonal variation due to seasonal precipitation variation. Periods of high rainfalls typically result in sufficient freshwater discharge at the submarine springs to maintain low salinity and head conditions. During extended periods of low precipitation, the hydraulic gradient between the fresh groundwater filled conduits and the denser seawater at the submarine springs vent can reverse. Under such conditions, a submarine spring no longer acts as a point of freshwater discharge for the local aquifer system, but may become a point of seawater intrusion and siphons seawater directly into the conduit system. The high-permeability conduit system normally supplies a submarine spring with freshwater, however, allows seawater to intrude very quickly into a coastal karst aquifer many miles inland via the submarine spring vents at the coast (Schmitter-Soto et al., 2002; Bauer-Gottwein et al., 2011). The flow pattern at a submarine spring are determined by the hydraulic gradient of equivalent freshwater head relative to the local potentiometric surface, and hydraulic conductivity of the coastal aquifers (Fleury et al., 2007). For example, long-distance seawater intrusion has been observed at the karst coastal aquifer in Yucatan Peninsula, Mexico, where open sinkholes, fractures, conduits and springs are widely distributed (Perry et al., 2002; Bauer-Gottwein et al., 2011). Zötl (2013) also used tracers to demonstrate that seawater emerges in brackish coastal springs situated 15 km away on the east coast of the Island of Cephalonia, Greece.

1.3 The Karst Features in the Woodville Karst Plain (WKP)

The Woodville Karst Plain (WKP) is the study site for the work of Chapter 2 and 3 in this dissertation. The numerical model in Chapter 4 also uses the values of hydrological characteristics of the WKP and quantitatively simulates the extents of seawater intrusion in the WKP. However, the VDFST-CFP model in Chapter 5 is a numerical model development but is still not used for any field application.

1.3.1 The Upper Floridan Aquifer (UFA) in the WKP

The Woodville Karst Plain (WKP) is located in north Florida, USA, which extends north to the Cody Scarp and the City of Tallahassee, and south to the Gulf of Mexico (Figure 1.1). The WKP is a geomorphic region that extends around Florida's Big Bend area and is characterized as a highly karstic, gently rolling surface of porous sand overlying Oligocene and Miocene aged limestone (Rupert and Spencer, 1988). Elevations in the WKP proper generally range from 0 to 35 ft above mean sea level, with a trending slope of less than 4 ft per mile in the southward direction (Bush and Johnson, 1988). The relic paleo-shoreline Cody Scarp is the border of the WKP to the north, while the Lowland river delta and terraces of the Apalachicola National Forest comprise the westernmost border, and the Gulf of Mexico the southernmost border.

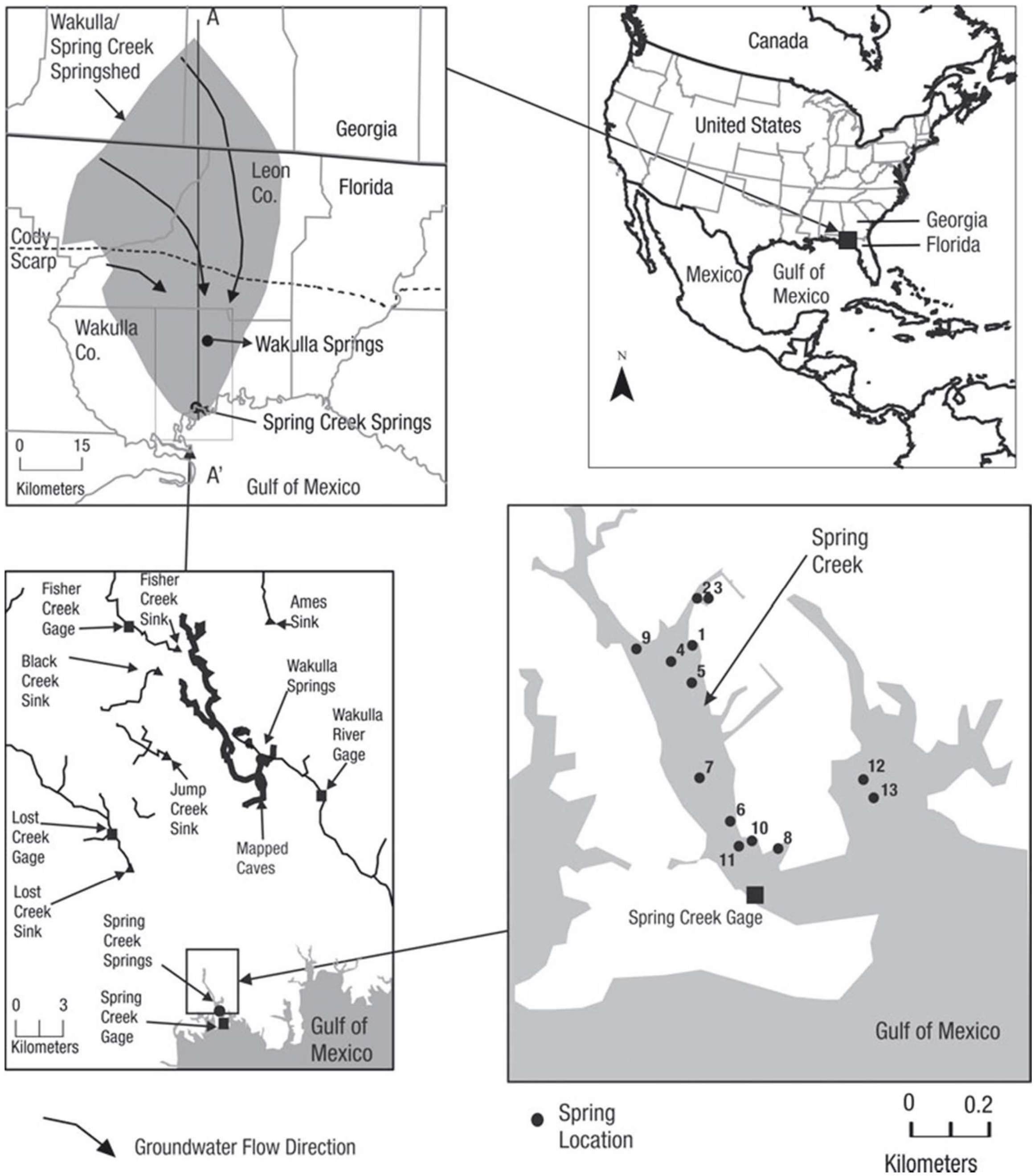

Figure 1.1. Location of the study area, Woodville Karst Plain (WKP) and two springs, Wakulla Spring and Spring Creek Springs. Modified from Davis and Verdi (2014).

Many of the surficial springs, sinkholes, karst windows and sinkholes found throughout the WKP. Geologically, the immediate surficial bedrock in the WKP is comprised of the Oligocene age St. Marks Formation, a pale orange to white calcarenite, highly karstic morphologically, well indurated and fossiliferous dolomitic limestone that extends to depths of around 100 ft throughout the study area (Rupert and Spencer, 1988). The Miocene age Suwannee

Limestone is beneath the surficial St. Marks limestone in the WKP. This unit is comprised of a white to light-tan, cream or brown recrystallized, fossilferous, dolomitic calcarenite limestone (Rupert and Spencer, 1988). In the areas to the west and north of the WKP, the permeable limestone units are capped by the relatively impermeable, clay-bearing Hawthorn Group sediments, which are absent in most parts of the WKP at the south of the Cody Scarp (Miller, 1986).

The hydrogeological setting of the WKP is the Upper Floridan Aquifer (UFA), one of the world's most productive aquifers (Miller, 1986). Regionally, the potentiometric surface of the UFA slopes downward from the higher elevations to the west and the east of the study site until it encounters the flat expanse of the WKP (Lane, 2001). The carbonate St. Marks Formation and Suwannee Limestone form the bulk of the porous media in the study area, and are notable for their uneven distribution of heterogeneous permeability with highly permeable subsurface fractures (Bush and Johnson, 1988), and openings in loosely cemented limestone and mosaics of many fractures and solution-widened conduits are common in the area (Davis, 1996). The ultimate sources of recharge for the UFA in the vicinity of the WKP are precipitation and regional recharges from the Red Hills region (Davis, 1996; Lane, 2001). Along the north margins of the WKP, the impermeable Hawthorn units collect allogenic recharge over large areas, often funneling surficial runoff into a single large swallet feature. Rainfall over the WKP surface is autogenic in nature, and surface waters are rapidly transmitted into the aquifer system via the numerous karstic surface features. The average annual temperature in Tallahassee is 67 ^{o}F and the average annual precipitation is about 61.3 inches per year (in/yr) during the study period. The average potential evapotranspiration in the WKP ranged from 51.91 to 54.23 in/yr from 2007 to 2010, which was calculated by USGS Florida Water Science Center.

The deeper Suwannee Limestone unit also hosts an extremely well-developed network of horizontal underground conduits that interconnect many of the karst features found at the surface. The large, human-navigable conduit system is vertically terraced and generally found at one of three elevations: 100 ft (the general elevation where the shallower St. Marks Formation uncomfortably contacts the underlying Suwannee Limetsone), 200 ft, and 280 ft below sea level (Werner, 2001). The vertical distribution of the conduit system is tied to the paleo-history of sea level elevation, the subsequent dissolution of the sedimentary limestone bedrock, and additional terrace levels that formerly possessed both springs and paleo-inhabitants have been found off-shore in the Gulf of Mexico, now underwater (Florea and Vacher, 2006).

Tracer tests were conducted to verify the possible conduit network distribution and connection with Wakulla Springs, Spring Creek Springs and Lost Creek swallet (Dyer, 2015). High permeability characteristics were also observed between the Southeast Sprayfield, St. Mark Spring, sinkholes and karst windows such as Black Sink and Fisher Sink connected with Wakulla Springs by tracer tests (Kincaid and Werner, 2008). Regional transmissivity distribution in the UFA is heterogeneous, ranging from 1.3×10^3 to 1.3×10^4 feet squared per day (ft^2/d), and can be as large as 1.3×10^6 ft^2/d due to highly permeable karst conduit texture (Davis, 1996).

1.3.2 Wakulla Spring

The predominant karst feature in the study area is Wakulla Spring, one of the "largest and most dramatic of Florida's springs" and one of the largest springs in the southeastern US (Davis, 1996; Scott et al., 2004). Wakulla Spring is located 11 miles north from the coastal shoreline of Wakulla county, and its spring run forms the 14.3 miles long Wakulla River, eventually discharging in the Gulf of Mexico. Wakulla Spring has the greatest known discharge range among Florida's Springs, with a minimum flow of 25.2 cubic feet per second and a maximum discharge of 1910 cubic feet per second (Scott et al., 2004). Kulakowski (2010) reported the water balance of recharges coming from the creeks and sinkholes including Black Creek (Black Sink), Monson Slough (Ames Sink) and Fisher Creek (Fisher Sink) to Wakulla Spring.

Wakulla River comes from the extensive submerged cave system and flows out through Wakulla Spring, which is consist of a single giant vent and several small vents nearby. The depth of Wakulla Spring cave is estimated to be about 200 ft near the origin, extended horizontally to 300 ft and could be 360 ft deep at some locations (Scott et al., 2004). The vent at Wakulla Spring is approximately 5.0 ft above sea level and forms a horizontal ellipse estimated to measure 50 ft. by 82 ft, discharging into a large, sloping basin (Scott et al., 2004). This single, giant vent connects to an extensive branching underwater conduit system that supplies Wakulla Spring with its water. The conduit system proximate to the vent is one of the most extensively mapped underwater cave systems in the world, with divers successfully traversing and mapping more than 37 miles of underwater conduits (Davis et al., 2010).

The initial exploration of the conduit system was conducted by an expert cave diving team in 1987 and 1988. This exploration effort was excellently chronicled by Stone (1989), and the alphabetic lettter designations for the various interconnected tunnel segments that were established by the original cave diving team are still used today (Figure 1.2C). Starting at the main vent, the cave system follows a generally southward direction through the Grand Junction, which joins the main cave system with B and C tunnels. Groundwater within the B and C tunnels are sourced from deeper in the aquifer system, with B tunnels initially trending east before turning eastward and C tunnel trending almost due south. Continuing southward, the Grand Junction turns westward near the join with the unexplored G tunnel until it ends at the junction of A and D tunnels. The D tunnel trends northward for a short distance until it becomes impassible, while the A tunnel branches to the south. Continuing south along A tunnel, the next major point of intersection is the junction of A and K tunnels. The western K tunnel eventually joins up with the east-west running R tunnel. The R tunnel (and by extension, the K tunnel) is one of the major source of surficial waters in the Wakulla conduit system, and it trends west from the K-R junction for approximately 0.8 miles before turning sharply runs, uninterrupted, over 7 north miles into southern Leon County. A tunnel, by contrast, connects sequentially with the M, O and Q tunnels all of which run southwards towards the Spring Creek Springs complex. The current limit of southern exploration of the explored cave system lies within the Q tunnel is known as the Q-Terminus.

1.3.3 Spring Creek Springs

The other major karst feature of note in the study area is the Spring Creek Springs complex, a group of 14 submarine spring vents opening into the Gulf of Mexico south of Wakulla County. The two major discharge points are vents #1 and #10 (Figure 1.1 and 1.2) (Lane, 2001). The exact locations, diameters, depths, and discharges of the numerous Spring Creek vents are difficult to accurately explore and measure, as they are physically located beneath the brackish waters of the Spring Creek embayment. Current exploration indicates that the Spring Creek vents are supplied by an extensive, interconnected and highly complex horizontal conduit network joining deep and as-yet unexplored vertical conduits. The ultimate depth of the vents at Spring creek are believed to be approximate 300 ft at the major outlets vents #1 and #10 based on the depth of the conduit system at Wakulla Spring (Davis and Verdi, 2014).

Unfortunately, the veracity of the assumed depths of the conduit system at Spring Creek is almost entirely unknown, as the brackish and turbid waters at the Spring Creek vents are extremely dangerous for diving and exploration.

The vagaries of flow patterns at Spring Creek are highly dependent on the complex interplay amongst local sea levels, the inland potentiometric surface, the interconnections of surface features to the conduit system, and the salinity of the water in the Spring Creek embayment. The aggregate flow at the Spring Creek complex makes it one of the largest freshwater springs in Florida, with Scott et al. (2004) estimating the combined freshwater discharge of the 8 vents known at the time at approximately 2,000 cubic feet per second. Freshwater discharge at Spring Creek Springs dramatically increases after a high rainfall event, sometimes a tropical storm or a hurricane. Meanwhile, seawater can be pushed out at the submarine caves. Time-dependent groundwater discharge significantly affects salinity at Spring Creek Springs and controls the condition of seawater intrusion simultaneously.

On the other hand, the pressure of freshwater discharge is too weak to prevent seawater intruding into the conduits during low rainfall periods. The giant interconnected conduits system has a large storage capacity that keeps tons of seawater during when rainfall and surface water recharge are low. The equivalent freshwater head in the conduit system will overwhelm the outflowing freshwater, and some or all of the 14 Spring Creek vents will reverse and begin siphoning seawater into the aquifer, rather than discharging freshwater into the gulf. Spring Creek begins to siphon seawater from the gulf until a high-rainfall event recharges the freshwater inland potentiometric surface and supplies enough energy to purge the seawater out of the conduit system. In recent decades, it has been more often that Spring Creek Springs becomes a significant point of seawater intrusion during periods of low recharge, despite their large aggregate outflow during periods of high rainfall. These periodic reversals of flow have been known to occur since at least 2001, and have come under increasing scrutiny in recent years as a phenomenon of concern (Lane, 2001; Davis and Verdi, 2014).

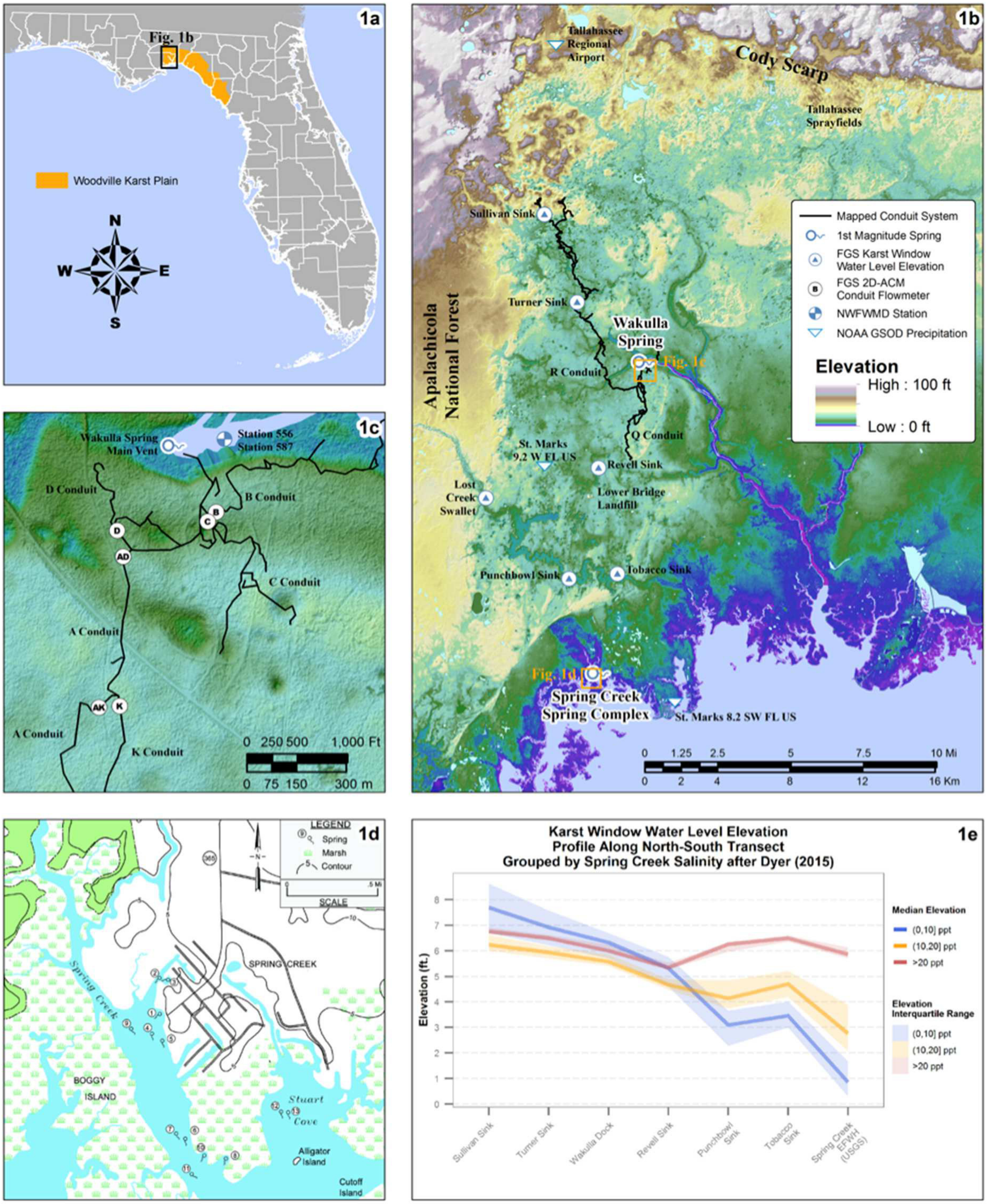

Figure 1.2 A) Locations of the Woodville Karst Plain and the study site; B) Map of the Woodville Karst Plain, showing the locations of features of note within the study area; C) Locations of Falmouth 2D-ACM meters and Wakulla Spring cave system; D) Locations of Spring Creek Spring vents, from Lane (2001); E) Groundwater elevation profile in major karst windows grouped by Spring Creek salinity, after (Dyer, 2015). Cartography by Seth Bassett.

CHAPTER TWO

FIELD OBSERVATION OF SEAWATER INTRUSION THROUGH KARST CONDUIT NETWORKS IN THE WOODVILLE KARST PLAIN (WKP)

2.1 Methods and Data Collection

In late 2003, Florida Geological Survey (FGS) installed six Falmouth 2D-ACM acoustic flowmeters in the conduits proximal to the main vent at Wakulla Spring. These flowmeters are located approximately 280 ft below land surface in the B, C, D, AD, AK, and K conduits (Figure 1.2). In late 2009, three additional meters were installed in at three sites south of the Wakulla vent: one meter was placed in the conduit beneath Revell Sink approximately 3.96 miles southwest of Wakulla Spring, and two meters were installed at Spring Creek Vent #1 and Spring Creek Vent #10. These nine flowmeters record five parameters at 15 minute or hourly intervals: average speed of flow (ASPD), electrical conductivity (COND), water pressure (PRES), water temperature (TEMP), and flow direction (AVDIR). These meters are used in conjunction with a network of In Situ Level Troll devices measuring the water level elevations in karst windows connected to the deeper conduit system.

Several additional datasets were utilized to augment the FGS conduit flowmeter data. The USGS installed a gage at Spring Creek in 2007 recording gage height, electrical conductivity, salinity and the aggregate discharge 12 of the 14 vents at Spring Creek Springs. Precipitation data from the National Oceanic and Atmospheric Administration (NOAA) Global Summary of the Day (GSOD) dataset were used to track rainfall at three stations: St. Marks 8.2 SW FL US, St. Marks 9.2 W FL US and Tallahassee Regional Airport (Figure 1.2). These stations represent the daily rainfall at Spring Creek Springs, Crawfordville and Tallahassee from south to north, respectively. Two Northwest Florida Water Management District (NWFWMD) stations, #587 and #556, were used to measure the aggregate electrical conductivity and discharge at the Wakulla vent and verify the accuracy of the 2D-ACM conductivity data. Finally, NWFWMD provided a dataset containing the results of over 30 years of intermittent, laboratory based geochemical analyses conducted on grab samples taken by the NWFWMD, FGS, USGS, and other government agencies at the Wakulla vent.

2.2 Conceptual Model

The conceptual model of seawater intrusion through conduit system was established by Schmidt et al. (1998); FGS (2004); Loper et al. (2005); Davis and Verdi (2014); Dyer (2015); Xu et al. (2015b) among many others. These earlier works show that the discharge of Wakulla Spring and Spring Creek Springs are reliant upon conditions at the margins of the WKP. Groundwater recharge flows to Wakulla Spring from the north and west in a regional scale, and the topographic boundaries of the Cody Scarp and Apalachicola National Forest coincide with a relatively steep, upward sloping potentiometric gradient. Tides also play a role, with both the matrix and conduit components of the aquifer proximal to the Gulf of Mexico at Spring Creek Springs. Tidal cycles are clearly evident in both water elevations of karst windows and monitor wells connected to the conduit system throughout the springshed. Thus, the area immediately southwest of Wakulla Spring is bounded on the west and north by regional groundwater pressure, to the east by the Wakulla River, and to the south by the Gulf of Mexico. Within this wider hydrogeologic setting, Wakulla Spring and Spring Creek Springs exhibit a strong coupling flow behavior, and flow conditions at one spring are closely related to the other.

The constant hydraulic head at Wakulla Spring is only 5.0 ft above sea level (ASL), and acts as a constant head boundary for the local potentiometric surface. Comparatively, the estimated equivalent freshwater head at Spring Creek Springs complex is highly variable and changes dynamically both with the tides and with the elevation of the local potentiometric surface: during periods when Spring Creek is discharging it can be as low as 0 ft as the spring pool elevation of sea level, versus 7.5 ft when the conduit system at Spring Creek Springs is filled with seawater (Davis and Verdi, 2014). Multiple dye trace studies conducted by the FGS show that water entering the conduit system at Lost Creek Swallet transits southward when Spring Creek Springs is flowing, but transits northward to Wakulla Spring following low-rainfall periods when Spring Creek ceases to flow (Kincaid and Werner, 2008; Dyer, 2015). Succinctly, the freshwater that flows to the Gulf of Mexico when it is actively discharging can no longer exit at the Spring Creek Springs vents once the conduits are filled with saltwater. This inland freshwater is rerouted via the conduit system northward to the vent at Wakulla Spring. The rerouting of water results in the increasing discharge at Wakulla Spring noted by Davis and Verdi (2014). Numerical modeling conducted by Xu et al. (2015b) has confirmed the speculation that a rise in sea level can cause the water flowing to Spring Creek Springs to shift landward to the inland Wakulla Spring.

Dyer (2015) found that water level elevations increase 3.18 ft in the karst windows south of Revell Sink during periods of negative discharge at Spring Creek (Figure 1.2F). The local hydraulic gradient is reversed during the periods when Spring Creek Springs is no longer discharging, but remains normal seaward during periods of positive discharge. Thus, under low rainfall conditions, the potentiometric gradient southwest of Wakulla Spring reverses and runs against the prevailing regional gradient. Meanwhile, the constant low hydraulic head at Wakulla Spring attracts water that was formerly flowing south to Spring Creek Springs.

2.3 Conductivity Measurement Results

Figure 2.1A shows the rainfall at the three selected NOAA GSOD stations in the study area. Figure 2.1B illustrates the time-series electrical conductivity data collected by 2D-ACM flowmeters in the B, C, D, AD, AK, K conduits, the conduit beneath Revell Sink, and both the FGS and the USGS data recorded at Spring Creek Springs Complex. Figure 2.1C displays the NWFWMD discharge and conductivity measures at the main vent at Wakulla Spring. Figure 2.2 displays selected analytes from the NWFWMD geochemical dataset.

Importantly, the 2D-ACM data illustrates that the nominal electrical conductivity in the conduits remains a relatively constant 0.28 – 0.30 mmho/cm during the period of observation. However, there are five distinctive episodes of rising conductivity values exceeding the nominal background values: 2007/08/13 – 2008/02/28; 2008/04/15 – 2008/08/31; 2011/05/13 – 2012/03/24; 2012/06/26 – 2012/07/06; and 2012/10/31 – 2013/03/16. The discussion section focuses on these five periods, labeled Period 1-5, respectively. For the sake of convenient comparisons and graphical clarity, four of the five periods have been blocked in grey in all parts of Figure 2.1 and 2.2. Period 4, an abnormally short period due to the extreme rainfall and storm surge of Tropical Storm Debbie, is blocked in orange to distinguish it from the others.

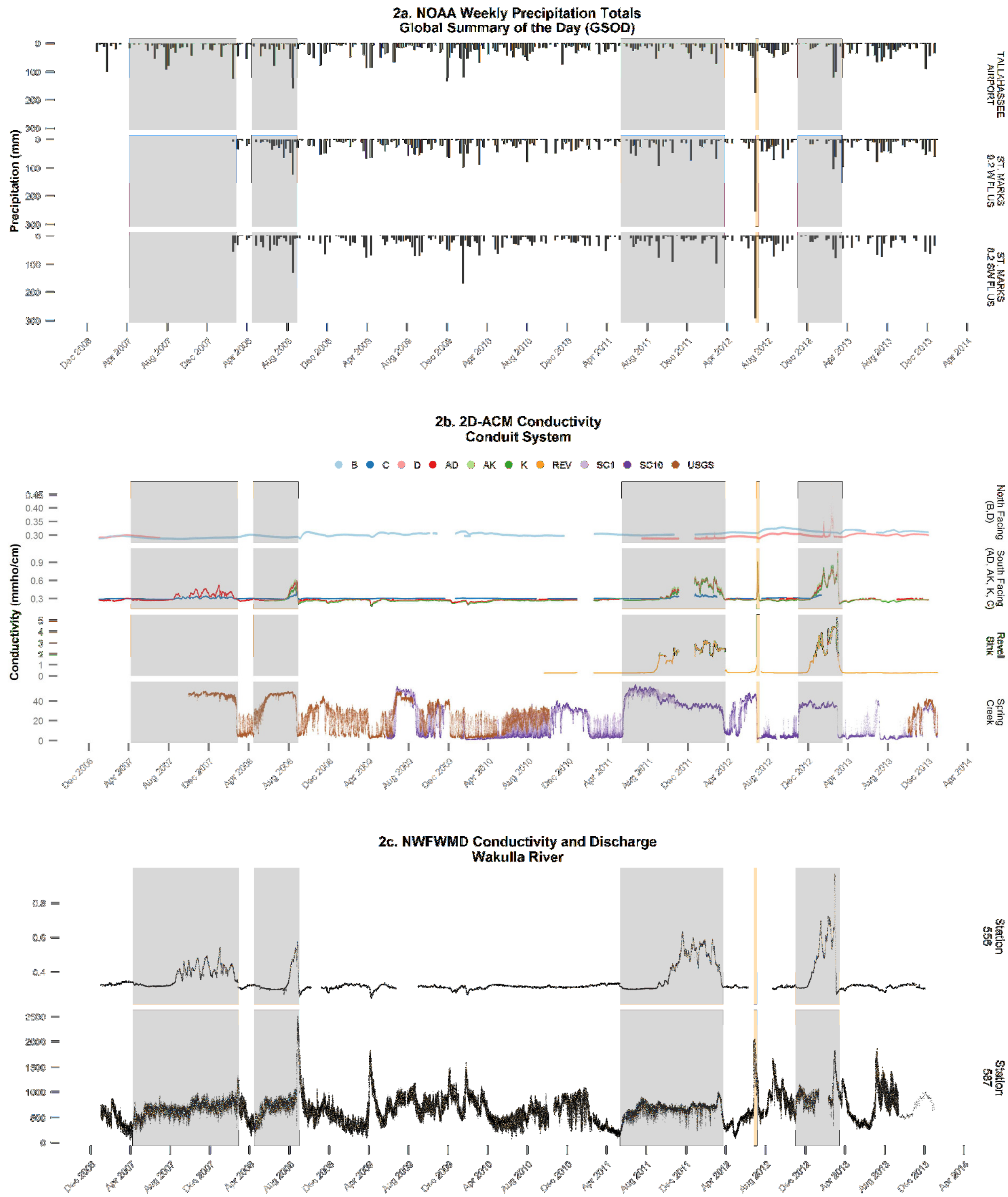

Figure 2.1 A) NOAA weekly precipitation totals; C) Falmouth 2D-ACM electrical conductivity data in the conduit system; B) Electrical conductivity and discharge at Wakulla River. Cartography by Seth Bassett.

2.4 Discussion

Three lines of evidence indicate that the rising conductivity observations in the conduit system are indicative of coastal seawater intrusion: the spatial orientation of the conduits in which the rising conductivity values are measured; the geospatial gradient of electrical conductivity values within the tunnels; the spatiotemporal pattern associated with the periods of rising conductivity values.

The spatial orientation of the individual conduits provides strong evidence that the increases in conductivity have their origins in coastal seawater intrusion. The northward oriented conduit (B & D) show little to no increases in conductivity during most of the identified periods that represents recharges from the north; whereas the southward oriented tunnels (AD, AK, C & K) all exhibit a similar pattern of rising conductivity (Figure 2.1B). The increased conductivity values in the northward oriented D tunnel during Periods 4 and 5 are posited to be related to the sensor's location relative to the conduit geometry. The increased conductivity values in D tunnel could be the result of more conductive water flowing northward past the A-D junction and continuing to the D tunnel sensor (Figure 1.1C).

The geospatial gradient of the increasing conductivity values within the conduit system also indicates that seawater sourced from the Gulf of Mexico is slowly migrating northward in a manner that agrees with the conceptual model established outlined above. Examining the maximum conductivity values for each station, there is a distinct pattern of decreasing conductivity values as one moves landward from Spring Creek Springs to Wakulla Spring: 50 mmho/cm at Spring Creek Springs; 5 mmho/cm at Revell Sink; 1 mmho/cm at AK and K tunnels; and 0.5 mmho/cm in C tunnel.

Additionally, the spatiotemporal pattern of rising and falling conductivity clearly tracks from south to north over time and space. The rising conductivity at Spring Creek Springs indicates that Spring Creek has ceased to discharge freshwater and begun to siphon saltwater. As the conductivity at Spring Creek Springs increases to highly saline (>30 mmho/cm), the conductivity beneath Revell Sink begins to increase approximately 28-77 days after the initial flow reversal at Spring Creek Springs (Figure 2.1B). The increases in conductivity at the AK/K/AD trio lag behind Revell Sink by 7-11 days and behind the spike at Spring Creek Springs by 35-110 days. The most northern of the south oriented conduits, C, lags behind all of the other stations, with increases in conductivity occurring 5-24 days after the AK/K/AD trio and 39-115 days after Spring Creek Springs. The only exception to this spatiotemporal pattern is Period 4. This period is tied to two abnormal events: the historic drought of 2011 and the extreme rainfall and storm surge produced by Tropical Strom Debby. The abnormal amounts of rainfall, large storm surge and rising tidal stage generated by Debby, combined with the long period of low rainfall before the tropical storm, forced conductive water proximate to the coast northward.

Similar to the pattern of rising electrical conductivity, there is also a discernable spatiotemporal pattern of the return to nominal conductivity in the conduit system. Falling conductivity values generally follow heavy rainfall events that provide sufficient recharge to reestablish flow at Spring Creek Springs. The allogenic recharge from the Apalachicola National Forest is particularly important, flow into the Lost Creek Swallet in enough volume to force the denser mixing saline water out of conduit systems at Spring Creek Springs (Davis and Verdi, 2014). Thus, there is a reversal of the spatiotemporal trend outlined in the preceding paragraph, beginning with a resumption of freshwater flow at Spring Creek Springs complex. This resumption of flow is followed in turn by a return to nominal conductivity that tracks from north to south: first C tunnel, then the AK/K/AD trio, and finally Revell Sink return to their normal values in turn. The return to nominal conductivity occurs significantly faster than the initial increase, with a lag time of only 1-2 days between C/AK/K/AD and Revell Sink.

Unfortunately, the 2D-ACM conductivity measurements alone do not provide evidence that the conductive water being measured is saline water sourced from the Gulf of Mexico. Two alternative explanations of conductivity spikes are also possible, which could be related to either anthropogenic contamination or upwelling regional groundwater. In order to rule out these possibilities, the geochemical dataset provided by NWFWMD were also examined (Figure 2.2).

Deep regional groundwater recharge (i.e., upwelling connate water) generally has a relatively higher electrical conductivity when compared to groundwater closer to the surface. This high conductivity is a product of the longer residence time of deep groundwater and long-term geochemical interaction in the limestone matrix (Winter et al., 1998). Two parameters recorded in the NWFWMD dataset, total calcium and total dissolved calcium are associated with upwelling groundwater (Winter et al., 1998). During the period of study, the concentration of these analytes remained relatively constant, indicating their negligible contribution to the increases in total conductivity. It is a low probability that the increases in conductivity seen in the conduit system are related to upwelling groundwater.

Figure 2.2. Geochemical analytes at Wakulla Spring, including sources of anthropogenic runoff, upwelling recharge connate water and seawater. Cartography by Seth Bassett.

The other potential source of conductive water in the region considered is water sourced from anthropogenic runoff. There are at least two major sources of anthropogenic contamination present in the study area: the Tallahassee Sprayfields and the Lower Bridge Landfill Facility (LBLF) (Figure 1.1B). Tracer studies have shown that dye introduced into monitor wells at the sprayfields will transit to the main Wakulla vent (Kincaid and Werner, 2008; Davis et al., 2010). Despite being located to the north of Wakulla Spring, the geometry of the conduit system provides that conductive water sourced north of Wakulla Springs approaches the main conduit system from the south. The R tunnel connects Wakulla Spring with the southern portion of Leon County and intersects the main conduit system south of the AK/K junction (Figure 1.1B). The LBLF is located approximately 3.4 miles south of Wakulla Spring and immediately proximate to the both the conduit at Revell Sink and the Q Conduit (Figure 1.1B).

Nutrient and organic components associated with both of these anthropogenic sources of contamination include nitrates, organic carbon, Kjeldahl nitrogen, ammonia and phosphorous. Examination of Figure 2.2 reveals that these anthropogenic analytes show no periodic increases that correlate with the periods of high conductivity. Moreover, the intragroup pattern among the anthropogenic analytes shows a linear trend consistent with the declining impact of the Tallahassee Sprayfields after remediation efforts were begun in 2004 (Davis et al., 2010; Xu et al., 2015a). The levels of organic and nutrient components also increase during the summer months when the Sprayfields are in heavy use, which is consistent with previous studies focusing on the effects of the Sprayfields on the water quality at Wakulla Spring. Conversely, the increases in conductivity seen in the 2D-ACM data occur predominantly during the winter months, when Spring Creek Springs has typically ceased to flow. Therefore, we conclude that there is low probability that anthropogenic sources are responsible for the rising conductivity values seen at Wakulla Spring.

Finally, there is a striking similarity between analytes associated with seawater and the rising conductivity values in the conduit system. These analytes - chlorides, magnesium, potassium, sodium, boron and sulfates (Pilson, 2012) – are elevated during the same periods when Spring Creek Springs has ceased to flow and conductivity is on the rise in the conduit system. The concentrations of the seawater analytes then return to lower values during periods when Spring Creek Springs is flowing and conductivity in the conduits returns to nominal. This provides strong evidence that the increases in conductivity seen in the vent are associated with seawater intrusion sourced from Spring Creek Springs. Of the three potential sources of conductive water at Wakulla spring, we consider seawater intrusion to be the most probable source that contributes to the increasing electrical conductivity values, based on the best available data interpretation at hand.

CHAPTER THREE

THE DEVELOPMENT OF DISCRETE-CONTINUUM VDFST-CFP (VARIABLE-DENSITY FLOW AND SOLUTE TRANSPORT – CONDUIT FLOW PROCESS) NUMERICAL MODEL

3.1 Numerical Models and Governing Equations

3.1.1 Numerical Modeling of Seawater Intrusion

Numerical modeling of seawater intrusion process is a density-dependent issue, since seawater has higher density than freshwater. In the variable-density numerical modeling, transport model is calculated based on the solution of groundwater velocity field from flow modeling, while the salinity also determines the groundwater density and affects the simulation of flow field. There are some pre-existed density-dependent numerical codes or models, such as SEAWAT (Guo and Langevin, 2002; Langevin et al., 2003), SUTRA (Voss and Provost, 1984) and FEFLOW (Diersch, 2002; Diersch, 2005). None of those is designed to simulate groundwater flow and solute transport in a coastal karst aquifer with conduit. An optional solution is to use extremely large values of hydraulic conductivity and porosity to represent the conduit structures in a karst aquifer, however, flow rate within the conduit is overestimated by Darcy equation. In Chapter 5, a SEAWAT numerical model is setup to simulate seawater intrusion through karst conduit networks in a cross section.

The movement of constant density groundwater through the porous medium is described by the three-dimensional partial differential equation of Darcy's Law as follow, which is the same equation that used in MODFLOW (McDonald and Harbaugh, 1988),

$$\frac{\partial}{\partial x}\left(K_{xx}\frac{\partial h}{\partial x}\right)+\frac{\partial}{\partial x}\left(K_{yy}\frac{\partial h}{\partial x}\right)+\frac{\partial}{\partial z}\left(K_{zz}\frac{\partial h}{\partial z}\right)+W=S_s\frac{\partial h}{\partial t} \quad 1)$$

where K_{xx}, K_{yy}, K_{zz} are the hydraulic conductivities along x, y and z coordinate axes, respectively, which are assumed to be parallel to the major axes of the hydraulic conductivity [L/T]; h is the potentiometric head [L]; W is the volumetric flux per unit volume representing sources and/or sinks of water, with $W < 0.0$ for flow out of the groundwater system, and $W > 0.0$ for flow into the system [T^{-1}]; S_s is the specific storage of the porous material [L^{-1}]; t is the time [T].

SEAWAT is able to simulate three-dimensional density-dependent process, however, most applications are two-dimensional cross section due to large computational cost (Guo and Langevin, 2002; Werner et al., 2013). The governing equation is also simplified as two-dimensional in the newly developed VDFST-CFP model.

The concept of equivalent freshwater head is used in SEAWAT (Guo and Langevin, 2002), instead of measured head, to describe variable-density groundwater flow and saline water movement. The conversion between head and equivalent freshwater head can be made using the following relations,

$$h_f = \frac{\rho}{\rho_f} h - \frac{\rho - \rho_f}{\rho_f} Z \qquad 2)$$

and,

$$h = \frac{\rho_f}{\rho} h + \frac{\rho - \rho_f}{\rho_f} Z \qquad 3)$$

where h_f is the equivalent freshwater head [L]; ρ_f is the density of freshwater [ML^{-3}]; ρ is the density of saline groundwater [ML^{-3}]; Z is the elevation [L].

Specific discharges or volumetric fluxes in the Darcy equation for a fluid of variable-density in terms of pressure can be expressed as,

$$q_x = -\frac{k_x}{\mu} \frac{\partial P}{\partial x} \qquad 4)$$

$$q_z = -\frac{k_Z}{\mu} \left(\frac{\partial P}{\partial z} + \rho g\right) \qquad 5)$$

where q_x and, q_z are the specific discharges in *x* and *z* directions, respectively [LT^{-1}]; μ is the dynamic voscosity [$ML^{-1}T^{-1}$]; k_x and k_z represent the intrinsic permeabilities [L^2] in the two coordinate directions; g is the gravitational acceleration constant [LT^{-2}].

The governing equation with sink/source terms for variable-density flow in terms of equivalent freshwater head is transferred with a coordinate system aligned with the principal directions of permeability,

$$\frac{\partial}{\partial \alpha}\left(\rho K_{f\alpha}\left[\frac{\partial h_f}{\partial \alpha} + \frac{\rho - \rho_f}{\rho_f}\frac{\partial Z}{\partial \alpha}\right]\right) + \frac{\partial}{\partial \gamma}\left(\rho K_{f\gamma}\left[\frac{\partial h_f}{\partial \gamma} + \frac{\rho - \rho_f}{\rho_f}\frac{\partial Z}{\partial \gamma}\right]\right) = \rho S_f \frac{\partial h_f}{\partial t} + \theta \frac{\partial \rho}{\partial C}\frac{\partial C}{\partial t} - \bar{\rho} q_s \qquad 6)$$

where γ represents the direction normal to the bedding, α represents the principal direction of permeability parallel to the bedding; $K_{f\alpha}$ and $K_{f\gamma}$ are the freshwater hydraulic conductivities in the α and γ directions, respectively [LT^{-1}]; S_f is the specific storage in terms of the freshwater head [L^{-1}]; C is the solute concentration (salinity) [ML^{-3}]; $\bar{\rho}$ is the density of water entering from a source or leaving through a sink [ML^{-3}]; q_s is the volumetric flow rate per unit volume representing sink/source term [LT^{-1}].

Solute transport modeling in a porous medium needs to solve groundwater flow advection, molecular diffusion and mechanical dispersion. The second order partial differential transport equation that applied in MT3DMS (Zheng and Wang, 1999; Zheng and Bennett, 2002) and UMT3D (Spiessl et al., 2007), has been simplified as two-dimensional transport equation in this study as well,

$$\frac{\partial(\theta C)}{\partial t} = \frac{\partial}{\partial x_i}\left(\theta D_{ij}\frac{\partial C}{\partial x_j}\right) - \frac{\partial}{\partial x_i}(\theta v_i C) + q_s C_s \qquad 7)$$

where θ is the porosity of the porous medium [dimensionless]; v_i is the seepage or linear pore water velocity [LT^{-1}], which is related to the specific discharge or darcian flux through the relationship, $v_i = q_i/\theta$; C is the solute concentration [ML^{-3}]; D_{ij} is the hydrodynamic dispersion coefficient tensor [L^2T^{-1}]; C_s is the solute concentration of water entering from sources or flowing out from sinks [ML^{-3}]; q_s is the volumetric flow rate per unit volume of aquifer representing fluid source (positive) and sink (negative) [T^{-1}].

3.1.2 Numerical Simulation of Flow and Solute Transport in a Karst Aquifer

Physically based discrete-continuum numerical model has been developed and used to simulate groundwater flow and solute transport processes in a karst aquifer. Groundwater flows in the discrete pipe and continuum porous medium are coupled in the numerical model. There are some pre-existed discrete-continuum numerical codes or models, such as CAVE (Carbonate Aquifer Void Evolution) (Clemens et al., 1996; Liedl et al., 2003), MODFLOW-CFP (Shoemaker et al., 2008b), CCPF (Hu, 2010; Chen et al., 2012) and CFPv2 (Reimann et al., 2013; Reimann et al., 2014). None of those is designed to simulate density-dependent seawater intrusion process. An optional solution is to calculate the equivalent freshwater head prior to the simulation, however, there is no density-dependent vertical flux in the groundwater flow model.

In Chapter 4, a CFPv2 numerical model is setup to simulate groundwater flow cycling process in the WKP with pre-calculated equivalent freshwater head at a submarine spring.

When a pipe is fully saturated, groundwater flow within the pipe can be assumed to be one-dimensional along the axis of straight cylindrical pipe. The Darcy-Weisbach equation is used to simulate groundwater flow within the pipe, which is applicable to both laminar and turbulent flows (Shoemaker et al., 2008b),

$$\Delta h = h_L = f\frac{\Delta l}{d}\frac{v^2}{2g} \tag{8}$$

where Δh or h_L is the head loss [L] measured along the pipe Δl [L]; f is the friction factor [dimensionless]; d is pipe diameter [L]; v is the mean velocity [LT^{-1}]; g is the gravitational acceleration constant [LT^{-2}].

Groundwater advective flow exchange through the pipe wall between the conduit and porous medium is calculated using the linear relationship model (Shoemaker et al., 2008b),

$$Q_{n,ex} = \alpha_n\left(h_n - h_{i,k}\right) \tag{9}$$

where $Q_{n,ex}$ is the volumetric exchange flow rate between the conduit and matrix [L^3T^{-1}]; h_n is the head at conduit node *n* [L]; $h_{i,k}$ is the head at matrix cell *i, k* [L]; α_n is the pipe conductance at conduit node *n* [L^2T^{-1}], which is calculated by:

$$\alpha_n = \frac{\sum_f^2 K_l^f \pi d_l^f \frac{1}{2}\left(\Delta l_l^f \tau_l^f\right)}{r_l^f} \tag{10}$$

where the superscript *f* indicates either forward or backward direction of the pipe connected to node *n*; K_l^f is the conduit wall permeability term of pipe l [LT^{-1}]; π is the mathematical constant pi [dimensionless]; d_l^f is the diameter of pipe l [L]; Δl_l^f is the straight-line length of pipe l [L]; τ_l^f is the tortuosity of pipe l [dimensionless]; r_l^f is the radius of pipe l [L].

Solute transport in the conduit is describe by the one-dimensional advection equation as well, while mechanic dispersion within the conduit is ignored in the CFPv2 numerical model as well as the VDFST-CFP model in this study,

$$\frac{\partial C_l}{\partial t} = -q_l\frac{\partial C_l}{\partial x} \tag{11}$$

where C_l is the solute concentration in conduit tube l [ML^{-3}]; q_l is the conduit flow velocity in conduit tube l [LT^{-1}], which could be calculated by volumetric flow rate Q from the Darcy-

Weisbach equation [L^3T^{-1}]. Note there are no sink/source terms in the conduit transport equation, because the sink/source terms and exchanges with the surrounding porous media are computed at the conduit nodes only.

Advective exchange rate between a conduit node and the surrounding porous medium cells are determined by,

$$K_{ex} = \begin{cases} \frac{Q_{n,ex}^{+} C_{i,k}}{V_{i,k}}, Q_{n,ex}^{+} > 0 \\ \frac{Q_{n,ex}^{+} C_{n}}{V_{i,k}}, Q_{n,ex}^{+} < 0 \end{cases} \quad 12)$$

where $K_{ex,n}$ is the advective exchange rate between a conduit node *n* and respective matrix cell *i, k* [$ML^{-3}\ T^{-1}$]; $Q_{n,ex}^{+}$ is the exchange flow rate [L^3T^{-1}] at conduit node *n* ($Q_{n,ex}^{+} > 0$, flow direction is from matrix to conduit node; $Q_{n,ex}^{+} < 0$, flow direction is from conduit node to matrix); $C_{i,k}$ is the solute concentration of respective cell *i, k* in the porous medium at conduit node *n* [ML^{-3}]; C_n is the nodal concentration at conduit node *n* [ML^{-3}]; $V_{i,k}$ is the volume of respective cell *i,k* of the porous medium at conduit node *n* [L^3].

Spiessl et al. (2007) pointed out that mass transport within a conduit networks is determined by the flow velocity within the conduits, exchange coefficients between the conduit nodes and porous matrix, the magnitude of conduit sink/source terms and the lengths of conduit tubes. Mathematically, a weighted arithmetic mean of the nodal concentration value C_n [ML^{-3}] at conduit node *n* can be expressed as follow (Spiessl et al., 2007),

$$C_n = \frac{\sum_f^2 Q_{n,l}^{f+} C_{n,l}^{f} + Q_{n,ex}^{+} C_{i,k} + \sum_s Q_{n,s}^{+} C_{n,s}}{\sum_f^2 Q_{n,l}^{f+} + Q_{n,ex}^{+} + \sum_s Q_{n,s}^{+}} \quad 13)$$

where superscript *f* indicates either forward or backward direction of the pipe connected to node *n*; $C_{n,l}^{f}$ is the concentration of tube *l* connected to face *f* of the conduit node *n* [ML^{-3}]; $C_{n,s}$ is the concentration of the source or sink term to the conduit node *n* [ML^{-3}]. The superscript + represents the inflow terms at conduit node *n*, which means that only inflow terms are used to compute the nodal concentration; $Q_{n,l}^{f+}$ is the discharge of tube *l* connected to face *f* into the respective conduit node *n* [L^3T^{-1}]; $Q_{n,s}^{+}$ is the volumetric flow rate of a source term at conduit node *n* [L^3T^{-1}].

3.2 Modeling Methods and Governing Equations of the VDFST-CFP

3.2.1 Assumptions of the VDFST-CFP

A numbers of assumptions, listed below, are applied in the VDFST-CFP numerical model, which keep the mathematical model conceptually reasonable, guarantee the model accuracy but significantly reduce the coding effort, requirements of data preparation and computational demanding.

1) The model is two-dimensional with only one conduit network. The computational cost for three-dimensional or multiple conduit networks will be unaffordable. The extremely high computational cost is mainly due to the application of implicit iterative procedure, in which flow and transport equations have to be solved many times iteratively in each time step. The code could be extended into three-dimensional and multiple conduits in future study with parallel computing technique.
2) The aquifer is confined and the conduit is fully saturated. The governing equations and numerical implementation of groundwater flow in a confined aquifer are much simpler than that in an unconfined aquifer with variable thickness and transmissivity. The subsurface conduit network is usually existed in the deep coastal karst aquifer to avoid the complex calculation of variable saturation condition, for example, the karst conduit networks in the Woodville Karst Plain (WKP), north Florida, where submarine caves are believed as deep as 300 ft deep under surface.
3) Groundwater viscosity is assumed to be constant. Viscosity is basically dependent on temperature, which is assumed constant in this study as well. Density is a solely function of salinity in this study.
4) Matrix porosity is assumed to be constant. The physical and chemical processes that may change matrix porosity, including carbonate dissolution and precipitation, weathering and erosion, are not considered in this study.
5) The difference between the compressibility coefficients of saline water and freshwater is negligible.
6) The variation of density is linear to salinity. The advection dispersion of solute transport equation is applied without additional density terms, while the effect of variable density only affects groundwater flow.

7) The friction factor in the Darcy-Weisbach equation for pipe flow is constant and assigned at the beginning of the VDFST-CFP model. In MODFLOW-CFP, the Colebrook-White equation is used to calculate the friction factor based on the roughness of the conduit wall micro-topography and Reynolds number in each time step (Shoemaker et al., 2008b), but is not applied in the VDFST-CFP model. The constant friction factor assumption can greatly save the computational cost, however, the impacts will be discussed later in this paper.
8) Darcy-Weisbach equation is directly applied in the groundwater flow simulation in the conduit, no matter laminar or turbulent condition. In MODFLOW-CFP simulation, Reynolds number of groundwater flow in the conduit is calculated to determine the flow is either turbulent or laminar.

3.2.2 Variable-Density Groundwater Flow in the Conduit

The variable-density non-laminar conduit flow equations are analytically derived in this study. Bernoulli equation including head loss in the two sides of a conduit tube section could be written as:

$$\frac{p_1}{\rho g} + z_1 + \frac{{v_1}^2}{2g} = \frac{p_2}{\rho g} + z_2 + \frac{{v_2}^2}{2g} + h_L \quad 14)$$

where p_1 and p_2 are the fluid pressures at the two points [MLT^{-2}], z_1 and z_2 are the elevations at the two points [L], v_1 and v_2 are the velocities [ML^{-1}] at the two points, respectively; h_L is the head loss [L] for the water flow through the two points. The head loss term in Bernoulli equation and Darcy-Weisbach equation can be reformulated as,

$$h_L = \frac{p_1 - p_2}{\rho g} + z_1 - z_2 = f\frac{\Delta l}{d}\frac{v^2}{2g} \quad 15)$$

The mean pipe flow velocity v, is equal to the volumetric flow Q [L^{3}T^{-1}], divided by the cross-sectional area A [L^2] that perpendicular to flow direction. The Darcy-Weisbach equation can be reformulated to solve for volumetric flow rates Q [L^{3}T^{-1}] in term of head loss as,

$$Q = A \cdot v = A\sqrt{\frac{\Delta h\, d\, 2g}{\Delta l\, f}} = A\sqrt{\frac{2gd}{f\Delta l}\left(\frac{p_1 - p_2}{\rho g} + z_1 - z_2\right)} = A\sqrt{\frac{2gd}{f}\left(-\frac{1}{\rho g}\frac{dp}{dl} - \frac{dz}{dl}\right)} \quad 16)$$

In order to derive the variable-density groundwater flow in the Darcy-Weisbach equation, the relationship of pressure term and equivalent freshwater head has been demonstrated by Guo and Langevin (2002) as,

$$p = \rho_f \cdot g \cdot (h_f - z) \tag{17)}$$

Therefore, the relationship of flow rate respect to equivalent freshwater head and density could be presented by substituting the pressure differential term in equation 27) as follow,

$$Q = A\sqrt{\frac{2gd}{f}\left(\frac{\rho_f g}{\rho g}\frac{dh_f}{dl} - \frac{\rho_f g}{\rho g}\frac{dz}{dl} + \frac{dz}{dl}\right)} = A\sqrt{\frac{2gd}{f}\left(\frac{\rho_f}{\rho}\frac{dh_f}{dl} + \frac{\rho - \rho_f}{\rho}\frac{dz}{dl}\right)} \tag{18)}$$

3.2.3 Numerical Implementation and Code Structure

The VDFST-CFP numerical model is written in Fortran language with packages solving groundwater flow and solute transport in the conduit and the porous medium, respectively. Standard finite difference method is applied to solve the two-dimensional governing equations of variable-density darcian flow in the continuum porous medium domain. The two-dimensional advection dispersion solute transport equation in the porous medium is numerically solved by standard finite difference method as well. Fortran LAPACK (Linear Algebra PACKage) routines are used to solve the linear algebra matrix of finite difference method in the VDFST-CFP model. In general, the numerical approaches that used in the porous medium part of the VDFST-CFP model are very similar to those used in MODFLOW (Harbaugh, 2005) and the standard finite difference solvers in MT3DMS (Zheng and Wang, 1999). The variable-density terms in the governing equation that used in the VDFST-CFP are the same as those in SEAWAT model (Guo and Langevin, 2002). The coupling of groundwater flow and solute transport between the conduit and porous medium is similar to the method used in the discrete-continuum CFPv2/UMT3D model.

The derived variable-density Darcy-Weisbach equation demonstrates that the volumetric flow rate in the conduit is non-linear respect to the gradient of equivalent freshwater head. Therefore, the Newton-Raphson method is applied to calculate the head (equivalent freshwater head) by forming the Jacobian matrix and solving the system of linear equations iteratively in the VDFST-CFP model as well as MODFLOW-CFP (Shoemaker et al., 2008b). Node heads from the previous time step are used to start Newton-Raphson iterations for the current time step.

Specifically, nodal heads are set equal to the head in the porous medium at the first iteration of the first time step.

Implicit finite difference method with backward-difference in time is applied to solve the one-dimensional advection equation in the conduit. Explicit scheme is used more often with less computational cost, however, the numerical stability criterion of explicit method for solving the advection equation requires the Courant number (N_{co}) is lower or equal to 1,

$$N_{co} = \left|\frac{v\Delta t}{\Delta l}\right| \leq 1 \qquad 19)$$

where v is the average velocity in the conduit [LT^{-1}]; Δt is the length of timestep [T]; Δl is the length of conduit tube [L].

It is difficult to guarantee the Courant number is always satisfied the criterion of explicit scheme since the conduit flow is always rapid and can be turbulent. Therefore, the implicit scheme is used instead of explicit scheme because of its advantage of unconditionally stable. Other explicit semi-Lagrangian scheme such as the EMCNOT by Liu et al. (2001) is applied in CFPv2/UMT3D simulation (Spiessl, 2004), but not in this study because of the intensive coding demand and enormous computational cost. Each conduit tube is subdivided to 10 segments in the one-dimensional advection transport simulation with higher resolution of spatial discretization to avoid the numerical oscillation and provide more accurate results in the implicit scheme. Dispersion and diffusion are negligible and not considered in the conduit transport process to save computational cost, because solute transport in the conduit is advection dominated. However, the assumption could result in uncertainty in salinity estimation along the conduit network.

Groundwater flow and solute transport equations in the conduits and porous medium are coupled and calculated iteratively by an implicit procedure. The acceptable density differences in a matrix cell and conduit node need to be very small, especially in the highly permeable conduit network. The implicit approach solves the groundwater flow and solute transport equations in an iterative sequence in each time step, until the consecutive differences of the calculated head and density are less than the specified convergence values. In the beginning of an implicit coupling iteration loop, the variable-density flow equations for the porous medium and the conduit are solved by finite difference method and Newton-Raphson method, respectively. After that, the two-dimensional advection dispersion transport equations in the porous medium and one-dimensional advection transport equation in the conduit are solved by implicit finite difference method. The conduit nodal concentrations are calculated by the weighted arithmetic mean relationship expressed in equation (13). The computational cost and model running time are tremendous because the implicit coupling approach is needed to solve the flow and transport equations many times iteratively in one time step.

3.3 Model Validation

3.3.1 Benchmark Comparison Study

The VDFST-CFP model is developed and compared with other numerical models, such as SEAWAT, in which a variable-density groundwater flow model is coupled with a solute transport model, as well as MODFLOW/MT3DMS and CFPv2/UMT3D models, which are constant density continuum model and discrete-continuum model, respectively. In order to validate the VDFST-CFP numerical model, two groups of numerical models are generated to compare with the simulation results of the VDFST-CFP model.

Groundwater flow in the conduit networks is simulated by Darcy equation in a continuum model, either MODFLOW or SEAWAT, with large values of hydraulic conductivity, specific storage and porosity. However, Darcy-Weisbach equation is applied to simulate the one-dimensional, non-laminar conduit flow in the discrete-continuum models, and then couples with the Darcy equation used for groundwater flow in porous media. The flow equations are further coupled with solute transport equations in the conduit and the porous medium, as well as the advective water mass and solute exchanges between the conduit nodes and surrounding pore matrix. In the constant density MODFLOW/MT3DMS and CFPv2/UMT3D models, the equivalent freshwater heads are needed to compute and substitute in the constant head boundary conditions. However, the equivalent freshwater heads are calculated directly in the density-dependent numerical models without any prior computation, such as SEAWAT and the VDFST-CFP in this study. For comparison purpose, all numerical models in one case have the same values of hydrological parameters in both the conduit and porous medium, including the hydraulic conductivity, specific storage, porosity and dispersivity.

Porosity and specific storage of the conduit network in the continuum model are simply calculated by the volume of void spaces, while the mechanic dispersion and diffusion are ignored in the conduit. The following approach is used to calculate the conduit parameters used in the discrete-continuum models, including diameter and friction factor, to be equivalent with hydraulic conductivity of the conduit network in the continuum models. The conduit is represented as continuum cells with extremely high hydraulic conductivity in MODFLOW and SEAWAT models, in which groundwater flow is still simulated by laminar Darcy equation. The transition between laminar and turbulent flow is governed by the Reynolds number,

$$Re = \frac{qd}{v} \tag{20)}$$

where Re is the Reynolds number [dimensionless]; q is the specific discharge [LT^{-1}]; defined as discharge per unit cross-section flow area; d is the specific length dimension [L] (mean void diameter of porous media or conduit diameter for discrete elements); v is the kinematic viscosity of the fluid [L^2T^{-1}].

On the other hand, laminar flow in cylindrical conduits in the discrete-continuum model can be described with the linear Hagen-Poiseuille equation (eq. 21) that derived from the Darcy-Weisbach equation if $f = 64/Re$, where f is the friction factor [dimensionless] (Reimann et al., 2011b),

$$\frac{\partial h}{\partial x} = -f\frac{q^2}{2gd} \tag{21)}$$

$$q = -\frac{gd^2}{32v}\frac{\partial h}{\partial x} \tag{22)}$$

On the other hand, Darcy equation states that the laminar groundwater flow rate is linear to the hydraulic gradient with the hydraulic conductivity K [LT^{-1}], which is applied in the continuum model and used to simulate laminar groundwater flow as follow (Harbaugh et al., 2000),

$$q = -K\frac{\partial h}{\partial x} \tag{23)}$$

Therefore, the relationship of hydraulic conductivity in the continuum model and conduit diameter in the discrete-continuum model could be obtained from equations (22) and (23) and described as,

$$K = -\frac{gd^2}{32v} \tag{24)}$$

However, the estimation of equivalent hydraulic conductivity and conduit diameter is under laminar flow conditions with Reynolds number is smaller than the critical Reynolds number, usually about 2000 (Reimann et al., 2011b; Bear, 2013). The uncertainty of this approximation on non-laminar flow condition will be discussed later. The friction factor is assumed to be constant in the VDFST-CFP model and pre-calculated by the following Colebrook-White equation at the beginning of modeling simulation, which is the same method used in MODFLOW-CFP and CFPv2 when groundwater flow in the conduit is non-laminar,

$$\frac{1}{\sqrt{f}} = -2log\left(\frac{k_c}{3.71d} + \frac{2.51}{Re\sqrt{f}}\right) \quad 25)$$

where f is the friction factor [dimensionless], k_c is the mean roughness height of the conduit wall micro-topography [L], Re is the Reynolds number [dimensionless].

Regarding of numerical techniques, standard finite difference approach in the PCG solver of MODFLOW and GCG solver of MT3DMS with the upstream weighting scheme are applied to solve the partial differential groundwater flow and solute transport equations, respectively, in SEAWAT, MODFLOW/MT3DMS and CFPv2/UMT3D models. The newly developed VDFST-CFP model uses very similar numerical methods to other models.

3.3.2 Conceptual Model of Benchmark Cases

Two synthetic numerical models are designed as benchmarks to validate the VDFST-CFP model. A horizontal case is created to validate the discrete-continuum approach of groundwater flow and solute transport simulation in the conduit and porous medium. On the other hand, a vertical case in a cross section is developed to test the density-dependent groundwater flow and solute transport performance of the new numerical model.

The conceptual model and boundary conditions of the two-dimensional horizontal benchmark are shown in Figure 3.1. The spatial discretization of the model domain using the finite difference method consists of 21 rows, 120 columns and 1 layer in the horizontal benchmark The rows and columns width of each cell is 500 ft by 500 ft, with 50 ft thickness in the horizontal layer. The conduit network is located along row #11 in the middle of the domain, starts from the left to right boundary. The elevation of horizontal plane is assumed at the deep confined aquifer layer, starts from 334 ft BSL (below sea level) on the left and gradually rises to 319 ft BSL on the right.

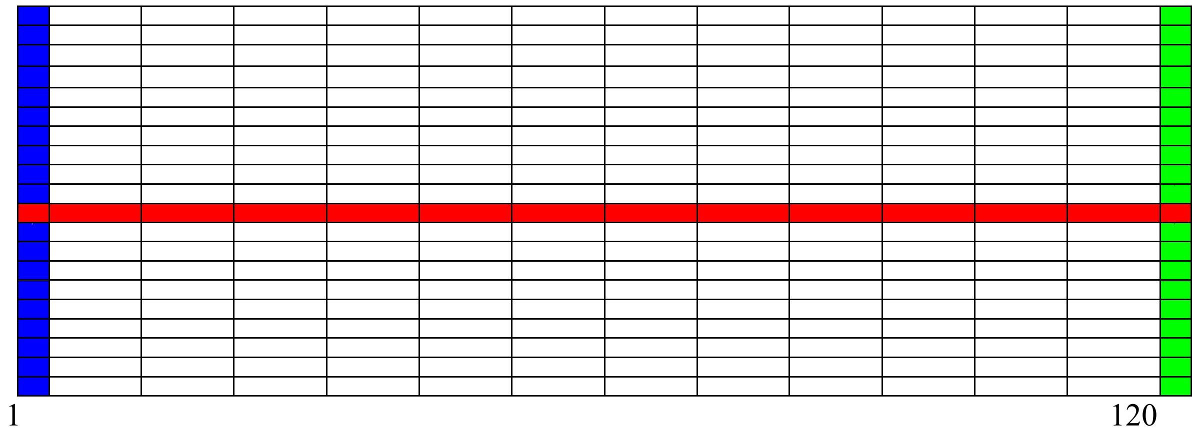

Explanations:

Seawater boundary: constant head (0.0 ft) and constant concentration (35 PSU)

Freshwater boundary: constant head (5.0 ft) and constant concentration (0 PSU)

Conduit system: relatively large values of hydraulic conductivity, porosity and specific storage in continuum models, or conceptual pipe network in discrete-continuum models

Porous medium: relatively small values of hydraulic conductivity, porosity and specific storage

Figure 3.1 Schematic figure of finite difference grid discretization and boundary conditions applied in the horizontal benchmark cases. Every tenth cells in horizontal are shown, except the boundary on the two sides with small width. The conduit system is located at row #11 in the middle of the spatial domain, starts from column #1 on the left to #120 on the right.

The freshwater boundary on the right side is assigned as constant head (5.0 ft) and constant concentration (0.0 PSU) to represent freshwater regional recharge; while the saline water boundary on the left is assigned as constant measured head (0.0 ft) and constant concentration (35.0 PSU) to represent hydrostatic condition of seawater. In the horizontal benchmark, the measured head boundary condition of the conduit is set as 1.0 ft on the left, which is higher than that in porous media to accelerate the exchanges between conduit and surrounding porous media, but remains 5.0 ft on the right to be the same as that in the porous medium. As mentioned, the equivalent freshwater heads are directly calculated in the density-dependent models, but need to be pre-calculated by measured head, salinity, density and elevation, and then substituted in the constant density models. The upper and lower boundaries are no flow boundaries.

In the continuum SEAWAT and MODFLOW/MT3DMS models, 100 time steps are required to run 1-day simulation period with the specified time step size as 0.01 days. However, for the discrete-continuum models including CFPv2/UMT3D and the VDFST-CFP, 1000 time steps are needed to run the same period of time with much smaller time step size specified as 0.001 days, because of the more rigorous convergence criteria for the coupled flow and solute transport in the discrete-continuum numerical models.

On the other hand, a two-dimensional variable-density SEAWAT numerical model is created to compare with the VDFST-CFP model in the vertical benchmark case (Figure 3.2). Results of constant density groundwater flow models such as MODFLOW and CFPv2 are not shown, which are not applicable for vertical benchmarks, because simulations of groundwater flow field and vertical flux are physically inappropriate in terms of variable density effect. The finite difference model grid used to discretize the benchmark domain consists of 1 row, 140 columns and 37 layers in the vertical benchmark case. The rows and columns width of each cell is 50 ft by 50 ft with 10 ft thickness in each layer. The conduit system starts from the top of column #22, downward to layer #29, horizontally extends from column #22 to column #139, finally upward to the surface through column #139. The surface layer in the vertical case is simulated as confined aquifer, which starts from 34 ft BSL on the left and gradually rises to 19 ft BSL on the right. The vertical conceptual model is very similar but in a smaller spatial scale with the numerical model setup in Xu et al. (2016), which are designed to quantitatively simulate and evaluate seawater intrusion through the deep conduit networks connecting with submarine springs and caves in the Woodville Karst Plain (WKP), north Florida.

The boundary conditions of the porous medium in the vertical case are exactly the same as those in the horizontal case, in which the constant head and concentration boundary of freshwater (5.0 ft, 0.0 PSU) and seawater (0.0 ft, 35.0 PSU) are on the right and left, respectively. The initial conditions of conduit system are the same as those in the surrounding porous medium. The top and bottom boundaries are no flow. In the continuum SEAWAT model, 40 time steps are required to run 0.2-day simulation period with the specified time step size as 0.005 day. However, in a discrete-continuum model such as VDFST-CFP, 400 time steps are needed to run the same simulation period with much smaller time step size specified as 0.0005 day, due to the more rigorous convergence criteria for both conduit and porous medium in the discrete-continuum numerical model.

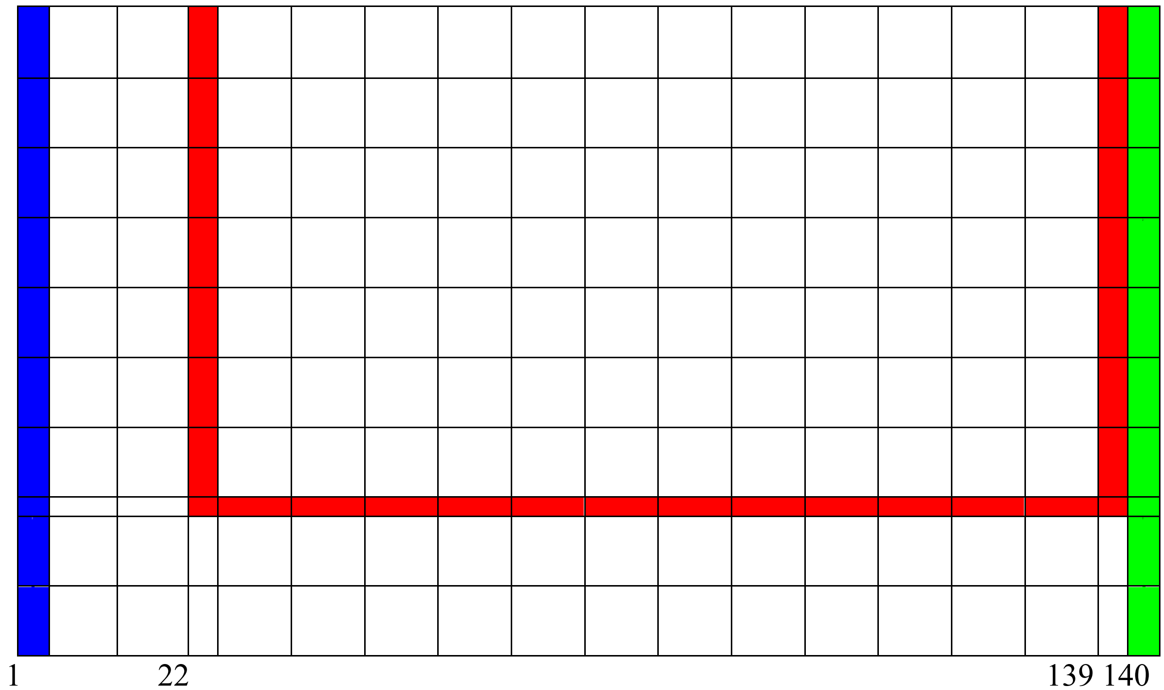

Explanations:

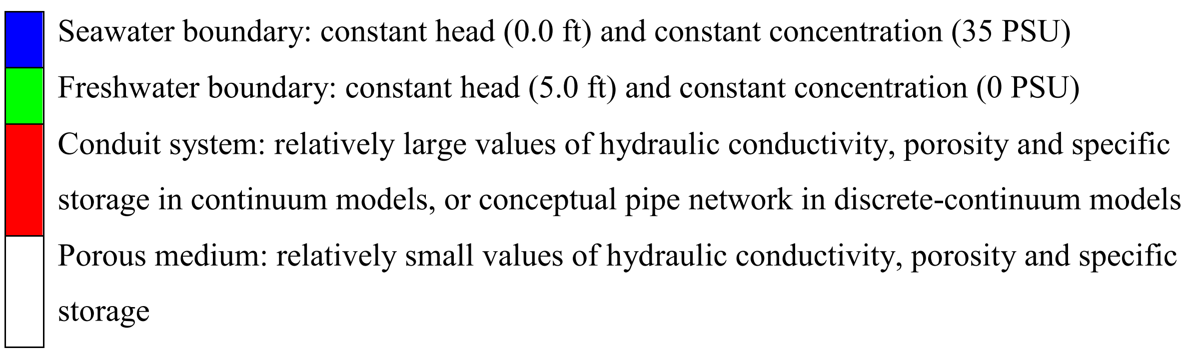

Figure 3.2 Schematic figure of finite difference grid discretization and boundary conditions applied in the vertical benchmark cases. Every tenth cell in horizontal and every fourth cell in vertical are shown, except the boundary on the two sides and conduit layer with small width. The conduit system starts from the top of column #22, downward to layer #29, horizontally extends to from column #22 to column #139 and then upward to the top through column #139.

The detailed definitions and values of hydrological parameters in the porous medium and conduit are listed in Table 3.1. Conduit diameters and friction factors in the discrete-continuum models are calculated to be equivalent as those in the continuum model. Most parameters of the porous medium used in the synthetic models are assigned based on the parameter values of the Upper Floridan Aquifer (UFA) in the WKP, which were calibrated in a regional-scale numerical model by Davis et al. (2010) and then applied in many subsequent modeling studies (Gallegos et al., 2013; Xu et al., 2015a; Xu et al., 2015b). The diameter and friction factor of the conduit network are synthetic and do not match with the field conditions, because of the limitations of discrete-continuum model assumptions and the issues of numerical convergence, which will be discussed later.

3.3.3 Simulation Results

The salinity simulation of the horizontal benchmark case by SEAWAT, MODFLOW/MT3DMS, CFPv2/UMT3D and the newly developed VDFST-CFP numerical models are presented in Figure 3.3. Generally speaking, high-density seawater intrudes landward along the high-permeability conduit system with the rapid groundwater flow, and then transports into the matrix domain through the exchange between the conduit and matrix. Simulation results of continuum SEAWAT and MODFLOW/MT3DMS are exactly the same, and the simulation results of discrete-continuum CFPv2/UMT3D and the VDFST-CFP are similar as well. In the constant density cases, the equivalent freshwater head is calculated at seawater boundary condition on the left. The density-dependent vertical flow does not exist and is not simulated in the horizontal benchmark case. In other words, simulation results of the constant density case should be same as those of the density-dependent case, if the equivalent freshwater head has been converted and applied at the seawater boundary in the horizontal case.

The positions of mixing zone extend significantly further along the conduit in the continuum SEAWAT and MODFLOW/MT3DMS models than those in the discrete-continuum CFPv2/UMT3D and VDFST-CFP models, and the reasons are explained below. The groundwater flow rate is no longer linear to the head gradient in the conduit under non-laminar condition. Volumetric flow rate and specific discharge are significantly overestimated under non-laminar condition with large hydraulic gradient, if the linear Darcy equation (eq. 23) is still used in the continuum models, result in simulations of faster groundwater flow and further seawater intrusion in the continuum SEAWAT and MODFLOW/MT3DMS models. The Darcy-Weisbach equation in the discrete-continuum models, such as CFPv2 and VDFST-CFP, provide more accurate simulation of flow rate in the highly permeable conduit network.

Table 3.1. Parameters values of the conduit and porous medium in the horizontal and vertical benchmarks. MODFLOW/MT3DMS and SEAWAT are continuum models, while MODFLOW-CFP/UMT3D and the VDFST-CFP are discrete-continuum models. Conduit parameters including diameters and friction factors are different in horizontal and vertical benchmarks.

	Porous media	Conduit (Continuum model)	Conduit (Discrete model), Horizontal benchmarks	Conduit (Discrete model) Vertical benchmarks
Conductivity (ft/day)	7500	2×10^{6}	-	-
Porosity	0.003	0.031	-	-
Specific storage	5.0×10^{-5}	1.0×10^{-4}	-	-
Dispersivity (ft)	32.80	0	-	-
Diameter (ft)	-	-	3.00	0.891/1.333*
Friction factor	-	-	0.0178	0.03

* In vertical benchmarks, the conduit diameters of horizontal part are calculated as 0.891 ft, but are calculated as 1.333 ft in the vertical parts of the conduit.

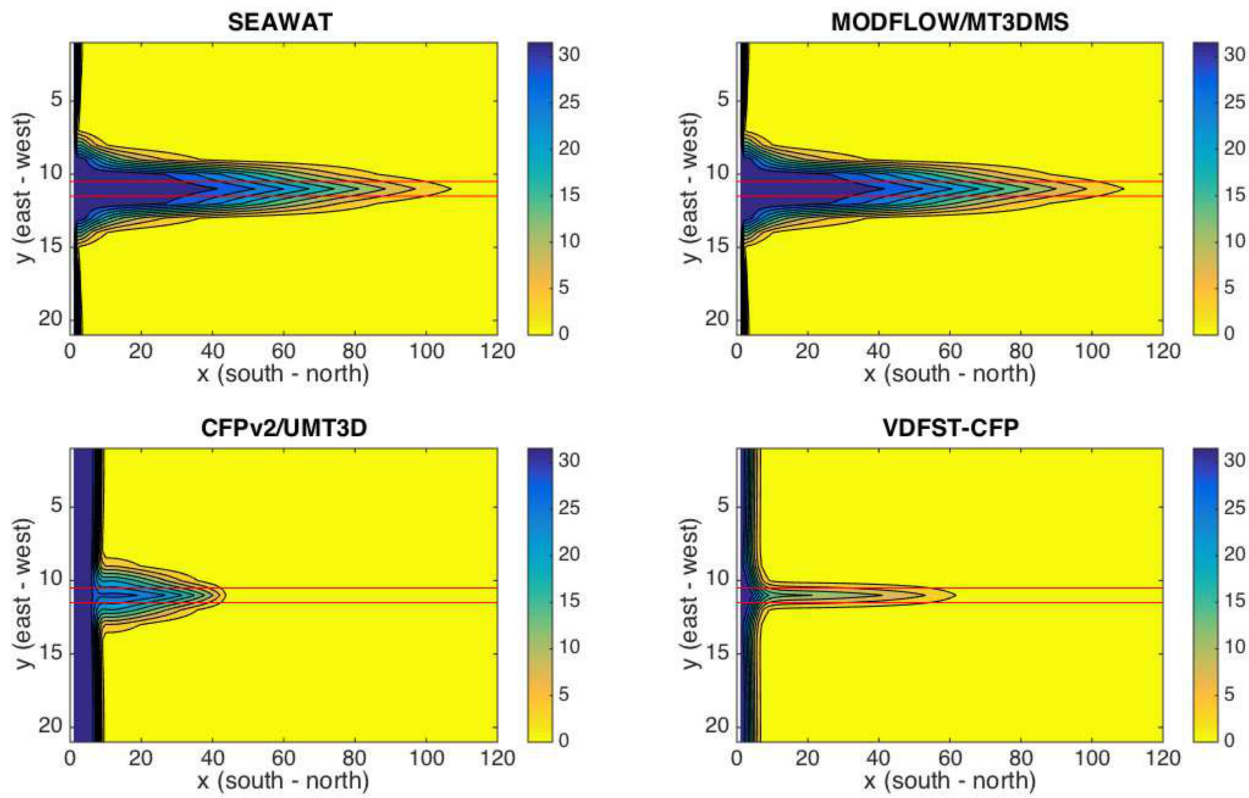

Figure 3.3 Salinity simulations by the two continuum numerical model and the other two discrete-continuum numerical model in the horizontal case: 1) SEAWAT (upper left); 2) MODFLOW/MT3DMS (upper right); 3) CFPv2/UMT3D (lower left); 4) VDFST-CFP (lower right).

Comparing with the simulation results of CFPv2/UMT3D, the position of mixing zone in the conduit moves further landward in the VDFST-CFP simulation, but the salinity plume is less significant near the left seawater boundary in the porous medium. The difference is probably due to the different governing equations and estimation of friction factor in the two discrete-continuum models. In the VDFST-CFP model, a uniform pre-assigned friction factor is applied in Darcy-Weisbach equation to calculate groundwater flow in the conduit to keep the coding structure simple and save the computational cost. In the CFPv2 model, friction factor is calculated for every conduit tube at each time step. The friction factor in the VDFST-CFP model is estimated by assuming the Reynolds number is 100,000 and uniform along the conduit in the horizontal benchmark case, which is about the average Reynolds number calculated in the CFPv2 model. However, the friction factor can be less than the uniform value in some parts of conduit network when Reynolds number is higher than the averaged value, results in overestimation of groundwater flow and moves position of mixing zone further landward along the conduit in the VDFST-CFP simulation. The underestimation of friction factor is a potential reason for the smaller simulated salinity plume in the porous medium by the VDFST-CFP model. The uncertainty of friction factor estimation is evaluated by parameter sensitivity analysis and discussed in Section 5.3 in detail.

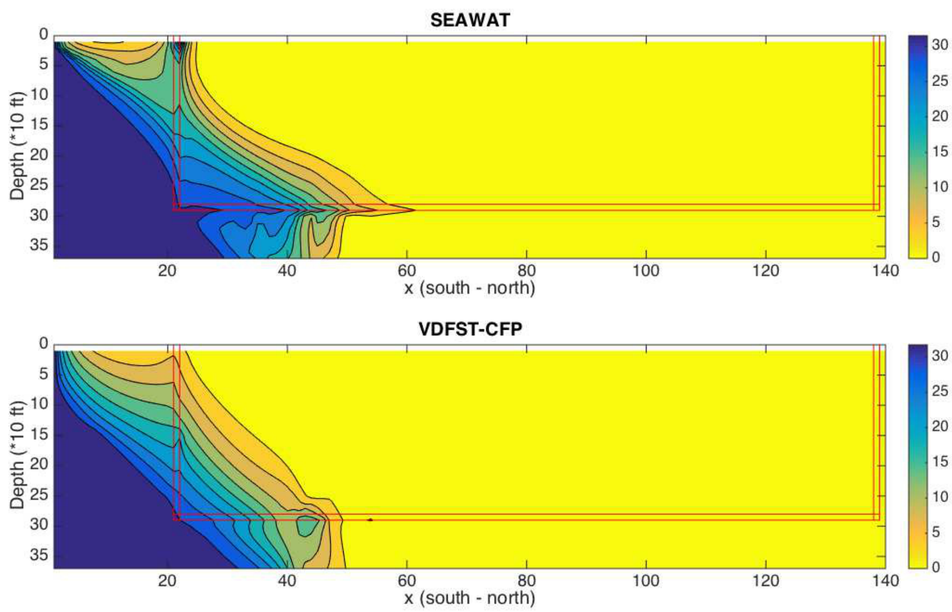

Figure 3.4 Salinity simulations by two density-dependent numerical models in the vertical case: 1) SEAWAT (upper); 2) VDFST-CFP (lower).

The salinity simulation of the vertical benchmark case by SEAWAT and the newly developed VDFST-CFP numerical models are presented in Figure 3.4. Seawater intrudes through both the seawater water boundary on the right and the submarine cave opening to the sea, travels further landward in the high-permeability conduit than surrounding porous medium. The simulated salinity distributions in the porous medium are roughly the same by the two numerical models, while the position of mixing zone moves further landward along the conduit simulated by the continuum SEAWAT model than that by the discrete-continuum VDFST-CFP model, because of the overestimation of non-laminar specific discharge by linear Darcy equation. The fingering effect along the conduit system in SEAWAT simulation is probably due to the numerical instability of groundwater flow, solute advection and density distribution between the highly permeable conduit system and surrounding porous medium with relatively low hydraulic conductivity. However, the phenomenon is not shown and the numerical stability is improved in the discrete-continuum VDFST-CFP model, since the exchange between the conduit and the porous medium is calculated internally within numerical cells where conduit nodes are located.

3.3.4 Parameter Sensitivity Study

The sensitivities of several factors on salinity distribution simulation are studied in order to investigate the importance of parameters in the VDFST-CFP model. The evaluated factors include the diameter and friction factor of the conduit system, conduit-matrix exchange interaction, hydraulic conductivity and porosity of the porous medium. The sensitivity results of conduit parameters and exchange permeability are shown in Figure 3.5, and the results of matrix parameters are shown in Figure 3.6. The results of sensitivity analysis for the horizontal benchmark case are presented but not for the vertical benchmark case, which exhibit the similar pattern. The positions of the mixing zone, defined as the column number with salinity as 10.0 PSU, are evaluated in the conduit network and the matrix cell where conduit nodes are located.

The conduit diameter is allowed to vary from 2.0 ft to 4.0 ft with an interval of 0.5 ft in the sensitivity study. Simulation results indicate the position of mixing zone moves further landward in the cases with larger diameter because of the faster groundwater flow rate in the conduit (Figure 3.5A). The position of mixing zone in the porous medium is lag behind but affected by the diameter more significantly than that in the conduit. Result of parameter sensitivity analysis demonstrates that the conduit diameter is an important factor for groundwater flow and solute transport simulations in both the conduit and porous medium. The positions of mixing zone in the porous medium change instantly in some cases because of the numerical instability for calculation of the water and salt exchanges between conduit and matrix system. The VDFST-CFP models with large values of conduit diameter may have the numerical convergence issue due to the limitations of numerical calculation required in the variable-density discrete-continuum numerical model, which will be discussed later in Section 5.3.

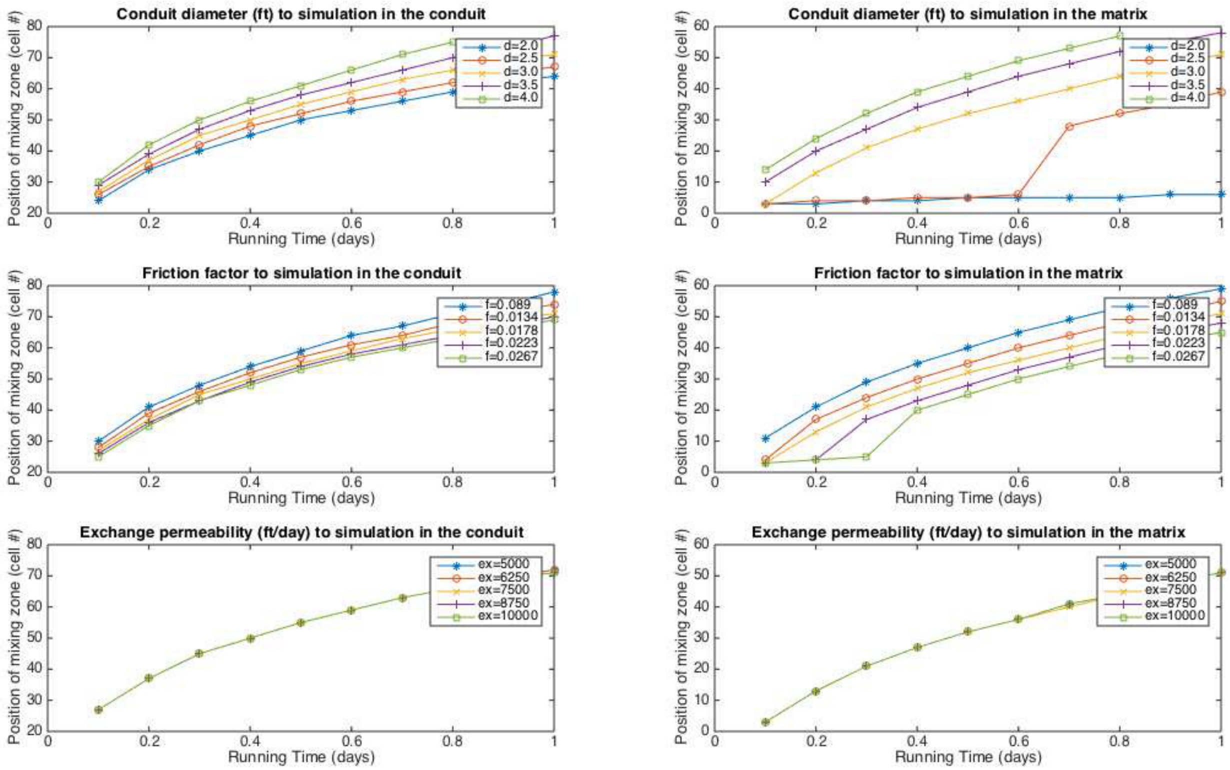

Figure 3.5 Parameter sensitivity analysis: variation of the position of mixing zone by different values of conduit parameters and conduit-matrix interaction. The subplots on the left are simulations in the conduit, and the subplots on the right are simulations in porous media. The parameter variation from top to bottom are: A) d: conduit diameter; B) hy: hydraulic conductivity in porous medium; C) ex: exchange permeability.

The friction factor is adjusted from 50% to 150% of the originally used value to evaluate its effect on salinity simulations in both the conduit and porous medium (Figure 3.5B). Seawater intrudes further landward through the conduits with smaller friction factor due to the faster groundwater velocity in a smooth pipe. Friction factor of the conduit also significantly affects the positions of mixing zone in porous medium. Overall, the friction factor on the simulation results is less important than the conduit diameter, but with a similar pattern.

To investigate the influence of conduit-matrix interaction on salinity simulation, the exchange permeability or pipe wall conductivity is adjusted from 5000 ft/day to 10000 ft/day with an interval of 500 ft/day (Figure 3.5C). The salinity simulations in both the conduit and porous medium are insensitive and vary trivially to the variation of parameter, probably due to the relatively stable groundwater flow and solute transport between the two domains. The exchanges on the pipe wall are not significant, since the difference of equivalent freshwater heads between the conduit and porous medium is relatively small in the horizontal case of the VDFST-CFP model. However, the exchange permeability could become an important parameter in other studies when conduit-matrix interaction is significant and the head differences between two domains are large.

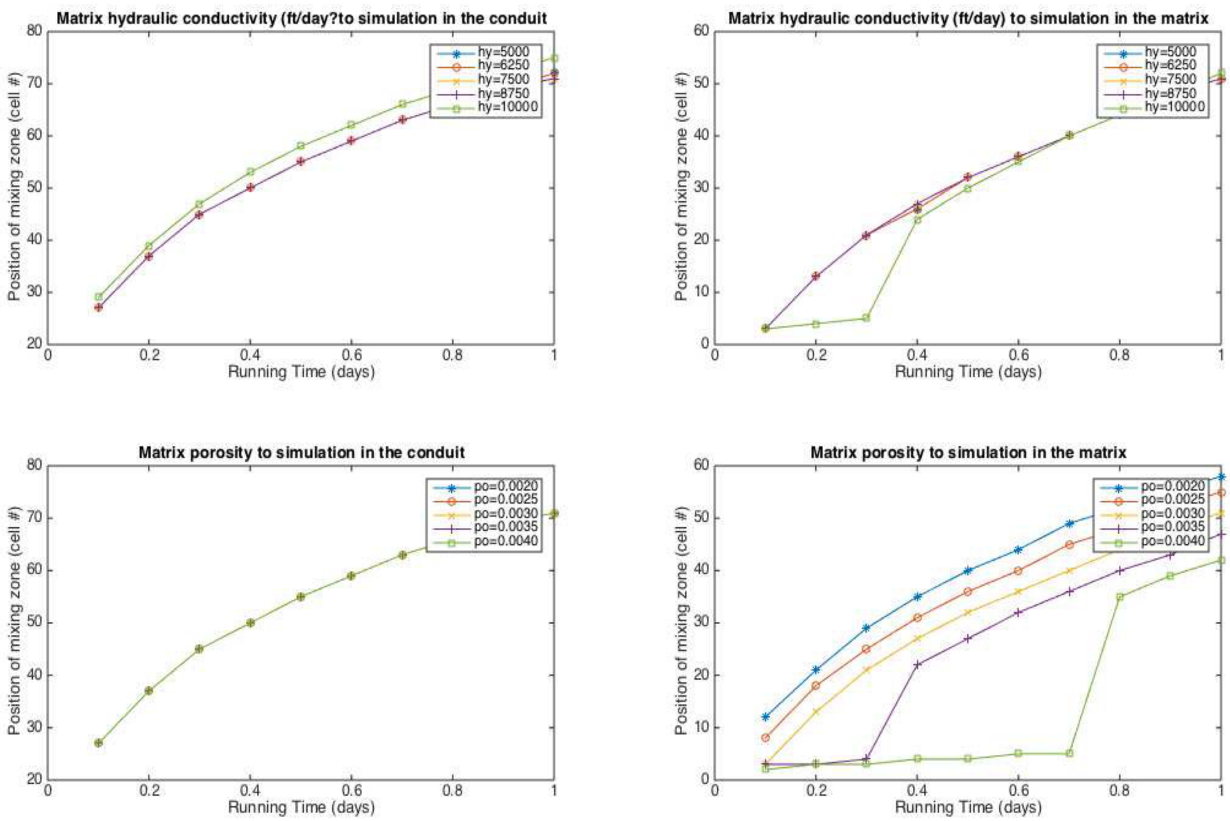

Figure 3.6. Parameter sensitivity analysis: variation of the position of mixing zone by different values of matrix parameters. The subplots on the left are simulations in the conduit, and the subplots on the right are simulations in porous media. The parameter variation from top to bottom are: A) hy: matrix hydraulic conductivity; B) po: porosity.

For the sensitivity study of matrix hydraulic conductivity on solute transport, its value is adjusted from 5000 ft/day to 10000 ft/day with an interval of 500 ft/day, and the conduit-matrix exchange permeability on the conduit wall is set as equal to the matrix conductivity. The position of mixing zone moves further landward in the conduit but backward in the porous medium with higher matrix hydraulic conductivity values (Figure 3.6A). Because of the more rapid seepage velocity in porous medium and more dynamic exchange with the increasing values of matrix conductivity and conduit wall permeability, groundwater flow and solute transport in the conduit are accelerated and result in further landward high-density seawater movement. Salinity plume extends broadly and moves quickly away from the conduit in the matrix domain with large values of hydraulic conductivity, but results in the relatively backward position of mixing zone in the porous medium surrounding the conduit due to the faster groundwater seepage and higher dispersion effects in the porous medium. Similar to what is shown in the sensitivity study of conduit diameter, the numerical instability of the VDFST-CFP model could cause fingering phenomenon around the mixing zone position in the porous medium.

Matrix porosity is another parameter determining groundwater flow and solute transport. Its value is changed that from 0.02 to 0.04 with an interval of 0.005 in the sensitivity study. Variation of the matrix porosity does not significantly affect the seawater movement in the conduit, but greatly influences the salinity distribution in the porous medium (Figure 3.6B). The salt plume of high salinity is concentrated near the conduit network with relatively slower groundwater seepage velocity in the porous medium; therefore, the position of mixing zone moves further landward with lower porosity. However, porosity is not as important as hydraulic conductivity especially in the porous medium, since the matrix hydraulic conductivity affects the salinity simulation not only in the porous medium but also in the conduit system.

3.4 Discussion of the VDFST-CFP model

The uncertainties of the newly developed VDFST-CFP simulation are originated from the concepts of discrete-continuum model, numerical methods, governing equations and code structures. The uncertainty sources are discussed in details below.

The concept of hybrid discrete-continuum numerical model requires that the conduit diameter must be significantly smaller than the size of matrix cell in the finite difference grid where conduit nodes are located. The storage and volume of the conduit system are negligible comparing with the size of matrix grid, in order to keep the balance of water budget and guarantee numerical stability in the discrete-continuum coupling modeling system (Shoemaker et al., 2008b; Reimann and Hill, 2009; Reimann et al., 2014). On the other hand, density-dependent vertical flux in the variable-density numerical modeling requires the vertical discretization of spatial domain to be very small for the calculation accuracy (Werner et al., 2013). In the application of variable-density numerical SEAWAT model, Guo and Langevin (2002) pointed out that a very high grid resolution in the vertical direction is often required to represent the complex flow pattern with high concentration gradients for density-dependent flow and solute transport simulation. Generally speaking, the thickness of a grid cell needs to be small to guarantee the simulation accuracy for a density-dependent vertical flux. Meanwhile, the conduit diameter needs to be significant smaller than the size of grid cell to satisfy the concept of a hybrid discrete-continuum numerical model. However, the conduit diameters sometimes can be extremely large in the field, especially in the horizontal direction. For example, many conduit diameters are about 20 ft to 30 ft in the Upper Floridan Aquifer (UPA) of Woodville Karst Plain (WKP), north Florida, and some can be as large as 50 ft at the outlet of conduit system (Bush and Johnson, 1988; Gallegos et al., 2013). The total 400 ft thickness of the UPA needs to be discretized as very thin vertical layers, for example, 40 layers with 10 ft thickness of each layer to accurately simulate density-dependent vertical flux. At the same time, the conduit diameter simulated in the discrete-continuum model is required to be even smaller than the thickness of grid cell. Therefore, the balance between a large conduit diameter in the field versus the small size of grid cell and tiny conduit diameter required in the numerical model becomes a difficult problem. Constant density discrete-continuum numerical model does not have this issue, since the vertical discretization is not required to be very small. The entire aquifer can be discretized as only one or two layers in the previous applications of discrete-continuum modeling studies (Xu et al., 2015a; Xu et al., 2015b). Many testing cases for the VDSFT-CFP model suggest that the conduit diameter significantly control the mass balance discrepancy, which dramatically becomes unacceptably large with the increasing ratio of conduit diameter and grid cell size.

The application of numerical method is important to the model uncertainty and accuracy as well. Numerical solution to the advection dispersion equation has a heavy computational demanding, since the spatial first derivative term (advection) and the spatial second derivative term (dispersion and diffusion) are coexisted in the solute transport governing equation for the porous medium (Zheng and Wang, 1999). MT3DMS provides several numerical methods for solving the advection dispersion equation, such as the Eulerian standard finite difference, mixed Eulerian-Lagrangian and third-order TVD (Total Variance Dimishing) method (Zheng and Wang, 1999). In order to keep the numerical implementation and coding structure simple and consistent, a standard finite difference method is used in the VDFST-CFP model to solve the advection dispersion solute transport equation in the porous medium. An oscillation-free solution of upstream weighting scheme is applied to determine the interface concentration of two matrix cells. The solution of variable-density flow field is coupled with the solute transport simulation. However, the solution of advection term is only accurate to the first order by the finite difference method and could lead to significantly numerical dispersion when it applied to advection-dominated problems (Zheng and Wang, 1999). Zheng and Bennett (2002) also pointed out that the application of a standard finite difference method requires the Peclet number, P_e, to be smaller than 4 to guarantee the numerical stability and mass balance, which is defined as,

$$P_e = \frac{|v|L}{D} \leq 4 \qquad 26)$$

where v is the seepage velocity [LT^{-1}]; L is the characteristic length, commonly taken as the grid cell width [L]; and D is the dispersion coefficient [L^2T^{-1}].

Because of the dynamic interaction on the conduit wall and relatively large matrix hydraulic conductivity, the non-laminar conduit flow is able to accelerate the groundwater seepage velocity in the porous medium. Therefore, the VDFST-CFP model becomes an advection-dominated problem in the porous medium that near the conduit, and the Peclet number (P_e) may exceed the maximum value for numerical stability of the finite difference method. In other words, the benchmark cases in this study could be advection-dominated in parts of the porous medium that are close to the conduit system, which results in large truncation error of solute transport simulation. The small grid size and multiple vertical layers of the finite difference discretization are important to reduce the Peclet number and truncation error. Generally speaking, the physical dispersivity should be large enough or the grid spacing is made sufficiently small in the VDFST-CFP models, which significantly increase the computational burden.

The estimation of friction factor in the conduit is another major uncertainty for the calculation of non-laminar groundwater flow rate and conduit nodal head. Friction factor is not only a solely function of the physical characteristics of conduit wall roughness, but also depends on flow velocity and Reynolds number in the conduit. MODFLOW-CFP and CFPv2 uses the Colebrook-White equation (eq. 25) to calculate the friction factor, and then applies Darcy-Weisbach equation to calculate flow rate along the conduit network in each time step.

MODFLOW-CFP provides a better estimation of friction factor and flow rate but significantly increases the computational cost (Shoemaker et al., 2008b). Friction factor is assumed to be constant in the VDFST-CFP model, which is calculated as an estimation of the averaged Reynolds number in the entire conduit system by another numerical model, such as MODFLOW-CFP and CFPv2 model. In other word, the effect of Reynolds number variation on friction factor is assumed to be negligible in the VDFST-CFP model. However, flow velocity and Reynolds number vary along the conduit and affect friction factors in each pipe discretization. The friction factor is overestimated when the actual groundwater flow velocity is higher than the simulation result. Meanwhile, the Reynolds number that used in the calculation of friction factor is underestimated. On the other hand, the friction factor is underestimated when the actual Reynolds number in the conduit is smaller than the estimated average value. In this case, the groundwater flow rate will be overestimated corresponding with the overestimation of Reynolds number.

In the horizontal and vertical benchmark cases, the continuum SEAWAT and MODFLOW/MT3DMS models are used to compare with the discrete-continuum CFPv2/UMT3D model and validate the newly developed VDFST-CFP model. The conduit diameter and friction factor in the discrete-continuum models are calculated to be equivalent as the conduit hydraulic conductivity in the continuum model using the methods introduced in section 5.2.1. Since Darcy equation is still applied in the continuum model with the assumption of linear relationship between specific discharge and hydraulic gradient, Hagen-Poiseuille equation (eq. 21) is applied in a cylindrical conduit with the estimation of friction factor and Reynolds number ($f = 64/Re$) under laminar flow condition. Therefore, the combination of Hagen-Poiseuille equation and Darcy equation yield the equivalent hydraulic conductivity, but its uncertainty for turbulent flow in the conduit is still unknown. Darcy equation is not able to provide an appropriate solution for non-laminar groundwater flow, and significantly overestimates the groundwater flow rate if applied under turbulent flow condition. The friction factor and Reynolds number under a turbulent flow condition can be approximated using the Blasius estimation ($f = 0.316 \times {R_e}^{-1/4}$) or the Colebrook-White equation (eq. 25), but is significantly underestimated by $f = 64/Re$ that used for laminar condition. However, neither the Blasius estimation nor the Colebrook-White equation can be combined with non-laminar Darcy-Weisbash equation to generate a simple relationship between equivalent turbulent hydraulic conductivity and conduit diameter without flow velocity or Reynolds number. Although friction factor is not a solely function of conduit wall roughness, equivalent hydraulic conductivity is a physical parameter of the conduit system. Therefore, the comparison of the numerical model results in the benchmark study assumes that the equivalent hydraulic conductivity under turbulent flow condition is nearly the same as that under the laminar flow condition. The assumption is reasonable since the effects of overestimation of flow rate and underestimation of friction factor would offset more or less under turbulent flow condition, although the quantitative uncertainty of the approximation is hard to know.

There are two important convergence criteria for numerical methods in the VDFST-CFP model. The convergence criterion for the Newton-Raphson method determines the numbers of iteration loops for conduit flow solution, also controls the calculation accuracy for head and flow rate in the conduit system using the density-dependent Darcy-Weisbach equation. The convergence criteria of implicit coupling approach include the maximum values of head and density differences from the previous loop in the conduit and porous medium, respectively. In addition, the temporal discretization of time step size and the spatial discretization of grid cell size also significantly control the numerical stability, simulation accuracy and mass balance.

CHAPTER FOUR

NUMERICAL STUDY OF GROUNDWATER FLOW CYCLING CONTROLLED BY SEAWATER/FRESHWATER INTERACTION IN THE WOODVILLE KARST PLAIN (WKP) USING CFPV2

In this chapter, CFPv2 is applied instead of MODFLOW-CFP to simulate the seawater and groundwater interaction processes, since MODFLOW-CFP is not applicable to a time dependent boundary condition in the numerical model. The CFPv2 model is setup to numerically represent the conceptual model of the groundwater flow cycling in the Upper Floridan Aquifer (UPA) of Woodville Karst Plain (WKP), north Florida, USA. The modeling study focuses on the impacts of precipitation and rainwater recharges, hydraulic gradient variation and seawater intrusion through the conduit system on discharges of springs and groundwater flow cycling.

4.1 Governing Equations

4.1.1 Hybrid Discrete-continuum Flow Modeling

According to Darcy equation and mass conservation, the three-dimensional continuum equation for groundwater flow in a porous medium including source/sink term is described as follows:

$$\frac{\partial}{\partial x}\left(K_{xx}\frac{\partial h}{\partial x}\right)+\frac{\partial}{\partial y}\left(K_{yy}\frac{\partial h}{\partial y}\right)+\frac{\partial}{\partial z}\left(K_{zz}\frac{\partial h}{\partial z}\right)\pm W = S_s\left(\frac{\partial h}{\partial t}\right) \tag{27)}$$

where K_{xx}, K_{yy} and K_{zz} are values for hydraulic conductivity [LT^{-1}] along the x, y, z axis, respectively; h is the hydraulic head [L]; W is the volumetric flux per unit volume [T^{-1}] as sink/source term; S_s is the specific storage [L^{-1}].

Darcy equation is only appropriate for laminar flow with Reynolds number less than 10 but not for non-laminar or turbulent flow in the conduit (Bear, 2013). Therefore, Darcy-Weisbach equation is used to simulate groundwater flow in the high permeable karst conduit networks in which a conduit is conceptualized as a pipe,

$$\Delta h = h_L = f\frac{\Delta l}{d}\frac{V^2}{2g} \tag{28)}$$

where Δh or h_L is the head loss [L] measured along the pipe length Δl [L]; f is the friction factor [dimensionless]; d is the pipe diameter [L]; V is the mean velocity [LT^{-1}]; g is the gravitational acceleration constant [LT^{-2}].

Darcy-Weisbach equation can be reformulated to solve for volumetric flow rate in the conduit networks by MODFLOW-CFP (Shoemaker et al., 2008b) and CFPv2 (Reimann et al., 2013). MODFLOW-CFP and CFPv2 are able to solve non-saturated pipe flow but not applied in this study, because all layers are assumed as confined aquifers and conduits are fully saturated. Caves and conduits are defined as a discrete pipe network consisting of cylindrical tubes and nodes within the cells of grid defined in the model. The advective exchanges between porous media and conduit nodes are assumed to be linear with head difference as follow,

$$Q_{ex} = \alpha_{j,i,k}(h_n - h_{j,i,k}) \qquad 29)$$

where Q_{ex} is the volumetric flow exchange rate [L^{3}T^{-1}]; $\alpha_{j,i,k}$ is the pipe conductance at MODFLOW cell j, i, k [L^{2}T^{-1}]; h_n is the head [L] at pipe node n located at the center of the MODFLOW cell; and $h_{j,i,k}$ is the head [L] in the encompassing MODFLOW cell j, i, k.

4.1.2 Equivalent Freshwater Head at Spring Creek Springs

A schematic diagram of the submarine caves system at Spring Creek Springs is presented in Figure 4.1. In the mixing zone of freshwater/seawater in a coastal aquifer, hydraulic head and seawater pressure are dependent on salinity or density. To calculate spatial hydraulic gradient and flow field of seawater mixing, the concept of equivalent freshwater head is introduced to represent seawater pressure in the submarine caves at Spring Creek Springs. The equivalent freshwater head at Spring Creek Springs is calculated using the measured salinity data in each stress period, which is important to determine whether the submarine cave is flowing freshwater or siphoning seawater. A small change of seawater pressure at Spring Creek Springs would significantly affect groundwater discharge at Wakulla Spring, because the flat topography and small hydraulic gradient in the study area. If the submarine caves contains only freshwater while Spring Creek Springs are discharging freshwater such as phase 2 and 3 of the conceptual model, the equivalent freshwater head would be equal to the tide height or sea level. On the other hand, a direct use of spring altitude as equivalent freshwater head would be incorrect if the submarine caves are filled with higher density salt water while Spring Creek Springs are siphoning. The equivalent freshwater head is calculated by Ghyben-Herzberg equation,

$$h_f = \frac{\rho_s - \rho_f}{\rho_f} z \quad 30)$$

where z [L] is the height of the vertical column of salt water, or the depth of mixing interface below sea level in the conduits; ρ_f [ML^{-3}] is the density of freshwater; ρ_s [ML^{-3}] is the density of mixing seawater; h_f[L] is the equivalent freshwater head, which is also the height of freshwater rise above the top of the salt water in a static condition.

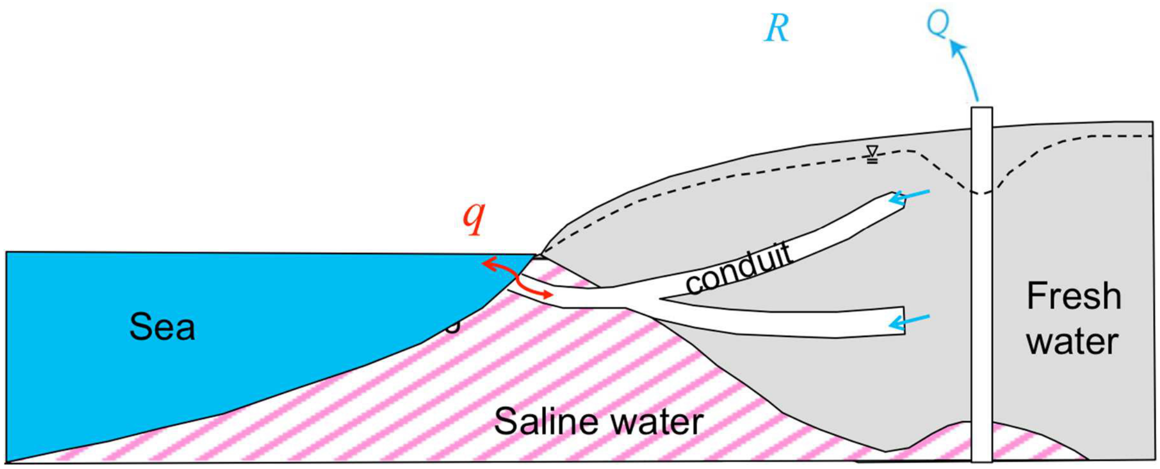

Figure 4.1. Schematic cross section of a coastal karst aquifer with conduit networks and submarine spring (Spring Creek Springs) opening to the sea. Flow direction q would be seaward when sea level drops, pumping rate Q is low and precipitation recharge R is large; however, reversal occurs when sea level rises, pumping rate Q is high or precipitation recharge R is small.

Seawater density ρ_s is calculated by the measured salinity using the equation that correlates fluid density and solute concentration (Langevin et al., 2003):

$$\rho_s = \rho_f + \alpha \times s \quad 31)$$

where $\alpha = \partial\rho/\partial s$ [dimensionless] is the change rate of density with salinity, slope of the linear equation of state that relates solute concentration to fluid density; s [ML^{-3}] is the salinity of mixing seawater.

In this study, salinity data are converted from the measured electrical conductivities. The height of the vertical column of seawater is assumed as nearly 300 ft deep during phase 1 in the conduit connecting to Spring Creek Springs, based on the assumption that the depth of Spring Creek Springs cave is almost same as Wakulla Spring conduit networks, where has been explored by cave divers. Meanwhile, the depth of seawater/freshwater mixing zone is also 300 ft in the conduit at the Spring Creek Springs during phase 1. Equivalent freshwater head at Spring

Creek Springs in phase 1 is calculated as 7.5 ft above sea level by the Ghyben-Herzberg equation. The equivalent fresh water head proportionally decreases if the caves are filled with a mixture of freshwater and seawater. For example, if the freshwater and seawater mixture is half-half, then the equivalent fresh water head would be 3.75 ft; if the freshwater is dominated in the cave as in phase 2 and 3 conditions, the equivalent freshwater head should be equal to sea level or tidal stage.

4.2 Model Implementations

4.2.1 Conceptual Model of Groundwater Flow Cycling

Based on the discharges of springs, rainfall recharges and salinity at Spring Creek Springs in the WKP from June 2007 to June 2010, Davis and Verdi (2014) proposed a conceptual model of three repeating phases for the groundwater interactions among Spring Creek Springs, Wakulla Spring and Lost Creek. During an extended low rainfall period of phase 1, seawater backflows and siphons into the conduit system at Spring Creek Springs with high salinity and very low freshwater discharge. Freshwater discharge is blocked at Spring Creek Springs by higher seawater pressure and diverted to Wakulla Spring. Phase 1 switches to phase 2 after a heavy rainfall event, results in temporarily high inflows from sinkholes to groundwater that purge seawater out of the Spring Creek Springs submarine conduits. Discharges of both the inland and submarine springs increase dramatically in this phase, especially at Spring Creek Springs. Phase 2 transforms to phase 3 when a low rainfall period returns. Surface rainwater recharge returns to base flow condition, but salinity at the submarine springs still remains low level with large quantity of freshwater discharge coming from groundwater storage.

4.2.2 Spatial and Temporal Numerical Discretization

In previous studies, a long-term (1968-2018) MODFLOW model was developed for groundwater flow in the Woodville Karst Plain (Davis et al., 2010). Afterwards, the model was modified to a discrete-continuum MODFLOW-CFP model in Gallegos et al. (2013). The CFPv2 groundwater flow model in this study is based on the previous long-term MODFLOW and MODFLOW-CFP models with the same spatial domain. The model domain consists of two confined aquifer layers because of the near absence of the overlying water table aquifer and Hawthorn clays, and the conduit system is assumed at the second layer except the major sinkholes and springs on the surface, such as Spring Creek Springs and Wakulla Spring (Figure 4.2). However, the temporal period of simulation is reduced to three years from June 2007 to June 2010. The numerical models in Davis et al. (2010) and Gallegos et al. (2013) have 58 stress periods with nearly one year for each. In this study, there are 156 stress periods in the three-year simulation, and the length of each stress period is seven days (one week). The temporal discretization is much shorter than previous models and generates simulations with higher resolution. The spatial discretization of grid cells, boundary conditions and hydraulic parameters are almost the same as previous MODFLOW-CFP model by Gallegos et al. (2013) in Figure 4.3. The southeastern boundary of the numerical model is assumed as no-flow because it follows approximately a groundwater flow line as delineated by the field measurements. Other boundaries are assigned as constant head conditions, which are determined by a regional groundwater flow model in previous works (Davis and Katz, 2007). The initial and boundary conditions on the shoreline are based on time-variable equivalent freshwater head at Spring Creek Springs, which has been explained in part 3.1.2.

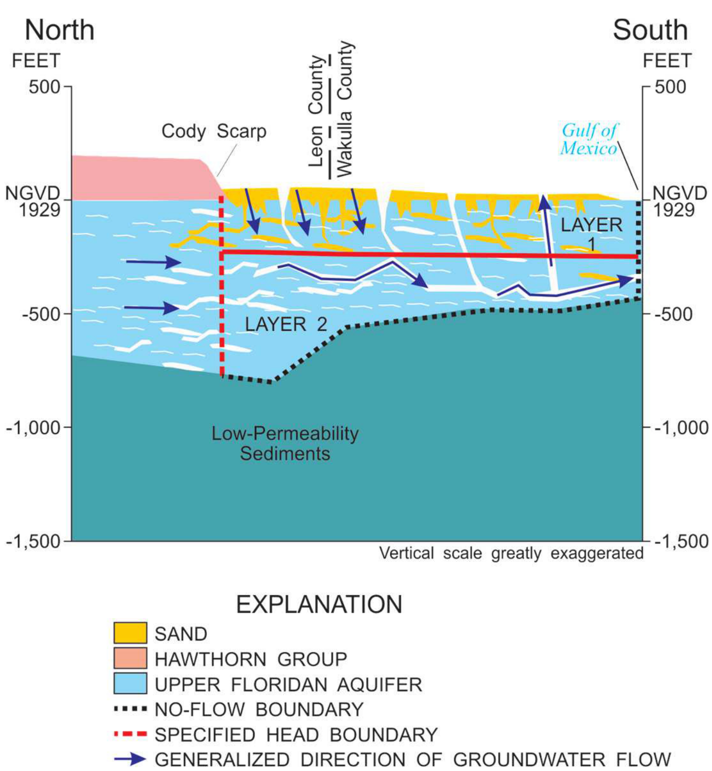

Figure 4.2. Generalized geological cross section in Woodville Karst Plain and model layers. Modified from Davis et al. (2010).

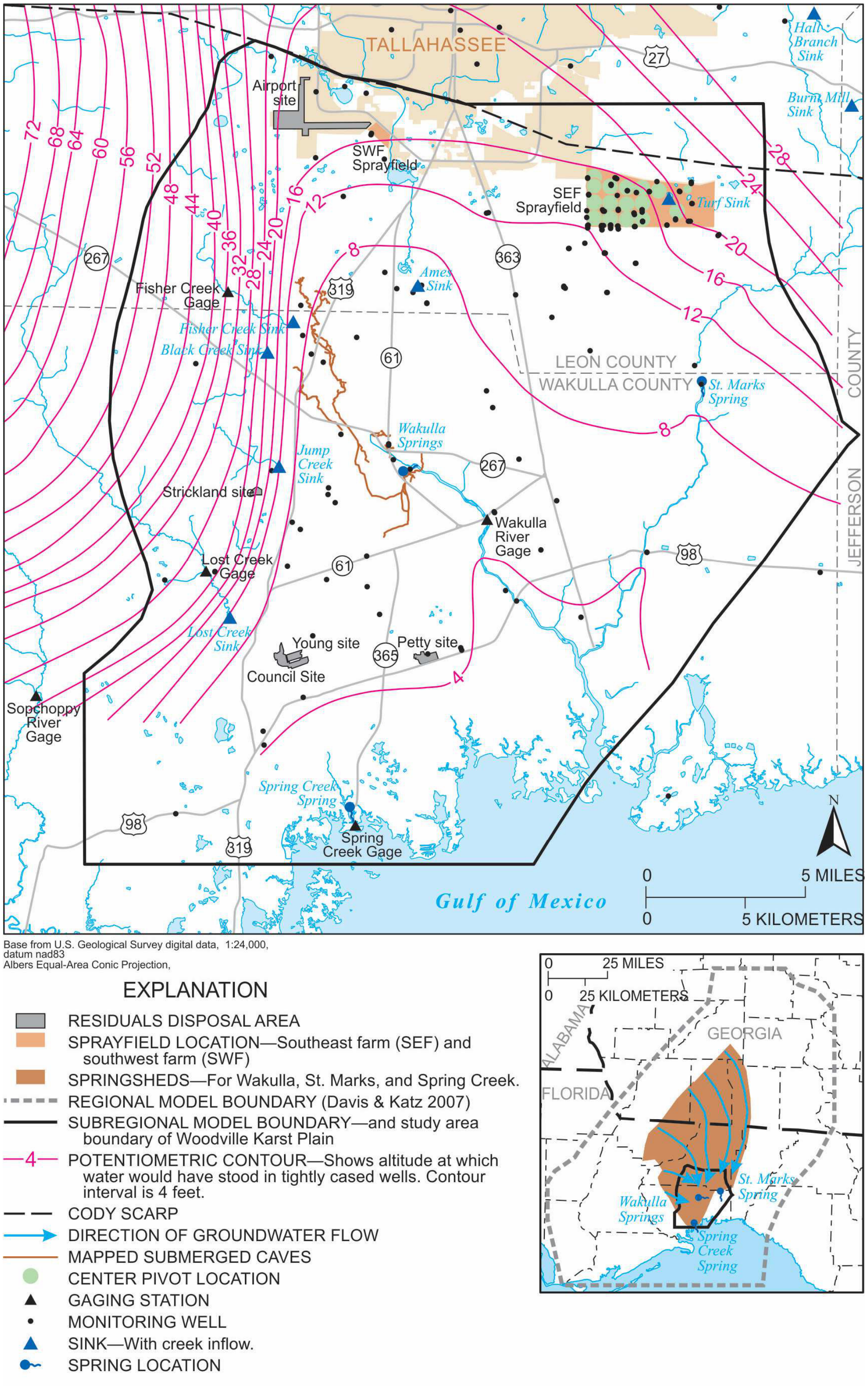

Figure 4.3. Sub-regional model boundary of the Woodville Karst Plain. Modified from Davis et al. (2010).

4.2.3 Tidal Stage

The variation of tide level during the simulation period is used to simulate the discharges at two major springs, Wakulla Spring and Spring Creek Springs. The difference of daily low and high tide heights ranges from 1.8 to 3.0 ft, but is not considered in this study because the length of each stress period is one week, and daily tidal changes are internal variation within each stress period. According to the long-term tide height observation by the USGS gage at Spring Creek Springs, average daily tide height level in summer is 0.8 ~ 1.2 ft above NAVD88 (North American Vertical Datum), but could be approximate -0.3 ~ 0.1 ft in winter time. The time-variable tide levels as well as measured sea levels from June 2007 to June 2010 are applied in the numerical modeling to calculate equivalent freshwater heads at Spring Creek Springs. Simulated discharge would be underestimated at Wakulla Spring and overestimated at Spring Creek Springs, if sea level is assumed constant as 0.0 ft all year around in the numerical model, because the actual tide level is slightly higher than 0.0 ft above NAVD88 at Spring Creek Springs, especially in summer time. Calibrated model matched better with the field observations than original simulation without adjustment of tide level variation.

4.2.4 Recharge and Evapotranspiration

The net recharges coming from creeks and rainfall are used to simulate the discharges at two major springs, Wakulla Spring and Spring Creek Springs. The consecutive precipitation data measured at Tallahassee Regional Airport station are used to calculate recharges in the north part of WKP, and the data from the other two stations at Crawfordville (St. Marks 9.2 W FL US) and Spring Creek Springs (St. Marks 8.2 SW FL US) are used for the middle and south parts of the study area, respectively.

Generally speaking, net recharge to an aquifer is equal to the difference of precipitation and evapotranspiration. The potential evapotranspiration data are calculated by USGS Florida Water Science Center, and then transformed to real evapotranspiration by an empirical correction factor of 0.7 (Farnsworth and Thompson, 1983). The temporal discretization of each stress period in the numerical model was as long as one week; therefore, net recharge could be underestimated during a hurricane or tropical storm, because huge amount of rainwater in a short period of time would be averaged and reduced by evapotranspiration in the entire stress period. For example, the net recharge of an instant rainstorm should be higher than that of an extended light rain for a long period of time with the same total precipitations, especially during the summer time when evapotranspiration level is high.

Surface water recharge at Lost Creek directly flows into the subsurface conduit networks, which can divert to either Wakulla Spring or Spring Creek Springs, depending on the equivalent freshwater head at Spring Creek Springs. In addition, Fisher Sink, Black Sink and Ames Sink are locations of point source recharge to the conduit system as well, but mostly flow to Wakulla Spring through the subsurface tunnels, especially during low rainfall periods. Some surface creeks including Fisher Creek and Lost Creek have large areas of runoff catchments that beyond the spatial domain of the numerical model. Since the soils and sands on the surface of the Woodville Karst Plain are extremely loose, most rainwater could directly infiltrate into aquifer and become groundwater very quickly, especially at the south of the Cody Scarp without the impermeable Hawthorn clay formation on the surface. In other words, point source recharges to conduit systems from surface creeks at sinkholes are only small part of total recharges in this study. Regional recharge from the northern boundary is more significant and simulated as constant head boundary conditions in the numerical model.

4.3 Simulation Results

Davis and Verdi (2014) proposed a conceptual model that describes the groundwater flow cycling and hydrological interaction between Spring Creek Springs and Wakulla Spring. The effects of precipitation and recharge flow rate at Lost Creek Sink were also introduced and analyzed in Davis and Verdi (2014). Time-variable recharges and seawater pressure in terms of equivalent freshwater head at Spring Creek Springs are the most important factors to groundwater interaction. Generally speaking, the numerical simulation match reasonably well with the discharge measurements at two springs. The correlation coefficients between simulation results and field measurements of spring discharges are 0.891 and 0.866 at Spring Creeks Springs and Wakulla Spring, respectively.

The three-year groundwater flow cycling was divided as 12 periods, basically according to the salinity at Spring Creek Springs and discharges of the two springs. The dates and periods of each phase in the conceptual model were documented in Table 4.1 (Davis and Verdi, 2014), as well as the averaged measured and simulated discharges at two major springs in each period. Hydrological conditions such as groundwater discharge, salinity at Spring Creek Springs, precipitation and surface water recharges were relatively stable in one period, while a new period began when those conditions changed.

4.3.1 Phase 1

Phase 1 occurs during an extended low rainfall condition for several weeks or even longer (Davis and Verdi, 2014). Surface creek discharges decrease to baseflow conditions due to low precipitation in the study area during this phase. Seawater moves landward and backflows into the aquifer through the caves of Spring Creek Springs, blocks most of freshwater discharge due to higher equivalent freshwater head. A slight rises of groundwater levels are found in the sinkholes and karst windows when freshwater discharge is blocked at the submarine caves during phase 1, along with the rises of the equivalent freshwater head at Spring Creek Springs (Dyer, 2015). The equivalent freshwater head at Spring Creek Springs is 7.5 ft when the submarine caves are filled with pure seawater, but is calculated by the measured salinity at Spring Creek Springs in the numerical model. The river stage or hydraulic head at Wakulla Spring is only 5.0 ft, which means that groundwater would prefer to discharge at the inland Wakulla Spring rather than Spring Creek Springs due to reversal hydraulic gradient in this phase. Wakulla Spring is the major discharge spring in the entire WKP aquifer; on the other hand, very low freshwater discharge is incapable to purge seawater out of the submarine caves and dilute salinity at Spring Creek Springs.

Phase 1 includes the periods 1, 4, 8 and 10 of the 12 periods in the three-year modeling study and occupies the longest time periods. The first period lasts almost eight months from June 2007 to February 2008, which is also the longest period of the conceptual model due to extended low rainfall period. Measured freshwater discharge of Spring Creek Springs was nearly zero or even negative in this phase, which means that Spring Creek Springs stopped flowing and began siphoning when seawater filled and intruded into the submarine conduits (Figure 4.4). Wakulla Spring was the major groundwater discharge spot of the entire WKP aquifer with an average flow rate of 700 - 800 ft^3/s in both measurement and modeling simulation during phase 1. Flow rate at Lost Creek remains baseflow condition, and its contribution to aquifer as well as groundwater flow cycling is negligible.

Table 4.1. Classification of flow periods, phases in the conceptual model, measured and simulated flow rates (SC: Spring Creek Springs; WK: Wakulla Spring; flow rates are in cubic feet per second (ft^3/s), negative values at Spring Creeks Springs indicate reverse flow).

Period	Start Date	End Date	Measured flow rate (SC)	Simulated flow rate (SC)	Measured flow rate (WK)	Simulated flow rate (WK)	Conceptual model phase
1	06/25/2007	02/19/2008	-2	184	707	602	1
2	02/20/2008	03/25/2008	951	925	693	532	2
3	03/26/2008	05/19/2008	468	336	466	393	3
4	05/20/2008	08/19/2008	-2	131	760	575	1
5	08/20/2008	09/30/2008	644	1023	934	704	2
6	10/01/2008	03/26/2009	443	395	483	412	3
7	03/27/2009	06/21/2009	875	861	691	533	2
8	06/22/2009	08/26/2009	-10	115	830	680	1
9	08/27/2009	10/23/2009	445	413	636	420	3
10	10/24/2009	12/02/2009	-224	100	698	546	1
11	12/03/2009	04/06/2010	1072	979	832	521	2
12	04/07/2010	06/22/2010	642	483	406	393	3

Generally speaking, simulated groundwater discharges are overestimated at Spring Creek Springs but are underestimated at Wakulla Spring, and the reasons will be explained in the discussion section. Discharge at Wakulla Spring is nearly 20% underestimated by simulation at the beginning of period 1 due to the inaccurate initial conditions, however, does not affect the simulation results in the later periods. Simulated discharges at Spring Creek Springs have relatively larger oscillations than measurements, but remain very low amount comparing with other phases in the model.

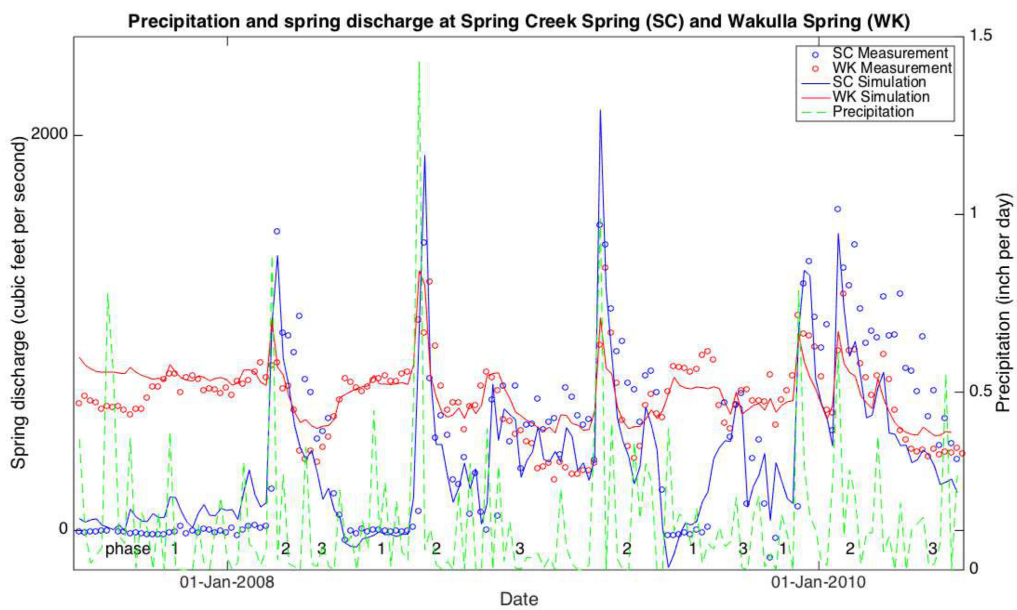

Figure 4.4. Measured and simulated results of discharges at Wakulla Spring and Spring Creek Springs, from June 2007 to June 2010, as well as precipitation.

4.3.2 Phase 2

A high precipitation event with large amount of rainfall occurs at the end of phase 1 or the beginning of phase 2, sometimes a tropical storm or hurricane. Phase 2 is always the shortest phase in the conceptual model of groundwater flow cycling, which only lasts a few weeks but can be extended if there is an additional rainfall. The abundant rainfall in short period of time leads to high surface runoffs in creeks, then flows into local sinkholes and becomes groundwater in the UFA. Lost Creek is the largest and most important creek in the study area that affects groundwater flow cycling, while its water flows and discharges through subsurface conduits north to Wakulla Spring and/or south to Spring Creek Springs. Fisher, Black, Jump and Ames

Sinks in the Wakulla Springshed also receive large amount of runoff from the north part of the WKP. Rainwater recharges raise water level at the entire aquifer and sinkholes with significant groundwater flow into the subsurface conduit networks, purge seawater out of submarine caves and dilute salinity at Spring Creek Springs. Freshwater is filled with Spring Creek Springs caves during this phase, in which great portion of freshwater comes from Lost Creek. The equivalent freshwater head is no longer 7.5 ft as phase 1 and needs to be re-calculated by the measured low salinity. When the entire caves are filled with freshwater, the equivalent freshwater head at Spring Creek Springs decreases to the altitude of sea level or tide level. Therefore, groundwater in the aquifer would prefer to discharge at Spring Creek Springs instead of the inland Wakulla Spring with seaward hydraulic gradient. As a result, freshwater discharges at Spring Creek Spring increased more dramatically than those at Wakulla Spring in phase 2.

Periods 2, 5, 7 and 11 are phase 2 in the conceptual model proposed by Davis and Verdi (2014). Discharges at both Wakulla Spring and Spring Creek Springs increase dramatically and reach the highest levels during this phase. The average measured discharges in this phase were 910 ft^3/s and 850 ft^3/s at Spring Creek Springs and Wakulla Spring, respectively. The peaks of Spring Creek Springs discharges are more significant than Wakulla Spring, could be 1500 ft^3/s in period 2 and 11, and even higher than 2000 ft^3/s in period 5 and 7, which are the most remarkable characteristics in the groundwater flow cycling conceptual model as well as numerical simulation. On the other hand, discharge at Wakulla Spring only slightly increased at the beginnings of period 2 and 11, but greatly increased at periods 5 and 7 due to higher rainfall recharges. Simulated results at Spring Creek Springs and Wakulla Spring match very well with measurements, except the peaks of discharge at Spring Creek Springs slightly overestimated the measurements at period 5 and 7. In general, rainwater recharges and surface runoff are dominated in the entire aquifer and discharge at both two springs during this phase.

4.3.3 Phase 3

After a high rainfall event in phase 2, the water cycling process moves to phase 3 when low rainfall condition returns. Lost Creek and other surface creeks return to baseflow condition, but Spring Creek Springs caves are still discharging large quantity of freshwater. As a result, equivalent freshwater head remains at or near the actual spring pool elevation of sea level because salinity is still very low at the submarine spring. In this scenario, discharges at both

Spring Creek Springs and Wakulla Spring come from the abundant groundwater storage in the UFA. Meanwhile, the groundwater level slowly drops with the reduction of storage during this phase. Phase 3 can last for as long as months but depends on groundwater storage, previous total precipitation and additional recharges. Extended low rainfall condition allows seawater once again siphons into the Spring Creek Springs caves when freshwater discharge is significantly decreased, then phase 3 terminates and returns to phase 1.

The length of phase 3 varies from six weeks as in periods 3 and 9, and can be as long as three months in period 6. Discharge at Spring Creek Springs decreases to almost half comparing with that in phase 2, but still much higher than that in phase 1. Discharge at Wakulla Spring decreases about 30% from that in phase 2 and can be even lower than that in phase 1. At this phase, the magnitudes of discharges at two springs are relatively similar. After streams return to baseflow conditions in phase 3, freshwater discharge at Spring Creek Springs remains a high flow rate of 500 ft^3/s in averaged for weeks to months; however, discharge at Wakulla Spring decreases to the lowest rate of 500 ft^3/s. Numerical simulation results match very well with the measurements of discharge at Spring Creek Spring, except for a nearly 15-20% underestimation of discharge in the last period of phase 3. Simulated discharge at Wakulla Spring is generally slightly lower, which may be due to the missing sources of recharge or underestimation of surface creek baseflows. In general, simulated results reasonably match with field measurements.

4.3.4 Prediction of Sea Level Rise

Sea level rise in the past 100 years has been verified by IPCC (2007) in a global scale, and has been also observed in the local monitoring gages by Davis and Katz (2007); Davis et al. (2010). IPCC (2007) estimated the global sea level is going to keep rising nearly 3 ft if half of the ice sheet on Antarctic and Greenland is melted at the end of this century. As a prediction, the effects of rising sea level on the groundwater flow cycling and discharges of springs in the WKP aquifer are quantitatively evaluated in this study. The discharges at Wakulla Spring and Spring Creek Springs are evaluated under the condition of 3.0 ft sea level rise by straightforwardly increasing the equivalent freshwater head at the submarine spring on the shore, but all other hydrological conditions remain the same as the previous calibrated model. It should be pointed out this approach is only a simplified prediction because other conditions and assumptions may also change with rising sea level.

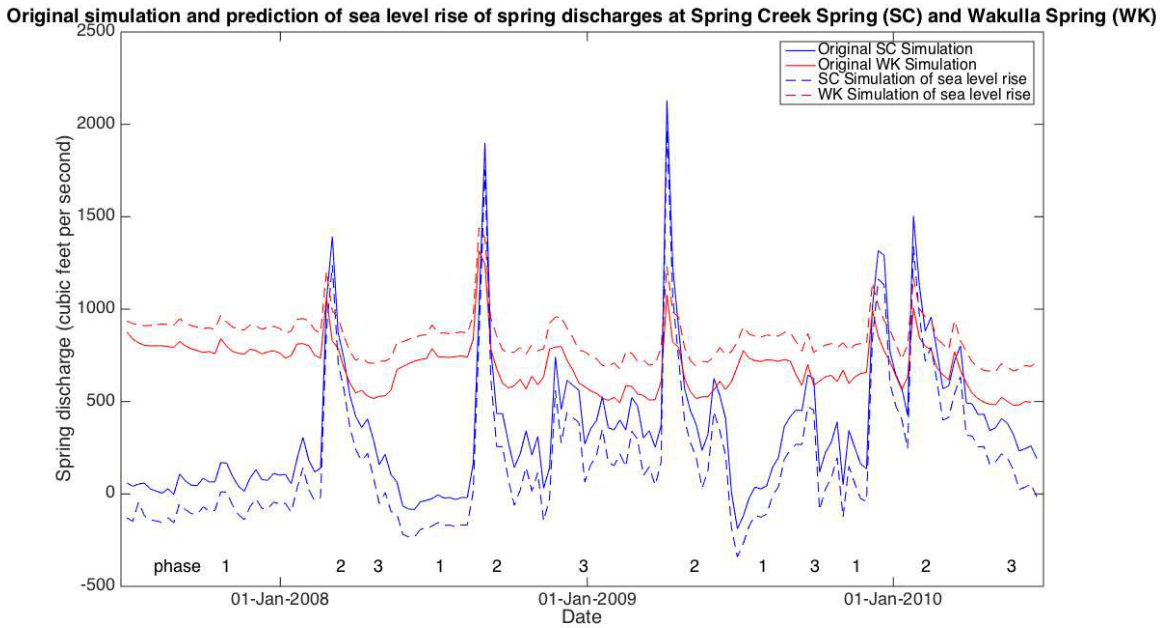

Figure 4.5. The original (calibrated) simulation results and the prediction of rising sea level of the discharges at Wakulla Spring and Spring Creek Springs, from June 2007 to June 2010.

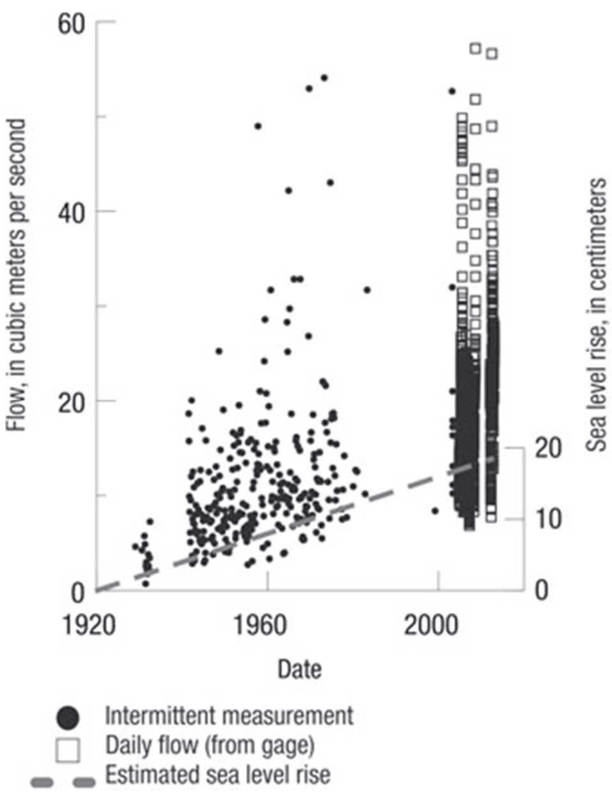

Figure 4.6. Flow from Wakulla Spring from 1930 to 2010 and estimated sea level rise from 1920 to 2020. Modified from Davis and Verdi (2014).

The simulation results are presented in Figure 4.5. As shown in the figure, discharge of springs will significantly increase at Wakulla Spring and decrease at Spring Creek Springs correspondingly when sea level rises 3.0 ft. Because of the rising sea level, seawater pressure and equivalent freshwater head at the caves of submarine springs rise simultaneously to block freshwater discharge from the Spring Creek springs, and groundwater will prefer to discharge at Wakulla Spring. The 3.0 ft rising sea level results in nearly 200 ft^3/s increase of freshwater discharge at Wakulla Spring, as well as 200 ft^3/s decrease at Spring Creek Springs by assuming the rainfall and recharges do not change in the numerical model. The effects of sea level rise on the peaks of discharges at both springs in phase 2 are not as significant as those in phases 1 and 3. Water levels in the sinkholes and potentiometric surface in the aquifer rise significantly after a high rainfall event, and then the magnitude of seaward hydraulic gradient increases dramatically along the conduit networks at the same time. Therefore, the differences of hydraulic gradient and discharges at both springs between the calibrated model and sea level rise case are small. On the other hand, the tidal stage rises as high as 4.0 ft if the high precipitation event in phase 2 is a tropical storm or hurricane. But generally speaking, higher tide level in terms of higher equivalent freshwater head would significantly reduce the discharge at Spring Creek Springs. The prediction results by numerical model have also been verified by Zervas (2001) and Davis and Verdi (2014), which reported the increasing discharge at Wakulla Spring from 1930 to 2010 along with the rising sea level in the Gulf of Mexico (Figure 4.5).

4.4 Discussion

Numerical CFPv2 groundwater modeling in this study provides a quantitative description of groundwater flow cycling and simulates the discharges at Spring Creek Springs and Wakulla Spring from June 2007 to June 2010, based on the three-phase conceptual model for groundwater interaction in the WKP (Davis and Verdi, 2014). Darcy equation in the MODFLOW model is appropriate to simulate groundwater flow in porous medium but no longer applicable in a karst aquifer with conduits, since groundwater flow could be non-laminar even turbulent in the conduit. The coupled discrete-continuum models MODFLOW-CFP and CFPv2 solve non-laminar flow in conduits and darcian flow in porous medium simultaneously, and provide more accurate estimation of the conduit networks effects on groundwater flow field in a karst aquifer. The calculation of equivalent freshwater head at Spring Creek Springs quantitatively represents the seawater pressure at the submarine spring and coastal conduit system.

The difference between simulations and measurements of discharge at Wakulla Spring is larger than that at Spring Creek Springs, especially in phase 3 in which simulation results are generally underestimated comparing with measurements. There are several uncertain factors for the numerical model. Firstly, it is difficult to guarantee the data quality and accuracy for all measurements. Most field measurements including the discharges of springs and water level are classified as fair quality, which means the error can be ±8% of the real values. Therefore, the measurement errors could lead to significant simulation error. Secondly, the temporal discretization of numerical model is set as seven days (one week) in each stress period, which is much shorter than one-year stress period used in the previous long-term model (Davis et al., 2010; Gallegos et al., 2013), but is still too long comparing with the daily or hourly measurements of rainfall, surface recharges and discharges of springs. However, it is not realistic to apply daily stress period in the numerical model due to the limit of computational capacity. The average of measurements in each stress period could cause significant error in the numerical simulation. For example, an instant heavy rainfall event is averaged in the seven-day stress period, and the peaks of springs' discharges could be underestimated and real evapotranspiration could be overestimated. Thirdly, the estimation of equivalent freshwater head at Spring Creek Springs is another possible error, which is calculated by Ghyben-Herzberg equation based on the assumption that the depths of Spring Creek Springs caves are nearly 300 ft. However, the exact cave depths are unknown and also hardly explored. The depth of Spring Creek Springs is assumed as same as that of Wakulla Spring, which has been well explored by cave divers. The equivalent freshwater head would be even higher if the caves of Spring Creek Springs are deeper than 300 ft, which means the position of seawater/freshwater mixing zone would be deeper than 300 ft as well. In addition, the uniform empirical correction factor is used to obtain the real evapotranspiration from the potential evapotranspiration in this study, which could be another source of uncertainty for surface recharge estimation. Last but not the least, some parts of the precipitation data in the middle and south part of the WKP are missing in this study and bring in imponderable error for the estimation of rainfall recharge, because precipitation in Tallahassee Regional Airport could be different from those in Crawfordville and Spring Creek Springs.

Generally speaking, simulation results of discharge match satisfactory with measurements, especially for the discharge peaks at Spring Creek Springs in phase 2. The correlation coefficients between measurements and simulation results at Spring Creek Springs and Wakulla Spring are 0.891 and 0.866, respectively. Most simulation results match well with measurements in phase 2 and phase 3, except for some specified periods. Groundwater discharge is generally overestimated at Spring Creek Springs but underestimated at Wakulla Spring in phase 1 with larger fluctuations as well (Table 4.1; Figure 4.3). The calculation of equivalent freshwater head at Spring Creek Springs is a possible reason for the mismatch, since the submarine caves might be deeper than 300 ft in the assumption. Another possible reason would be the data quality for measurements of discharge at Spring Creek Springs, because it is very difficult to accurately measure the total flow rate of a group of submarine springs by USGS gage is located at the mouth of the Spring Creek estuary bay. Tracer tests by Kincaid and Werner (2008) pointed out those vents and caves could have different hydrological characteristics; for example, tracer was strongly detected at Spring Creek Spring vent #10 but was not detected at vents #1 and #11. In other words, our knowledge of the submarine springs is still insufficient, and more future investigations are expected.

The numerical simulation results indicate that discharges at both Spring Creek Springs and Wakulla Spring are very sensitive to precipitation, especially for the discharge at Spring Creek Springs after a high rainfall event. Freshwater discharge and/or seawater intrusion vary under different rainfall conditions. Generally speaking, freshwater flows into the bay after a heavy rainfall event; on the other hand, seawater siphons reversely into the conduit during a low rainfall period. On the other hand, groundwater discharge at Wakulla Spring is not only controlled by precipitation recharge, but also affected by freshwater discharge and salinity fluctuation at Spring Creek Springs. During low rainfall periods such as phase 1 of the conceptual model, freshwater discharge at Spring Creek Springs is almost ceased or even reversed; however, seawater blocks the freshwater discharge and intrudes into the cave. Meanwhile, groundwater discharge at Wakulla Spring remains relatively high level. Discharges at both Wakulla Spring and Spring Creek Springs significantly increase at phase 2 with a heavy rainfall event. Spring Creek Springs remains high flow rate and low salinity in phase 3, but discharge at Wakulla Spring could be even lower than that in phase 1.

The phase transition is complicated in some cases. The periods from 7 to 9 did not show a sequential transition through each phase of the conceptual model (Davis and Verdi, 2014). Period 6 to 7 was a transition from phase 3 to 2 due to a heavy rainfall event that prevented phase 1 occurred. Period 7 to 8 was a transition from phase 2 to 1, because the springs had been discharging freshwater for approximately 10 months prior to period 8, and groundwater level of the UFA was extremely low due to the extended period of freshwater discharge and low rainfall. As a result, the caves of Spring Creek Springs are filled with siphoning seawater as the primary characteristic of phase 1. Period 8 to 9 was a transition from phase 1 to 3, and the salinity at Spring Creek Springs slightly decreased at this transition due to medium rainfall or surface recharges, which allows freshwater discharges at both Wakulla Spring and Spring Creek Springs. Davis and Verdi (2014) believed it is rare since the transition only happened once during the study period. However, a new description of the conceptual model may be needed if future observation indicates that it is more common.

The numerical model is very important to understand the conceptual model and evaluate the interaction of seawater and freshwater through conduit networks in the study site. High-density seawater and the mixing zone of freshwater/seawater could significantly affect groundwater flow field in terms of the equivalent freshwater head. The discrete-continuum MODFLOW-CFP and CFPv2 models are only able to simulate constant-density flow but not for variable-density flow. Therefore, the concept of equivalent freshwater head is introduced to represent seawater pressure in the conduit system and simulate the entire hydrological processes in the WKP. Equivalent freshwater head is calculated by the salinity measurements at Spring Creek Springs as time-variable boundary conditions in the numerical model.

Understanding the groundwater flow cycling processes plays a basic role in the study of seawater intrusion in a coastal karst aquifer, especially in the Woodville Karst Plain. Seawater is able to intrude into conduit networks when potentiometric surface of the entire aquifer is constant and low during phase 1 of the conceptual model. Meanwhile, salinity is high at Spring Creek Springs with little freshwater discharge. During phase 2 and 3, Spring Creek Springs discharges freshwater and purges seawater out of the submarine caves. However, these two phases are generally shorter than phase 1, which means seawater intrusion through submarine caves occurs at most of the time. Seawater intrudes further landward through the caves of Spring Creek Springs under sea level rise condition because of the higher seawater pressure at the mouths of caves. The discrete-continuum MODFLOW-CFP and CFPv2 models are insufficient evaluate the extent of seawater intrusion distance through the conduits without a transport modeling simulation of salinity distribution. More studies are conducted in the following chapters to provide the extent of seawater intrusion and gain a better understanding of variable-density seawater mixing process.

CHAPTER FIVE

NUMERICAL MODELING AND SENSITIVITY ANALYSIS OF SEAWATER INTRUSION IN A DUAL-PERMEABILITY COASTAL KARST AQUIFER WITH CONDUITS

5.1 Methods of Sensitivity Analysis

5.1.1 Local Sensitivity Analysis

The local sensitivity analysis evaluates the changes of model simulations with respect to model parameters for specified values, elucidates the importance of parameters to the simulated values (Hill and Tiedeman, 2006). The local sensitivities are generally calculated as the derivatives of simulations respect to each parameter at the specified parameter value. In this study, the forward difference approximation of sensitivity is calculated as the derivative of the *i*th simulation respect to the *j*th model parameters,

$$\left.\frac{\partial y'_i}{\partial b_j}\right|_b \approx \frac{y'_i(b+\Delta b) - y'_i(b)}{\Delta b_j} \qquad 32)$$

where y'_i is defined as the value of the *i*th simulation; b_j is the *j*th estimated parameter; b is a vector of the estimated parameter values, indicates that the sensitivity is calculated for the parameter values specified in vector b; Δb is a vector of zeros except that the *j*th parameter equals Δb_j.

The sensitivities are calculated by running the model once using the parameter values in b to obtain $y'_i(b)$, and then changing the *j*th parameter value and running the model again in $b + \Delta b$ to obtain $y'_i(b + \Delta b)$. Scaled sensitivities are introduced to compare the sensitivity of different parameters that may have different units. In UCODE_2005, a scaling method is used to produce the dimensionless scaled sensitivities (DSS) calculated by the following equation,

$$dss_{ij} = \left.\left(\frac{\partial y'_i}{\partial b_j}\right)\right|_b |b_j| {\omega_{ii}}^{1/2} \qquad 33)$$

where dss_{ij} is the dimensionless scaled sensitivity of the *i*th simulation respect to the *j*th parameter; ω_{ii} is the weight of the *i*th simulation.

In parameter sensitivity analysis, the weight ω_{ii} is always replaced by $1/\sigma$, where σ is the standard deviation of measurement error. However, the weight ω_{ii} can be artificially assigned to any value in this study since the parameter sensitivities are respect to simulation not measurement, and the importance of one parameter is relative to others. The DSS values of different simulations respect to each parameter are accumulated for each parameter to produce composite scaled sensitivities (CSS), which reflects the total sensitivities of all the simulations to each parameter. The CSS of the *j*th parameter is evaluated via,

$$css_j = \sum_{i=1}^{ND} \left[(dss_{ij})^2 \big|_b / ND \right]^{1/2} \quad 34)$$

Where ND is the number of observations or simulations.

5.1.2 Global Sensitivity Analysis of Morris Method

The local sensitivity analysis is conceptually straightforward and easy to evaluate, but the sensitivity indices are calculated for specified parameter values, not for the entire parameter ranges. In addition, the indices are limited to the linear (through the first order derivative) impacts of model parameters to simulations, and do not consider interactions between other parameters. Global sensitivity analysis provides the changes of simulations to parameters within the entire parameter range instead of a specified value in local sensitivity analysis.

In this study, Morris method is applied to evaluate the global sensitivity of parameters. It is a "one factor at a time" experiment, which means that only one input parameter is perturbed in each run. The *k*-dimensional vector *X* of the model parameters has components X_i, which can be divided into *p* uniform intervals. The effect of changing one parameter at a time is evaluated in turn by the elementary effect (*EE*), d_i, which is defined as,

$$d_i = \frac{1}{\tau_y} \frac{[y(x_1{}^*, \ldots, x_{i-1}{}^*, x_i{}^* + \Delta, x_{i+1}{}^*, \ldots, x_k{}^*) - y(x_1{}^*, \ldots, x_k{}^*)]}{\Delta} \quad 35)$$

where $\Delta = 1/(p-1)$, τ_y is the output scaling factor, and parameter set $\{x_i{}^*\}$ can be randomly selected by the Monte Carlo random sampling.

To compute the elementary effect for the *k* parameters, (*k*+1) simulations are needed in the same way as local sensitivity method for the perturbation of each parameter, which is called one "path". By having multiple paths of randomly generated parameter set, we have an ensemble of elementary effects for each parameter. The total number of calculation is *r*(*k*+1), where *r* is the number of paths.

However, the procedure of Monte Carlo sampling is not used in this study due to the expensive computational cost for large numbers of parameters and paths. To alleviate the computational burden, the trajectory sampling is commonly used in the global sensitivity analysis of Morris method to generate an ensemble of elementary effects. The method is developed by Saltelli et al. (2004) and applied in this study. The definition of *p*-level remains the same as Monte Carlo sampling, where Δ=*p*/[2(*p*-1)]. The trajectory design starts by randomly selecting a “base” value x^* for the vector X. Each component x_i of x^* is sampled from the set (0, 1/(*p-1*), 2/(*p-1*),…,1). The randomly selected vector x^* is used to generate the other sampling points but not one of them, which means that the model is never evaluated at vector x^*. The first sampling point, $x^{(1)}$, is obtained by increasing one or more components of x^* by Δ. The choice of components x^* to be increased is conditioned by that $x^{(1)}$ still being within the domain. The second sampling point, $x^{(2)}$, is generated from x^* with the property that it differs from $x^{(1)}$ in its *i*th component, which has been either increased or decreased by Δ. The third sampling point, $x^{(3)}$, differs from $x^{(2)}$ for only one component j, for any $j \neq i$, can be either ${x_j}^{(3)} = {x_j}^{(2)} + \Delta$ or ${x_j}^{(3)} = {x_j}^{(2)} - \Delta$. The design proceeds to produce a succession of (*k*+1) sampling points $x^{(1)}, x^{(2)}, \dots, x^{(k+1)}$, with the key property that two consecutive points differ in only one component, which is called a trajectory in the input parameters space. Therefore, any component *i* of the ‘base’ vector x^* has been selected at least once to be increased or decreased by Δ in order to calculate one elementary effect for each parameter.

Once a trajectory is constructed and evaluated at theMorris points in the model, an elementary effect for each parameter *i, i = 1,…, k*, can be computed. If $x^{(l)}$ and $x^{(l+1)}$, with *l* in the set in (*1,...,k*), are two sampling points differing in their *i*th component, the elementary effects associated with the parameter *i* is either,

$$d_i\left(x^{(l)}\right) = \frac{\left[y\left(x^{(l+1)}\right) - y\left(x^{(l)}\right)\right]}{\Delta} \qquad 36)$$

if the *i*th component of $x^{(l)}$ has been increased by Δ, or

$$d_i\left(x^{(l)}\right) = \frac{\left[y\left(x^{(l)}\right) - y\left(x^{(l+1)}\right)\right]}{\Delta} \qquad 37)$$

if the *i*th component of $x^{(l)}$ has been decreased by Δ.

A random sample of r elementary elements has to be selected at the beginning. Each trajectory sampling has a different starting point that is randomly generated. The points belonging to the same trajectory are not independent, but the r points sampled from each distribution belonging to different trajectories are independent. The goal of the experiment is to estimate the mean μ and standard deviation σ of the distribution of elementary effects, which are estimated with the r independent random paths in the global sensitivity analysis of Morris method,

$$\mu = \sum_{i=1}^{r} d_i / r \tag{38)}$$

$$\sigma = \sqrt{\sum_{i=1}^{r} (d_i - \mu)^2 / r} \tag{39)}$$

5.2 Model Developments

Numerical modeling is an effective method to quantitatively evaluate the extent of seawater intrusion and contamination of freshwater resources in a coastal karst aquifer. In this study, a two-dimensional SEAWAT model is setup to simulate variable-density flow and salt transport in a dual-permeability karst aquifer with a highly permeable conduit and surrounding porous medium. The conceptual model in this study is based on seawater intrusion through the subsurface conduit network of the coastal karst aquifer in the Woodville Karst Plain (WKP), where a submarine spring (Spring Creek Springs) is directly open to the Gulf of Mexico and connected to the conduit system (Figure 1.1 & 4.1). The conduit system in the WKP starts from the submarine spring and extends 11 miles landward to a constant head inland springs (Wakulla Spring).

5.2.1 Hydrological Conditions

The specified parameters values in the following local sensitivity analysis and scenarios of numerical simulation are assigned as the field hydrological characteristics of the Upper Floridan Aquifer (UFA) in the WKP (Table 5.1), which were calibrated in a regional-scale numerical model by Davis et al. (2010) and applied in many subsequent modeling studies (Gallegos et al., 2013; Xu et al., 2015a; Xu et al., 2015b). The two-dimensional seawater intrusion numerical model is not re-calibrated in this study due to insufficient field observation data. The head and salinity measurements in the conduit are generally unavailable, because the difficulties to investigate the exact location of subsurface conduit and install the monitoring devices. It is also extremely dangerous for cave divers to explore the conduit system from the submarine spring, especially during the period of seawater siphoning. However, the simulation results are still able to provide a general understanding and quantitative estimation of seawater intrusion through conduit network of the coastal karst aquifer in the WKP, since all parameters have been calibrated in the previous studies.

The hydrological characteristics of the conduit system can be significantly different from those of porous medium. Generally speaking, conduit system has larger values of hydraulic conductivity, specific storage and effective porosity. Hydraulic conductivity of the porous medium is assigned as 7500 ft/day, but is 2,000,000 ft/day for the conduit system. The hydraulic conductivity of a karst aquifer is higher than most of the alluvial aquifers due to numerous small fractures. Specific storage and effective porosity in the porous medium are assumed as 5×10^{-7} and 0.003, respectively. However, specific storage and effective porosity are 0.005 and 0.300 in the conduit layer, respectively. The longitudinal dispersivity is 32.80 ft in the porous medium, but is assumed very small in the conduit, in which solute advection is dominated and dispersion can be neglected.

5.2.2 Spatial and Temporal Discretization

The spatial discretization and boundary conditions of the two-dimensional SEAWAT numerical model is shown in Figure 5.1. The extent of model spatial domain is designed along the estimated conduit network between the submarine spring and the inland spring in the WKP. The numerical model simulates variable-density groundwater flow and salt transport in the area with a spatial discretization of 140 columns and 37 layers in a cross section. Guo and Langevin (2002); Werner et al. (2013) pointed out that the grid resolution in the vertical direction often requires a much greater level of detail to represent the complex density-dependent flow pattern with high concentration gradients. In the vertical direction, the study domain is uniformly discretized uniformly with 10 ft for a grid thickness, which has higher resolution than the previous numerical studies of non-density dependent simulations in the same study site by Davis and Katz (2007); Davis et al. (2010); Gallegos et al. (2013); Xu et al. (2015a); Xu et al. (2015b).

Table 5.1. The symbols and definitions of parameters used in this study, the specified evaluated values in local sensitivity study and evaluation ranges (lowest and highest values) of each parameter in global sensitivity analysis.

Parameter	Definitions	Lowest	Highest	Evaluated value	Unit
HY_P	Hydraulic conductivity (porous medium)	5000	15000	7500	ft/day
HY_C	Hydraulic conductivity (conduit)	1000000	3000000	2000000	ft/day
SS_P	Specific storage (porous medium)	4.00E-7	6.00E-7	5.00E-7	dimensionless
SS_C	Specific storage (conduit)	0.03	0.07	0.05	dimensionless
RCH	Recharge rate	0.00	0.10	0.03	ft/day
H_SL	Head (sea evel) at the submarine spring	-1.0	3.0	1.0	ft
PO_P	Porosity (porous medium)	0.001	0.005	0.003	dimensionless
PO_C	Porosity (conduit)	0.200	0.400	0.300	dimensionless
SC	Salinity at the submarine spring	0.0	35.0	35.0	PSU
DISP_P	Longitudinal dispersivity (porous medium)	20.00	40.00	32.80	ft
DISP_C	Longitudinal dispersivity (conduit)	0.50	2.00	1.00	ft

The horizontal discretization of the domain is also uniform with grid width of 500 ft, except columns #22 and #139 with the cell size of 50 ft to represent the submarine spring (Spring Creek Spring) and inland spring (Wakulla Spring), respectively. The sizes of the outlets of vertical highly permeable conduit system are calibrated in previous studies as well (Gallegos et al., 2013). Salt transport in the conduit system is originated from the shoreline at the cell of column #22 in layer #1. The conduit system starts from the submarine spring, vertically downward to layer #29 (nearly 300 ft below sea level), extends horizontally landward for nearly 11 miles to column #139, and then upward to the constant head inland spring on the surface. The inland spring is simulated by the DRAIN package as general head boundary condition in the SEAWAT numerical model. All layers are assumed in a confined aquifer with fully saturated conduit, based on the regional groundwater flow and transport model by Davis et al. (2010); Xu et al. (2015a); Xu et al. (2015b) in the WKP.

The numerical model is setup as one stress period of seven-day transient simulation in this study. The only exceptions are the scenarios of longer simulation time to evaluate the effect of extended low rainfall period in Section 4.4.4. The length of flow time step is set as 0.1 days but transport time step is calculated by SEAWAT code automatically.

5.2.3 Initial and Boundary Conditions

The initial condition of measured head in the numerical model is set 0.0 ft as current sea level for the cells from the left boundary to the shoreline (column #22), and gradually rises to 5.0 ft to the inland boundary on the right based on the elevation of inland Wakulla Spring in the WKP. The initial conditions of salinity are assumed to be constant vertically in each column, 35.0 PSU (Practical Salinity Unit) at the most left 10 columns representing pure seawater near the sea boundary of the aquifer. The mixing zone of seawater/freshwater is assumed to start from column #11 to column #45 in the initial condition, with a decreasing salinity gradient of 1.0 PSU per column. The salinity from column #46 to the inland boundary on the right is set uniformly as 0.0 PSU initially as an uncontaminated freshwater aquifer. Several test results indicate that the initial conditions do not affect the modeling results significantly.

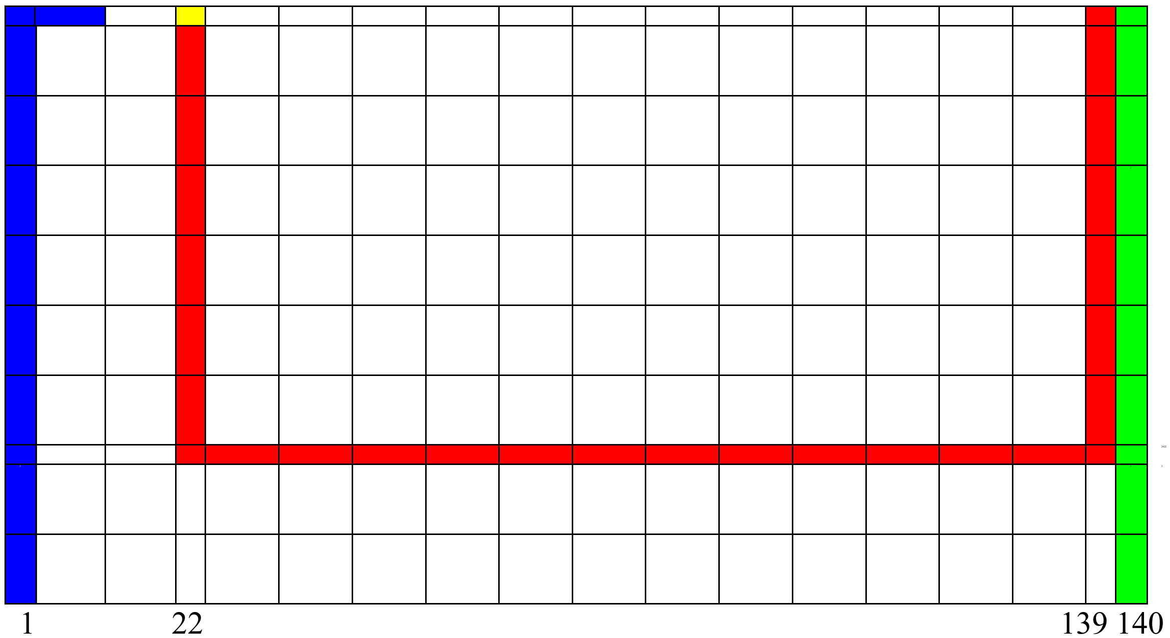

Explanations:

Constant head and constant concentration of the submarine spring and outlet of karst conduit system, however, various in different cases of numerical models

Seawater boundary: constant head (0.0 ft) and constant concentration (35.0 PSU), however, are different in each scenarios of simulation

Inland freshwater boundary: constant head (5.0 ft) and constant concentration (0.0 PSU)

Conduit: large values of hydraulic conductivity, porosity and specific storage

Porous medium: small values of hydraulic conductivity, porosity and specific storage

Figure 5.1. Schematic finite difference grid discretization and boundary conditions applied in the SEAWAT model. Every tenth cell in horizontal and every fourth cell in vertical shown, except the boundary and conduit layer with smaller width. The submarine spring is located at column #22, layer #1, and the inland spring is located at column #139, layer #1. The conduit system starts from the surface of column #22, vertically downward to layer #29, extends horizontally to column #139, and then vertically upward to the surface.

The boundary conditions are also presented in Figure 5.1. No-flow boundary condition is set at the bottom of the model domain as the less-permeable confining unit at the base of the UFA. The right inland boundary is set as 5.0 ft constant head as the elevation of inland Wakulla Spring and 0.0 PSU as pure freshwater in the aquifer. The seawater boundary on the left is assumed as hydrostatic equilibrium, which is 2.1 miles away from the shoreline, set as 0.0 ft constant head as sea level and 35.0 PSU constant concentration as pure seawater. The boundary conditions of head and salinity at the submarine spring (Column #22, Layer #1) vary in the different scenarios of sea level, salinity and freshwater discharge in Section 4.4. For example, the boundary conditions of the submarine spring are set as 0.0 ft constant head as the sea level and 35.0 PSU constant concentration as pure seawater in the case of the maximum seawater intrusion.

5.3 Sensitivity Analysis

The uncertainties of salinity and head simulations respect to eleven parameters in the seawater intrusion numerical model are evaluated in the following sensitivity analysis, which provides an overall understanding of the importance of hydrological characteristics and boundary conditions in a coastal karst aquifer with a conduit. The symbols and definitions of eleven parameters in the numerical models are listed in Table 5.1, as well as the evaluated values in local sensitivity analysis. Although all parameters are calibrated in previous study, the uncertainties of parameters and boundary conditions within ranges are estimated in global sensitivity analysis (Table 5.1). Six parameters (HY_P, HY_C, SS_P, SS_C, RCH and H_SL) are used in groundwater flow model, and the other five parameters (PO_P, PO_C, SC, DISP_P and DISP_C) are used in solute transport model. Groundwater flow and solute transport equations are coupled and solved simultaneously in the SEAWAT numerical model, and the sensitivities of eleven parameters are calculated together at the end of the simulation.

5.3.1 Local Sensitive Analysis

In local sensitivity analysis, the CSS (composited scaled sensitivities) values of parameters to head and salinity simulations at different spatial locations in the conduit and porous medium are calculated by UCODE_2005 (Poeter and Hill, 1998). The specified parameter values are identical with the hydrological characteristics of the UFA, and the boundary conditions of conduit system are evaluated as the pure seawater and current sea level in the local sensitivity study, which are the maximum seawater intrusion case in the Section 4.4.1 as well. Parameter sensitivities are calculated from column #25 to column #75 with an interval of 5 cells along the horizontal conduit (layer #29), where column #25 is very close to the shoreline and column #75 represents the uncontaminated aquifer. The sensitivities of simulations in a porous medium are evaluated at layer #24, 50 ft or 5 layers above the conduit layer, also starting from column #25 to column #75 with an interval of 5 cells. Generally speaking, the parameters with larger CSS value are relatively more important to simulations.

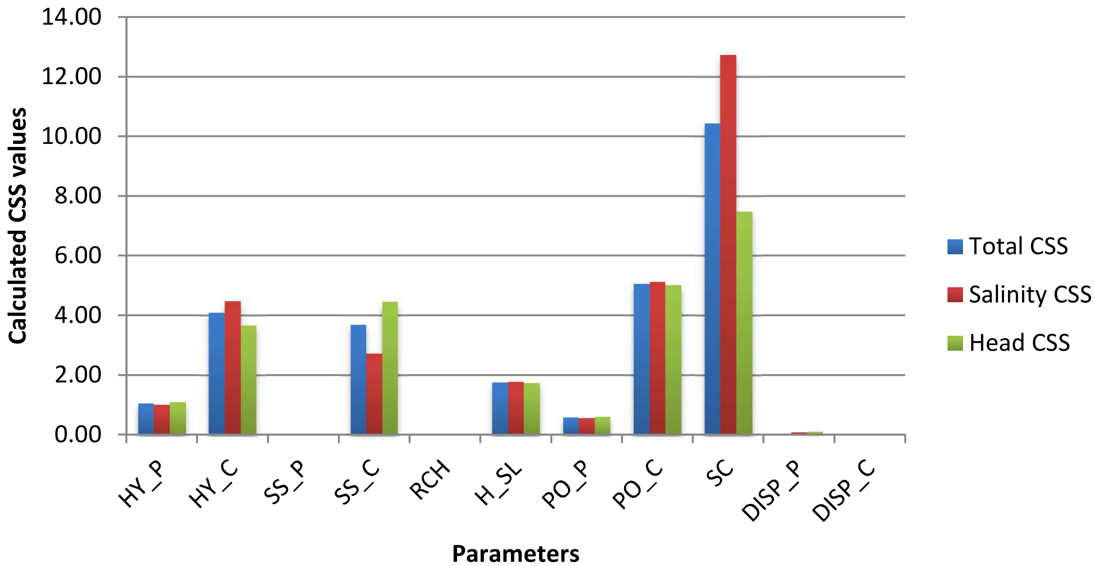

Figure 5.2. CSS (Composite Scaled Sensitivity) values of all parameters to simulations in the conduit (layer #29) by local sensitivity analysis.

The calculated CSS values of parameters to simulations in all evaluated locations along the conduit layer are shown in Figure 5.2. Salinity at the submarine spring (SC) is the most important parameter to both salinity and head simulations due to the largest CSS values. Hydraulic conductivity, specific storage and porosity of the conduit (HY_C, SS_C and PO_C) as well as sea level at the submarine spring (H_SL) are also important parameters. Parameters of hydraulic conductivity, specific storage and porosity of the porous medium (HY_P, SS_P and PO_P), recharge rate (RCH) and dispersivity (DISP_C and DISP_P) are less important than others.

Salinity at the submarine spring (SC) is the most important parameter and boundary condition in the seawater intrusion numerical model, because the salt plume and salinity distribution in the conduit is mainly determined by the advective transport that coming from the submarine spring, which is the outlet of conduit. The highly permeable conduit system significantly accelerates the groundwater flow in the conduit. Increasing salinity at the submarine spring directly results in severe seawater intrusion and moves the position of mixing zone further landward, and vice versa. The simulation results are more sensitive to the parameters of hydraulic conductivity, specific storage and porosity of the conduit (HY_C, SS_C and PO_C) than those properties of the porous medium (HY_P, SS_P and PO_P), since the simulations are evaluated in the conduit rather than the porous medium, and seawater mainly intrudes the aquifer through the conduit network. Sea level at the submarine spring (H_SL) is also an important boundary condition in the numerical model, but its relative small CSS value indicates that salinity simulation to sea level is not as sensitive as parameter SC. In other words, seawater intrusion is more sensitive to rainfall recharge and freshwater discharge that described by the parameter SC, rather than the variation of tidal stage or sea level. The small CSS value for recharge (RCH) indicates it is an unimportant parameter to the salinity distribution in this study, because rainfall and surface water recharges are only small parts of total recharge in the two-dimensional model. Regional recharge is the major source of freshwater in the model and controlled by the general head boundary condition at the inland boundary. Dispersivities of the conduit and porous medium (DISP_C and DISP_P) are not important to salinity and head simulations, because salt transport is dominated by advection in the highly permeable conduit with large values of hydraulic conductivity, porosity and specific storage.

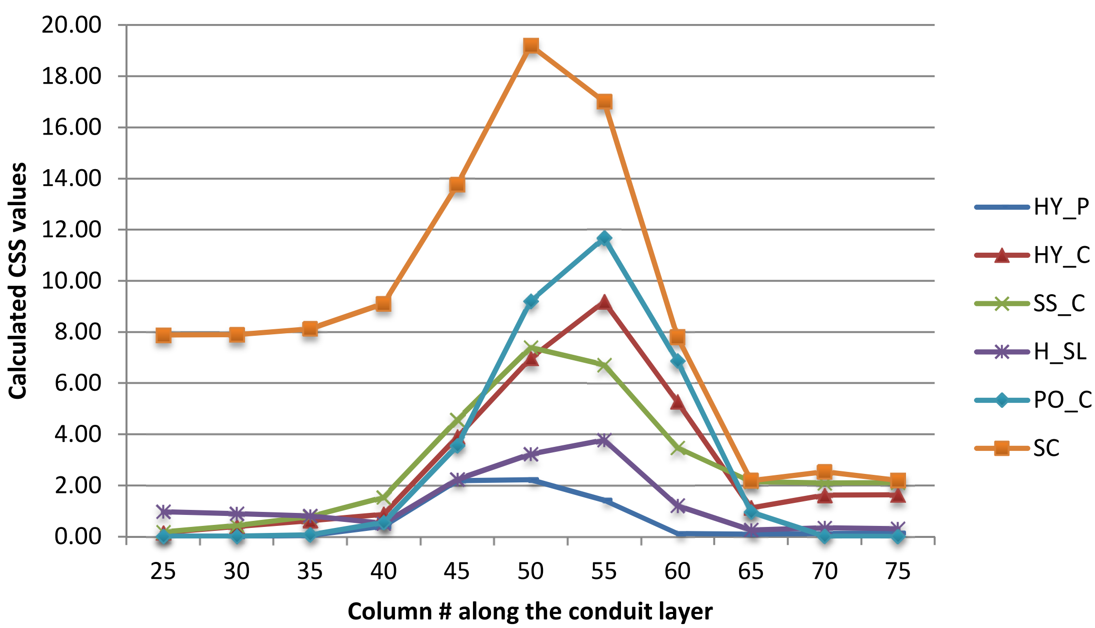

Figure 5.3. CSS (Composite Scaled Sensitivity) values at different locations along the conduit layer (from column #25 to column #75) in the spatial domain by local sensitivity analysis.

The six largest CSS values of parameters to the combination of head and salinity simulations are calculated in each evaluated location along the conduit in the spatial domain (Figure 5.3). The largest CSS values of all parameters are located at either column #50 or #55 along the conduit layer, which are exactly coincided with the position of mixing zone in the maximum seawater intrusion case that presented in section 4.4.1. The parameters are more influential at the mixing zone, because head and salinity simulations only change significantly near the mixing zone but remain relatively stable in other areas.

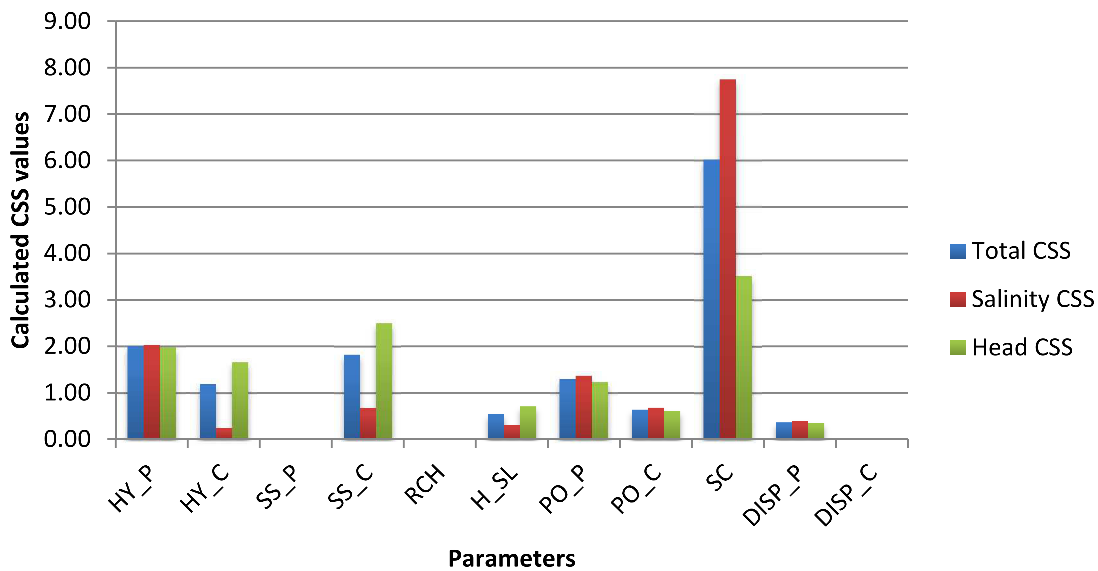

Figure 5.4. CSS (Composite Scaled Sensitivity) values of all parameters to simulations in porous medium (layer #24) by local sensitivity analysis.

The calculated CSS values of parameters to head and salinity simulations in all evaluated locations along the evaluated layer of the porous medium are presented in Figure 5.4. The largest CSS value of parameter SC indicates that salinity at the submarine spring is still the most important factor to simulations in the porous medium, although it is a boundary condition of the conduit system. The sensitivities of other parameters are different from the results of simulations in the conduit. Hydraulic conductivity and porosity of the conduit and porous medium (HY_C, HY_P, PO_C & PO_P), specific storage of the conduit (SS_C) and dispersivity of the porous medium (DISP_P) are not as important as parameter SC, but also play important roles in the numerical simulation. The other parameters (DISP_C, RCH, SS_P) are less important to the simulations in the porous medium. The eight largest CSS values of parameters along the evaluated layer of porous medium are presented in Figure 5.5. The largest CSS value of each parameter occurs at either column #35 or #40 in the spatial domain, which is the seawater/freshwater mixing zone, and exhibits similar pattern to the previous analysis of simulations in the conduit.

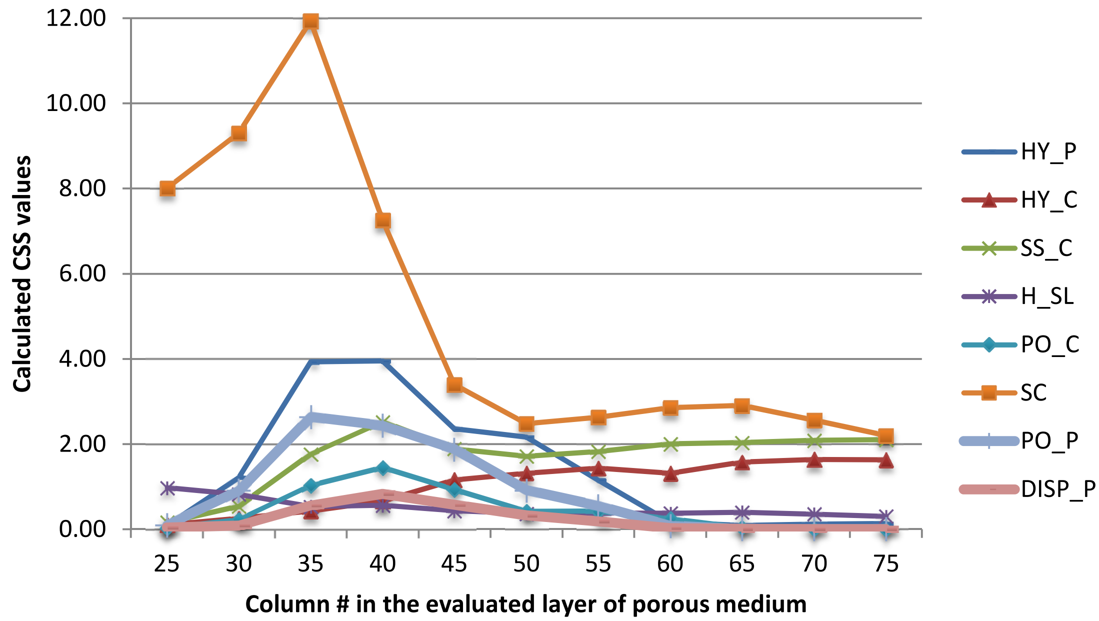

Figure 5.5. CSS (Composite Scaled Sensitivity) values at different locations in porous medium (from column #25 to column #75 at layer # 24) in the spatial domain by local sensitivity analysis.

In the numerical modeling of seawater intrusion in a dual-permeability karst aquifer, groundwater flow and salt transport through the conduit system significantly affect the head and salinity simulations in the surrounding porous medium. Seawater intrusion mainly starts at the submarine spring, travels through the conduit system and then exchanges water and solute with the surrounding porous medium. Therefore, the salinity of submarine spring (SC) is still the most important parameter for simulations in the porous medium as the salt source. Similarly, conduit parameters such as hydraulic conductivity, porosity and specific storage (HY_C, PO_C and SS_C) are also important to the simulations in the porous medium. On the other hand, relative large CSS values for hydraulic conductivity, porosity and dispersivity of the porous medium (HY_P, PO_P and DISP_P) also indicate that they are important parameters to simulations in the porous medium. The importance of matrix parameters is easy to understand, since groundwater flow and salt transport in a porous medium domain are significantly controlled by the matrix parameters in a local scale. The relatively large CSS values of the factors in both conduit and porous medium illustrate the importance of conduit-matrix interaction in the seawater intrusion process in a coastal karst aquifer. In general, parameter sensitivities for simulations in the porous medium are more complex than those in the conduit, and the conduit-matrix interaction plays a much more important role in the dual-permeability karst system than that in a relatively homogeneous medium.

5.3.2 Global Sensitivity Analysis

The head and salinity simulations respect to variations of parameters are evaluated in Figure 5.6. Simulation results are nearly unchanged to the variations of the unimportant parameters indicated in the local sensitivity study, for example, the dispersivity of porous medium (DISP_P). On the other hand, simulations in porous medium exhibit linear relationship to the parameter HY_P with a median calculated CSS value. However, both head and salinity simulations are non-linear to some parameters with large CSS values, such as the boundary condition of salinity at the submarine spring (SC) (Figure 5.6). Therefore, the results of local sensitivity analysis are imperfect in consideration of the parameter range and interaction of parameters.

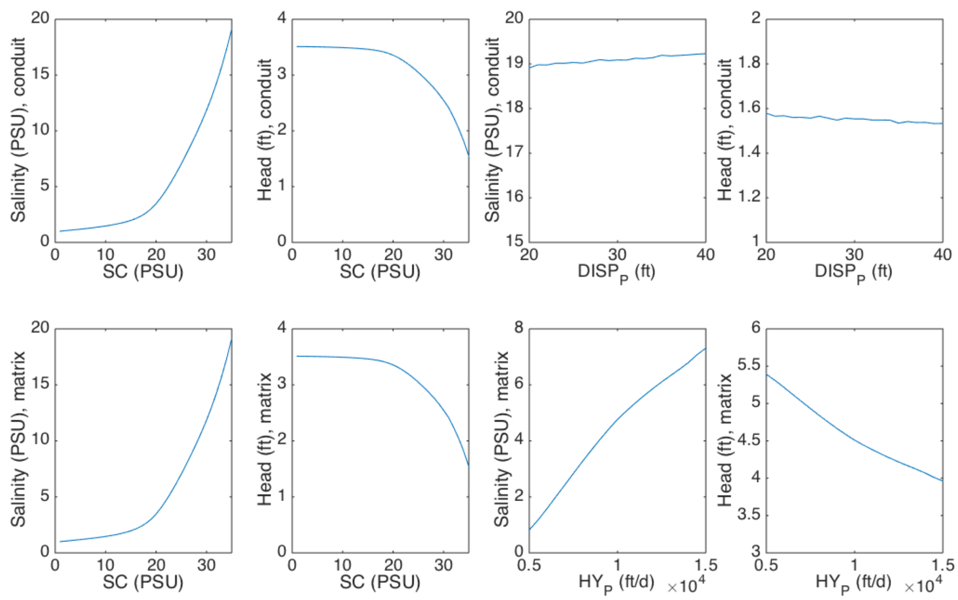

Figure 5.6. The relationship between head and salinity simulations in both the conduit and porous medium (matrix) respect to parameters SC, DISP_P and HY_P. (Note that the scale for each plot is different).

Global sensitivity analysis is able to provide a better understanding of parameters sensitivities in the seawater intrusion numerical model. Based on the results of local sensitivity analysis, global sensitive analysis based on Morris method is used to evaluate the parameters at the locations with the largest CSS values in the spatial domain, which are coincided with the position of mixing zone. Parameter sensitivities to both head and salinity simulations are evaluated in the conduit (column #50, layer 29) and porous medium (column #35, layer #24), respectively, in the following global sensitivity analysis.

Monte Carlo random sampling can be used in the global sensitivity analysis; however, it requires large numbers of elementary effects with heavy computational burden. Trajectory sampling method developed by Saltelli et al. (2004) is applied in this study to save computational cost. Three different trajectory cases of level p and random path r (Case 1: $p = 4$ and $r = 10$; Case 2: $p = 10$ and $r = 10$; Case 3: $p = 4$ and $r = 30$) have been tested and compared in the global sensitivity study. The results of the three testing cases with various level p and random path r do not show significant difference, which is identical with the conclusion made by Saltelli et al. (1999); Saltelli et al. (2004) that the choice of $p = 4$ and $r = 10$ in trajectory method are generally good enough. Therefore, the sensitivity results of $p = 4$ and $r = 10$ are presented and discussed in the following discussion.

The mean and standard deviation of elementary effects of parameters to salinity simulations in the conduit (column #50, layer #29) are presented in Figure 5.7A. Parameter SC is still the most important parameter to salinity simulations with the largest mean value, because salinity at the submarine spring is the boundary condition and the source of salt plume in the numerical model. The largest standard deviation value of parameter SC is due to the significant non-linear relationship to salinity simulation (Figure 5.6). The parameters HY_C, PO_C and H_SL are all important to salinity simulation with relatively large mean and standard deviation values of elementary effects, because they are either parameters or boundary conditions of the conduit system that directly affect seawater intrusion through conduit network. Other parameters are relatively unimportant with small mean and standard deviation of elementary effects. Generally speaking, the results of global sensitivity study are identical with those by the local sensitivity analysis.

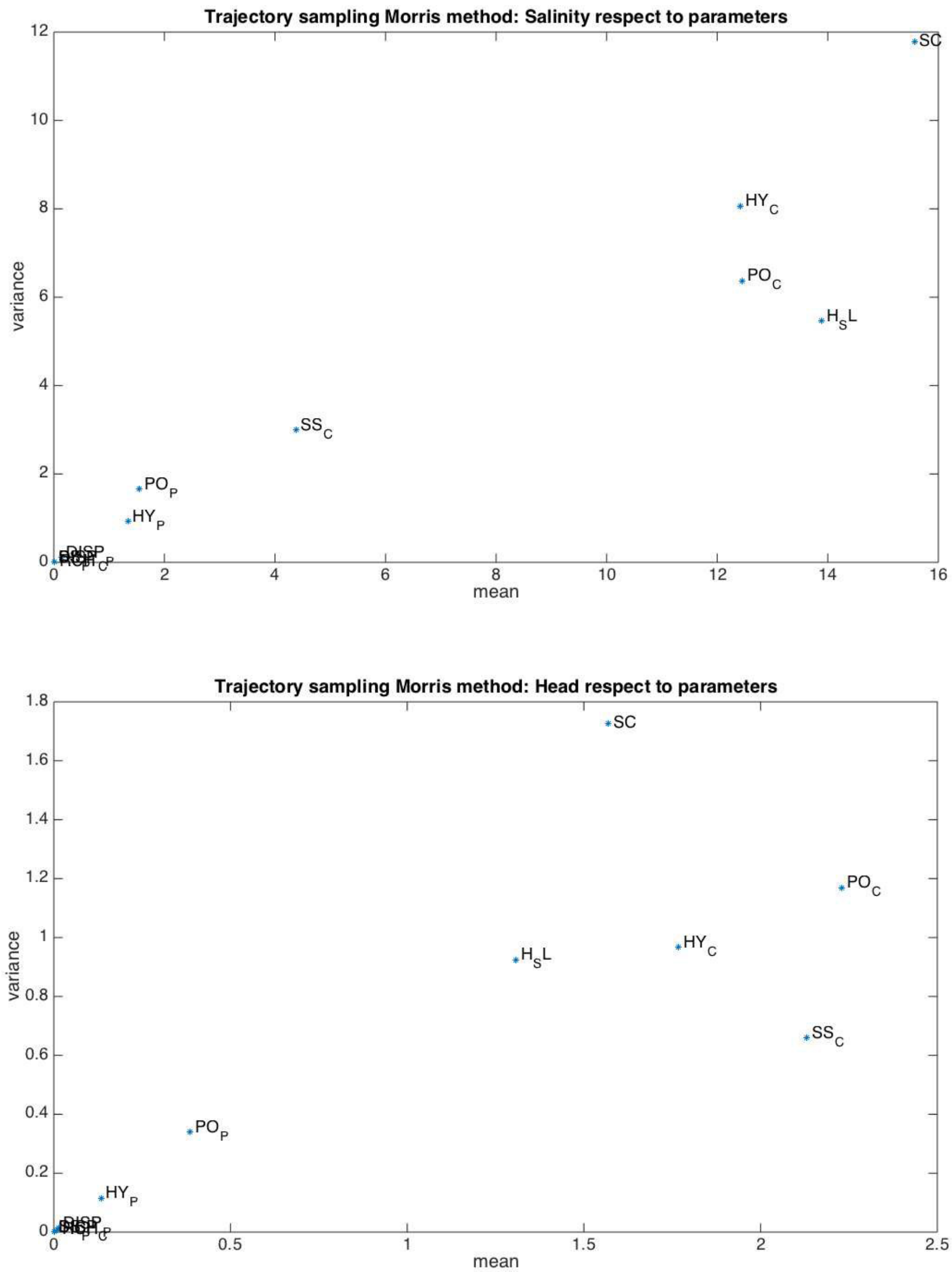

Figure 5.7. Mean and standard deviation of elementary effects to simulations in the conduit (column #50, layer #29) respect to each parameter by trajectory sampling Morris method global sensitivity analysis: A) salinity simulation (upper); B) head simulation (lower).

The results of global parameter sensitivity to head simulations are more complex than those to salinity simulation (Figure 5.7B). The absolute values of mean and standard deviation of elementary effects to head simulation are much smaller than those to salinity simulation, which indicates that salinity simulation is more sensitive to parameter variations than head simulation.

The largest mean values of elementary effects of the specific storage (SS_C) and porosity (PO_C) in the conduit indicate that they are the most important parameters to head simulation. Both specific storage and porosity are physically determined by the void space of porous medium, significantly control head and salinity simulations in the coupled groundwater flow and salt transport processes, respectively. Salinity at the submarine spring (SC) is still an important parameter for head simulation with a large standard deviation of elementary effects because of its non-linear relationship to head simulation as well (Figure 5.6). Salinity in terms of density is also an important factor to the equivalent freshwater head, which determines flow field and head simulation in the coupled variable-density numerical model. Hydraulic conductivity in the conduit and sea level at the submarine spring (HY_C and H_SL) are important to head simulation in the conduit with relatively large mean and standard deviation of elementary effects as well.

The means and standard deviations of elementary effects of the parameters PO_C and SS_C are much larger than those of parameter HY_C, which indicate that head simulation in the conduit is more sensitive to porosity and specific storage rather than the hydraulic conductivity. It is counterintuitive to empirical experience, but is actually reasonable in the dual-permeability numerical model. SEAWAT is a continuum numerical model that uses Darcy equation to simulate groundwater flow in the entire model domain, including both the conduit and porous medium system. Darcy equation in the continuum model is only accurate for laminar seepage flow in a porous medium with a linear relationship between flow rate and head gradient, but groundwater flow in the conduit could be non-laminar even turbulent. In other words, the uncertainties of hydraulic conductivity and specific discharge estimation by Darcy equation are significant in the conduit. Therefore, the sensitivity of hydraulic conductivity possibly does not well reflect the importance of permeability in the non-laminar conduit flow system. The continuum SEAWAT model is not inapplicable to simulate seawater intrusion in a dual-permeability karst aquifer; however, the uncertainty of groundwater flow estimation in the conduit will be significant. The importance of conduit system in the numerical model has been emphasized by the sensitivity of hydraulic conductivity in this study as well.

The means and standard deviations of elementary effects to salinity simulations in the porous medium are shown in Figure 5.8A. Parameters HY_P and SC are the two most important parameters to salinity simulation with the largest mean and standard deviation values. Hydraulic conductivity of matrix (HY_P) determines groundwater seepage velocity in flow simulation and significantly affects salt advection transport in a porous medium. The source of salt plume is originated from the boundary of conduit system, parameter SC, which controls salt transport in not only the conduit system but also in the porous medium. The importance of parameter SC highlights the significance of conduit-matrix interaction in the dual-permeability aquifer. However, salinity simulation is not sensitive to parameter HY_P in local sensitivity study, while the parameter SC has the largest CSS value. The importance of the salinity at submarine spring (SC) is significantly overestimated in local sensitivity analysis with the non-linear relationship and the largest derivative at the specified evaluated value (35.0 PSU) (Figure 5.6). Meanwhile, the importance of HY_P is relatively underestimated in local sensitivity study. Sea level at the submarine spring (H_SL) and porosity of the porous medium (PO_P) are important parameters to salinity simulations as well. Similar to parameter SC, the head boundary condition in the conduit system (H_SL) determines the equivalent freshwater head and affects the salinity simulation in the porous medium because of the dynamic exchange between the conduit and porous medium system in the coupled groundwater flow and salt transport dual-permeability model. The importance of conduit-matrix interaction is also represented by the relatively large mean and standard deviation values of porosity and specific storage (PO_C and SS_C) of the conduit to salinity simulation in the porous medium.

Parameter sensitivities for head simulation in the porous medium are more complex than those for salinity simulation. Hydraulic conductivity of the porous medium (HY_P) becomes the most important parameter to head simulation in the porous medium (Figure 5.8B) and directly determines the groundwater flow and head distribution by the Darcy governing equation. PO_P is also a relatively important parameter to head simulation because groundwater flow and salt transport equations are coupled and solved simultaneously in the SEAWAT numerical model. On the other hand, boundary conditions (SC and H_SL) and hydrological factors (SS_C, HY_C and PO_C) of the conduit system are another group of important parameters to head simulation in the porous medium. Sea level at the submarine spring (H_SL) is the most important conduit factor to head simulation in the porous medium, directly affects groundwater flow along the conduit and head simulation in the porous medium through conduit-matrix interaction. Parameter H_SL is even more important than parameter SC because the exchanges between the conduit and porous medium are directly determined by the head difference.

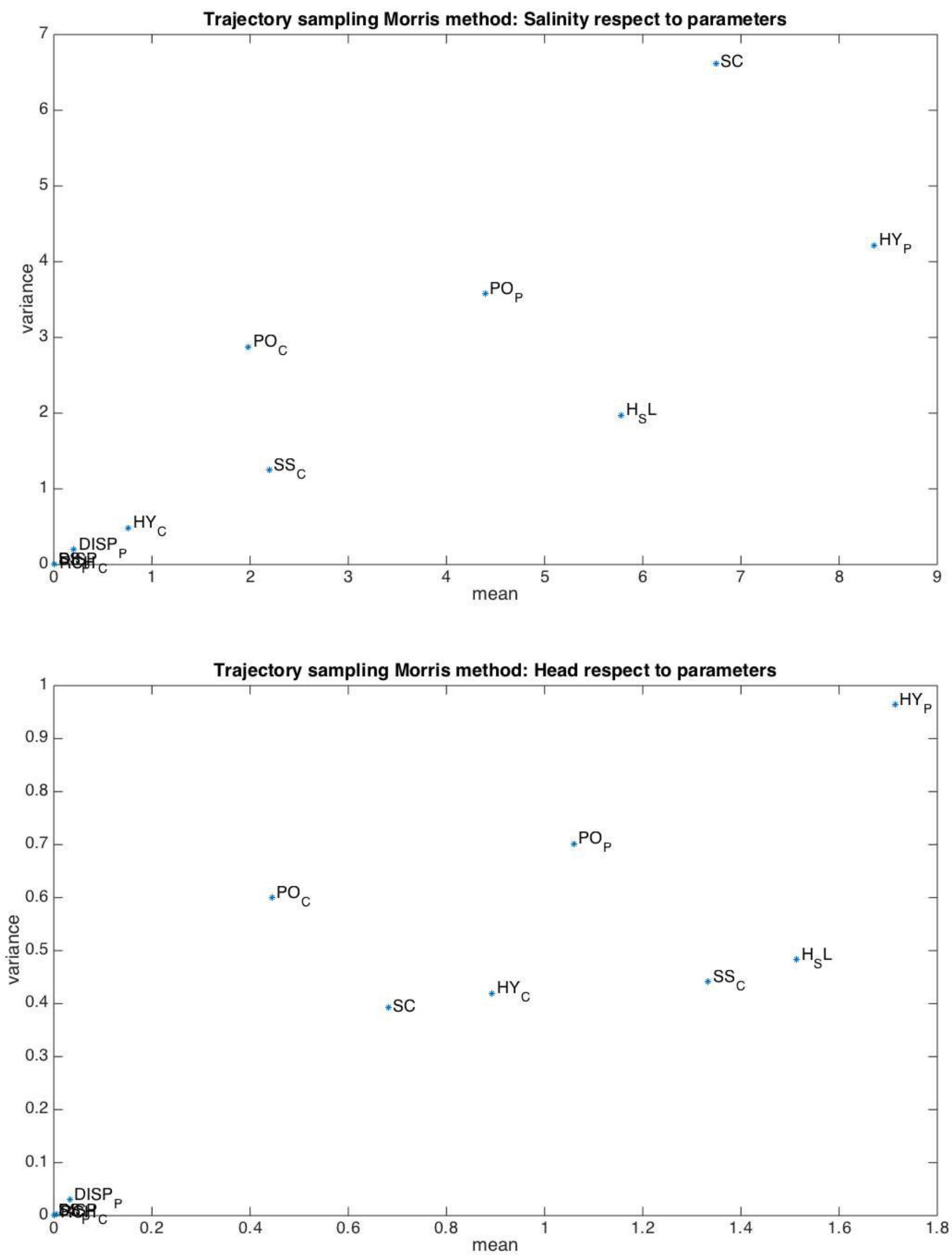

Figure 5.8. Mean and standard deviation of elementary effects for simulations in porous medium (column #35, layer #24) respect to each parameter by trajectory sampling Morris method global sensitivity analysis: A) salinity simulation (upper); B) head simulation (lower).

The large mean and standard deviation of elementary effects of conduit parameters to both salinity and head simulations indicate the significant effect of conduit system on simulations of seawater intrusion in a dual-permeability karst aquifer. Seawater intrudes the aquifer from the submarine spring, travels faster and further landward through the conduit system, and then flows into a surrounding porous medium domain. Salinity at the submarine spring is the major source of salt plume in a porous medium due to conduit-matrix interaction, and sea level determines the head difference between the conduit and surrounding matrix, which in turn controls groundwater exchanges between the conduit and porous medium. On the other hand, dispersivity parameters are not as important as those in the sensitivity analysis by Shoemaker (2004), in which the porous medium is homogeneous without preferential advective flow. In the dual-permeability system, advection is dominated in the conduit and its surrounding porous medium. Therefore, the effect of dispersion to solute transport is insignificant. Generally speaking, parameter sensitivities for head and salinity simulations in the porous medium are more complex than those in the conduit, especially for the head simulations. The results of global sensitivity analysis are similar to the local sensitivity analysis but provide an insight into the interaction of parameters and the non-linear relationship between simulation results with parameter SC.

5.4 Seawater Intrusion in Scenarios

Generally speaking, the boundary condition of salinity at submarine spring (SC) is the most important parameter to head and salinity simulations in both the conduit and porous medium. Sea level at the submarine spring (H_SL) is another relatively important boundary condition of the conduit system, although is not as significant as SC. The simulation results of numerical model in several scenarios with different boundary conditions are quantitatively studied to evaluate the effects of important parameters SC and H_SL to seawater intrusion in a dual-permeability system. Physically, those scenarios indicate the extents of seawater intrusion under various hydrological conditions at the submarine spring, such as freshwater discharge, sea level or tidal stage in the aquifer, etc. On the other hand, the length of simulation time is not evaluated in the parameter sensitivity study because of the extremely high computational burden. The extents of seawater intrusion through conduit network during the extended low rainfall periods are evaluated by extending the simulation time in section 5.4.4. In each scenario, only the parameter corresponding to the scenario is adjusted while others remain the same as the original values.

5.4.1 The Maximum Seawater Intrusion Case

Local sensitivity study evaluates the pre-calibrated parameters values and boundary conditions in the maximum seawater intrusion case. Therefore, the salinity and head simulation results of the maximum seawater intrusion case with seven-day simulation period in the cross section are presented in Figure 5.9, as a benchmark for following scenarios. The boundary conditions of measured head and salinity at the submarine spring are set as 0.0 ft as current averaged sea level or tidal stage, and 35.0 PSU as pure seawater filled with the conduit system, respectively. In other words, salinity dilution by freshwater discharge is negligible at the submarine spring and the extent of seawater intrusion is the maximum in this case.

According to Ghyben-Herzberg relationship, high-density seawater would intrude a relatively deep aquifer beneath the freshwater. The equivalent freshwater head at the submarine cave is calculated as 7.5 ft when seawater is filled with the submarine cave, which diverts the hydraulic gradient landward and allows seawater to intrude the coastal aquifer. Starting from the shoreline on the surface, seawater gradually intrudes landward with depth, and moves significantly faster and further landward through the conduit network due to the high hydraulic conductivity and porosity. Dynamic conduit-matrix interaction allows mixing seawater in the conduit to transport into surrounding matrix and result in a large area of salt plume in the aquifer. The position of mixing zone in the conduit is significant further inland than that in the shallow porous medium above the conduit, but only slightly further than that in the deep porous medium beneath the conduit since seawater moves downward from conduit layer into the deep aquifer. Simulation result shows that the position of mixing zone in the conduit reaches nearly 3.6 miles landward from the shoreline, defined as the spatial location with salinity as 5.0 PSU. The simulated width of mixing interface is about 7 grid cells or 0.7 miles in both the conduit and porous medium, defined as the distance between the spatial locations of simulated salinity as 1.0 PSU and 25.0 PSU. The relatively low salinity area to the left of the vertical conduit network is due to the dilution of freshwater discharge from the aquifer to the sea. However, the area may be significantly underestimated in the two-dimensional numerical model because freshwater discharge in the surrounding porous medium beyond the cross section is not simulated.

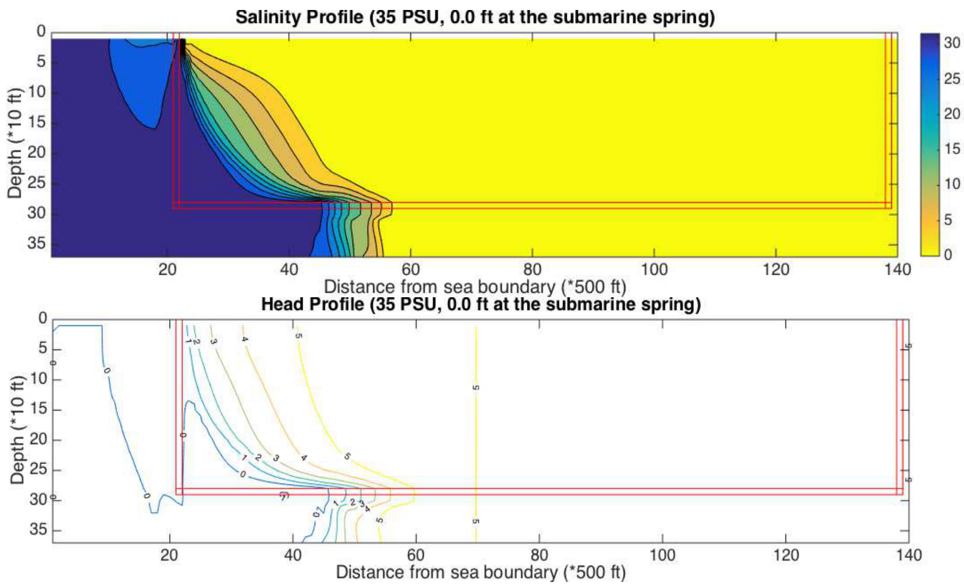

Figure 5.9. Salinity and head simulations of the maximum seawater intrusion case (35 PSU, 0.0 ft at the submarine spring).

5.4.2 Salinity Variation at the Submarine Spring (SC)

Both local and global sensitivity study results indicate that the salinity at the submarine spring (SC) is an important parameter to simulations in both the conduit and porous medium. However, the non-linear relationship between simulations and SC results in the variation of the evaluated values for different simulations (Figure 5.6). After a high precipitation event, salinity at the submarine spring is diluted by large amount of rainfall recharge and freshwater discharge, but would remain as saline water during a low rainfall period. The equivalent freshwater head at the submarine spring decreases to sea level if freshwater is filled with the conduit system. The equivalent freshwater head proportionally decreases if the seawater content in the conduit decreases.

In this study, rainfall and regional recharges are not directly simulated as the constant-flux boundary condition, because the exact recharge quantity are unknown and cannot be estimated in the two-dimensional numerical model. Meanwhile, salinity at the submarine spring represents the conditions of rainfall recharge and freshwater discharge in this study. The effects of freshwater discharge on the extent of seawater intrusion are evaluated in four scenarios of salinity at the submarine spring, 0.0 PSU, 10.0 PSU, 20.0 PSU and 30.0 PSU, as the model boundary conditions with sea level 0.0 ft (Figure 5.10). The positions of mixing zone in both the conduit and porous medium move significantly seaward to 2.5 miles and 2.8 miles away from the shoreline for the cases of salinity 10.0 PSU and 20.0 PSU at the submarine spring, due to rainfall recharge and freshwater discharge. The mixing zone is very close to the shoreline in the case of 0.0 PSU salinity at the submarine spring.

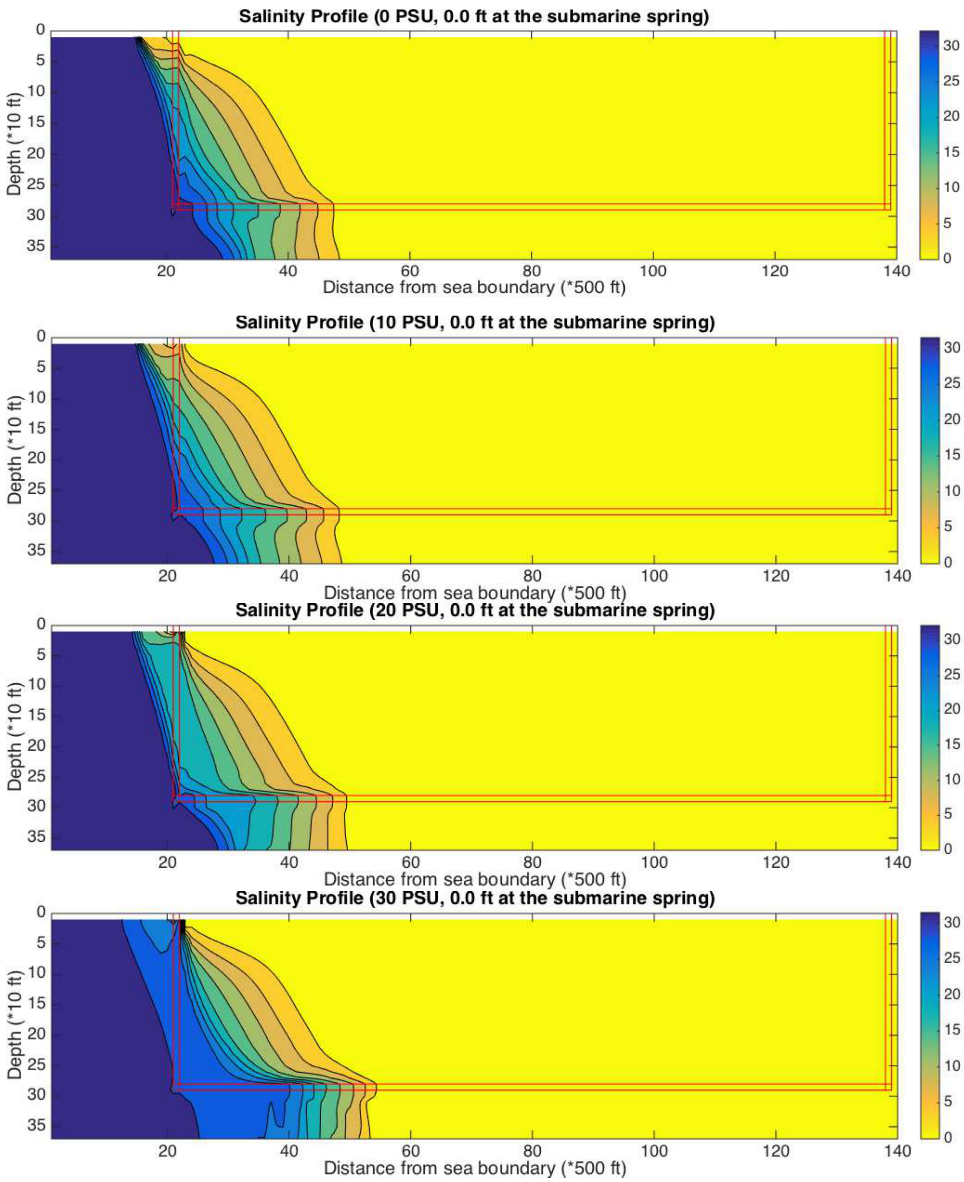

Figure 5.10. Salinity simulation of seawater intrusion with various salinity at the submarine spring under different freshwater discharge conditions: A) 0.0 PSU, 0.0 ft at the submarine spring; B) 10.0 PSU, 0.0 ft at the submarine spring; C) 20.0 PSU, 0.0 ft at the submarine spring; D) 30.0 PSU, 0.0 ft at the submarine spring (from upper to lower).

On the other hand, the width of mixing interface is much wider than that in the maximum seawater intrusion case due to freshwater discharge against seawater intrusion. At this time, advection may not be dominated while diffusion and dispersion become important in the numerical model with slower groundwater flow. However, the shapes of mixing interface are still similar to those in the maximum seawater intrusion case. Generally speaking, seawater intrusion is receded and no longer a serious problem when seawater is significantly diluted with freshwater in the conduit after a heavy rainfall event.

5.4.3 Sea Level Variation at the Submarine Spring (H_SL)

Both local and global sensitivity analysis indicate that sea level at the submarine spring is also a relatively important parameter. IPCC (2007) predicts that sea level will rise 3.0 ft in the beginning of next century, which can result in significant influences on seawater intrusion in a coastal karst aquifer. The effects of 3.0 ft and 6.0 ft sea level rise on the extents of seawater intrusion in the conduit and porous medium are evaluated by the numerical model and presented in Figure 5.11. The boundary condition of salinity at the submarine spring remains 35.0 PSU as the maximum seawater intrusion case, but the constant head at the submarine spring increases to 3.0 ft and 6.0 ft, respectively, represents the rising sea level. Meanwhile, the equivalent freshwater head increases along with the sea level as well. The width and shape of mixing zone are still similar to those in the maximum seawater intrusion case, but the position of mixing zone in the conduit moves to almost 4.4 miles from the shoreline if sea level rises 3.0 ft, defined as the spatial location of simulated salinity as 5.0 PSU. Another extreme case of 6.0 ft sea level rise predicts additional 0.6 miles further inland of the seawater intrusion. The cases of rising sea levels verify the concern that sea level rise would significantly increase seawater intrusion in a coastal aquifer, especially in a karst aquifer with conduit system opening to the sea. In addition, rising sea level could also affect the regional flow field and other hydrological conditions in a coastal aquifer; however, are hardly considered and simulated in the two-dimensional numerical model. Davis and Verdi (2014) reported the increasing groundwater discharge at the inland Wakulla Spring in the WKP associated with sea level rise in the past decades. The effects of sea level rise on groundwater flow field has been studied by a numerical model as well (Xu et al., 2015b).

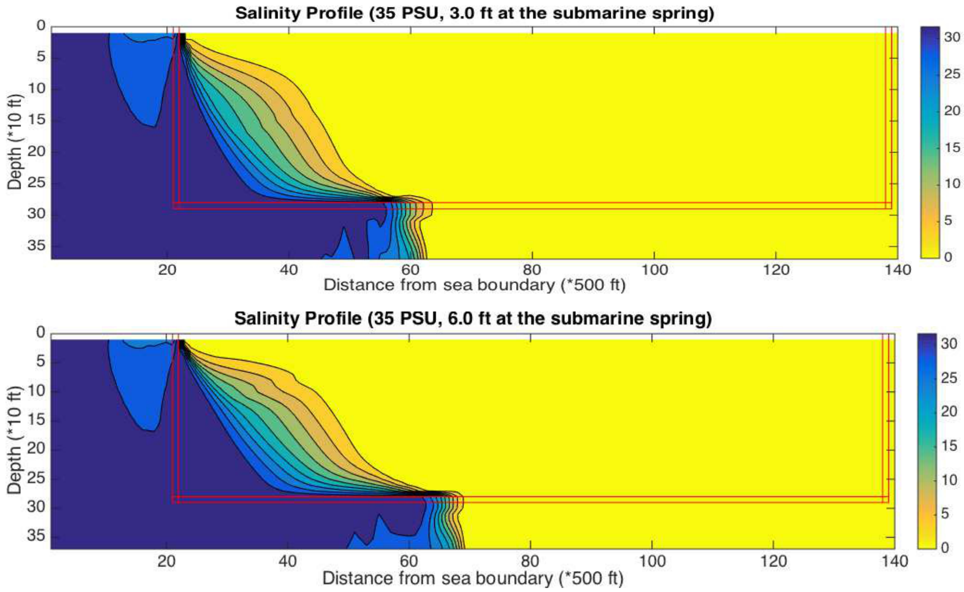

Figure 5.11. Salinity simulation of seawater intrusion with various sea level conditions: A) 35.0 PSU, 3.0 ft at the submarine spring; B) 35.0 PSU, 6.0 ft at the submarine spring (from upper to lower).

5.4.4 Extended Low Rainfall Period

Simulation time is not evaluated in the sensitivity analysis; however, its effect on the extent of seawater intrusion is quantitatively calculated here. The simulated time period is extended to simulate the seawater intrusion process during an extended low rainfall period. The boundary conditions of salinity and sea level at the submarine spring remain 35.0 PSU and 0.0 ft, respectively, as same as the maximum seawater intrusion case. The results of the numerical model are presented in Figure 5.12 with extended simulation time periods of 14, 21 and 28 days.

During an extended low rainfall period, seawater intrusion extends further landward in both the conduit and porous medium with time. The equivalent freshwater head at the submarine spring is higher than the inland freshwater boundary and allows seawater to intrude persistently. Comparing with the previous 7-day simulation of maximum seawater intrusion case, the position of mixing zone in the 14-day simulation moves additional 0.8 mile landward in the conduit, as well as in the surrounding porous medium. The positions of mixing zone keep intruding landward with slower speed in the simulations of extended time period due to the smaller landward hydraulic gradient at the inland parts of the conduit. The mixing zone will finally reach 4.9 miles from the shoreline after 28-day low rainfall period in the numerical model. As a result, the seawater intrusion through conduit network is significantly increased and becomes a serious environmental problem during an extended low rainfall period.

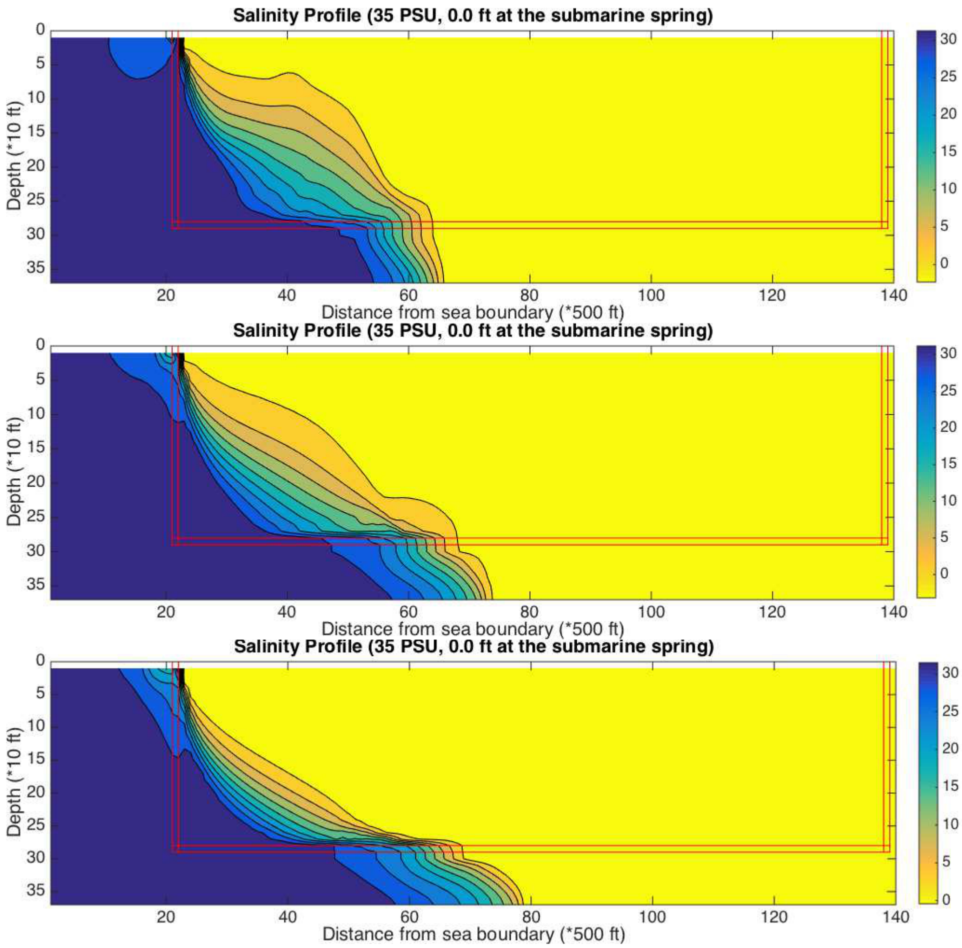

Figure 5.12. Salinity simulation of the maximum seawater intrusion case (35 PSU, 0.0 ft at the submarine spring) with extend simulation time during a low rainfall period: A) 14-day simulation period; B) 21-day simulation period; C) 28-day simulation period (from upper to lower).

CHAPTER SIX

CONCLUSIONS

In Chapter 2, the data analysis of electrical conductivity and geochemical components in the field provides strong evidence that seawater intrusion is migrating 14 miles inland to one of Florida's major first magnitude springs. The conceptual model established by previous researchers provides the mechanism by which seawater enters the conduit system at Spring Creek Springs and can migrate northward against the prevailing regional potentiometric gradient to Wakulla Spring. The analysis of the conductivity data allows us to establish that the increases in conductivity move from south to north over time, and the analysis of the geochemical data allow us to rule out both upwelling connate water and anthropogenic sources as the cause of the increased conductivity values. This is not only the first documented case of seawater intrusion at Spring Creek Springs migrating to Wakulla Spring; it is also the longest documented extent of seawater intrusion in the Woodville Karst Plain (WKP).

In Chapter 3, a discrete-continuum numerical model (VDFST-CFP) is developed to simulate density-dependent non-laminar and laminar seawater intrusion processes in the conduit and porous medium, respectively. Density-dependent Darcy-Weisbash equation is applied in the numerical solution of non-laminar groundwater flow in the conduit, and Darcy equation describes laminar groundwater flow in the porous medium. The one-dimensional advection equation and two-dimensional advection dispersion equation are used to estimate solute transport in the conduit and porous medium, respectively. Groundwater flow and solute transport equations in the continuum matrix domain are numerically solved by standard finite difference method, while the density-dependent non-linear Darcy-Weisbash equation is solved iteratively using the Newton-Raphson method. Groundwater flow and solute transport equations in both the conduit and porous medium are coupled and calculated simultaneously by an implicit iterative procedure within each time step. A horizontal plane model is setup to validate the conduit-matrix interaction in the VDFST-CFP model. The other model of vertical cross section is designed to test the effect of density-dependent flow in the newly developed model. Simulation of VDFST-CFP model is compared with other commonly used numerical models, including SEAWAT MODFLOW/MT3DMS and CFPv2/UMT3D models. The variable-density models have very similar result to the constant density models in the horizontal case, since only vertical flux is density-dependent. The discrete-continuum VDFST-CFP and CFPv2/UMT3D models provide more accurate results than continuum models, because Darcy equation overestimates the flow rate in the conduit under turbulent condition. In the vertical case, the simulation for density-dependent flow by VDFST-CFP model is similar to those by SEAWAT model. However, the discrete-continuum model improves the simulation in the conduit without overestimation of flow rate under turbulent condition.

The uncertainties of the developed VDFST-CFP model are discussed as well. Firstly, the large conduit size in the field is contradicted with the requirements of sufficient small vertical discretization in the variable-density model and tiny conduit diameter in the discrete-continuum model. The decreasing ratio between conduit diameter and grid cell significantly improves the numerical stability and model accuracy. Secondly, the standard finite difference numerical technique is used in the VDFST-CFP model to solve advection dispersion solute transport equation, which may generate significant truncation errors for advection-dominated transport in the porous medium near conduit system. Finally, friction factor is assumed to be constant in the VDFST-CFP model but actually varies with the fluctuation of flow velocity and Reynolds number along the conduit. In the model validation, an equivalent relationship is made between conduit diameter in the discrete-continuum model and hydraulic conductivity in the continuum model under a laminar flow condition, but is difficult to evaluate under non-laminar flow condition. The convergence criteria in the Newton-Raphson method and implicit procedure significantly control the model accuracy and mass balance. Overall, the VDFST-CFP model provides more accurate simulation for seawater intrusion in a coastal karst aquifer with conduits, but more future studies are expected to improve the accuracy, save the computational cost and extend the application in the field.

Numerical modeling is an important approach to simulate flow regime and study seawater intrusion in a coastal karst aquifer, since it is always difficult to collect data in the submarine conduit system. In Chapter 4, a numerical model provides quantitative description of the groundwater flow cycling conceptual model in Davis and Verdi (2014), to evaluate the effect of seawater/freshwater interaction in the WKP. The understanding of regional regime is important to analyze the water quality issues in the WKP, for instance, seawater intrusion, nitrate-N transport, groundwater contamination and water clarity at Wakulla Spring. Complex interactions between seawater, freshwater and rainfall recharge in a dual-permeability karst aquifer are numerically simulated by a discrete-continuum CFPv2 model. The well-match simulated results comparing with field measurements also verify the relationship of discharges at submarine springs and inland springs under different precipitation and hydrological conditions, while Spring Creek Springs and Wakulla Springs are competing with each other for freshwater discharges. On the other hand, high-density seawater plays an important role in regional flow field and affects significantly to the discharges of springs. The numerical modeling states the impacts of sea level rise to the hydrological conditions in the entire coastal aquifer, which would block freshwater discharge at the submarine spring and increase the flow rate at the inland springs. Overall, the application of numerical model in this study is important to understand the regional hydrogeology and helpful for future research, such as the effects of seawater intrusion and groundwater pumping.

In Chapter 5, density-dependent SEAWAT model is applied to evaluate the importance of parameters by local and global sensitivity analysis, and then simulate the extents of seawater intrusion in a coastal karst aquifer with conduit system. The composite scaled sensitivity (CSS) indicate that salinity at the submarine spring (SC) is the most important parameter to the simulations because it is the boundary condition of the conduit system and source of seawater intrusion to the aquifer. The sea level at the submarine spring (H_SL), hydraulic conductivity and porosity of the conduit (HY_C and PO_C) are important to the simulations in the conduit as well. Simulations in the porous medium are most sensitive to parameter SC and relatively sensitive to parameters of both the conduit and porous medium (HY_P, SS_C, PO_P, PO_C) due to the interaction between the two domains in the dual-permeability system. Local sensitivity analysis suggests that simulations are more sensitive to parameters around the mixing zone. This study confirms the conclusions by Shoemaker (2004) that parameters are more effective near the mixing zone, and salinity simulations are even more sensitive than head simulations. The study results also indicate the significance of conduit-matrix interaction and the less importance of dispersivity to seawater intrusion in a coastal karst aquifer. The results of global sensitivity analysis are similar to those of local sensitivity analysis, especially for the simulations in the conduit. The results of head simulation are more complex than those of salinity simulation. Porosity and specific storage of the conduit (PO_C and SS_C) are more important than hydraulic conductivity (HY_C) due to the non-linear relationship between flow rate and hydraulic conductivity under non-laminar flow condition. Salinity simulation in the porous medium is sensitive to both parameters SC and HY_P, but head simulation is more sensitive to HY_P due to the non-linear relationship between simulations and SC with the smaller mean but larger standard deviation of elementary effects. The effects of conduit-matrix interaction on simulations in the porous medium and the less importance of dispersivity are illustrated in the global sensitivity study as well.

The extents of seawater intrusion are evaluated under various boundary conditions of the two important parameters SC and H_SL. Simulation results indicate that seawater intrudes further landward in the conduit than that in the surrounding porous medium. The position of mixing zone in the conduit moves to 3.6 miles from the shoreline with the width of 0.7 miles in the seven-day maximum seawater intrusion case, in which salinity at the submarine spring is 35.0 PSU and sea level is 0.0 ft. Rainfall recharge and freshwater discharge dilute the salinity at the submarine spring (SC) and move the mixing zone significantly seaward. The importance of parameter H_SL is exhibited with additional 0.8 miles seawater intrusion landward with a 3-ft sea level rise in prediction. In addition, an extended low rainfall period would allow seawater to intrude further landward. These simulations are consistent with the results of sensitivity analysis in terms of the influence of model parameters on simulations.

There is still a lot of work can be done in the future. Additional field investigation is needed to provide further insights into the behavior of the local aquifer system southwest of Wakulla Spring, especially the effect of Lost Creek on regional flow regime. New stations and monitoring devices in karst windows need to be installed in order to establish the east-west extent of seawater intrusion, since it is unclear at present whether Spring Creek Springs is a single point of intrusion or whether it is indicative of wider saltwater intrusion. Field observation data at deep Punchbowl, Tobacco and Revell Sinks will be very useful to evaluate seawater intrusion through the subsurface conduit network. More measurements are expected at Spring Creek Springs as well to explore the flow conditions of each vent. Technologies such as mass spectrometry should also be applied to in order to confirm our results and definitively link the conductivity increases at Wakulla Spring to coastal saltwater along the conduit network.

In the numerical modeling prospective of view, the discrete-continuum VDFST-CFP model definitely needs more work of debugging and optimization to become a standard code. The model could be extended to simulate chemical reactions in the future, such as carbonate limestone dissolution/precipitation and/or nitrate-N denitrification processes. A multi-species transport model is required in reactive transport modeling although only one solute is density-dependent. The coupled reactive transport model can be further applied to evaluate the carbon sink effect in a karst aquifer, CO_2 sequestration and carbon cycle in a global scale. Parallel computing technique is necessary to extend the VDFST-CFP numerical model to three-dimensional spatial domain with multiple conduit networks. The application of other numerical techniques, such as finite element and finite volume methods, can be used to generate non-uniform spatial grid division, apply mesh adaptation and refine the conduit geometry.

REFERENCES

Bakalowicz, M., (2005). Karst groundwater: a challenge for new resources. Hydrogeology journal, 13 (1), 148-160.

Bauer-Gottwein, P., Gondwe, B. R., Charvet, G., Marín, L. E., Rebolledo-Vieyra, M. and Merediz-Alonso, G., (2011). Review: The Yucatán Peninsula karst aquifer, Mexico. Hydrogeology journal, 19 (3), 507-524.

Bear, J., (1999). Seawater intrusion in coastal aquifers, Springer Science & Business Media,

Bear, J., (2013). Dynamics of fluids in porous media, Courier Corporation,

Boesch, D. F., Field, J. C. and Scavia, D., (2000). The potential consequences of climate variability and change on coastal areas and marine resources. Report of the Coastal Areas and Marine Resources Sector Team US National Assessment of the Potential Consequences of Climate Variability and Change US.

Bush, P. W. and Johnson, R., (1988). Ground-water hydraulics, regional flow, and ground-water development of the Floridan aquifer system in Florida and in parts of Georgia, South Carolina.

Chen, K. and Jiao, J. J., (2007). Preliminary study on seawater intrusion and aquifer freshening near reclaimed coastal area of Shenzhen, China. Water Science and Technology; Water Supply, 2 (7), 137-145.

Chen, N., Gunzburger, M., Hu, B., Wang, X. and Woodruff, C., (2012). Calibrating the exchange coefficient in the modified coupled continuum pipe-flow model for flows in karst aquifers. Journal of hydrology, 414, 294-301.

Clemens, T., Hückinghaus, D., Sauter, M., Liedl, R. and Teutsch, G., (1996). A combined continuum and discrete network reactive transport model for the simulation of karst development. IAHS PUBLICATION, 309-320.

Covington, M. D., Doctor, D. H., King, J. N. and Wicks, C. M., (2011). Research in karst: A model for future directions in hydrologic science? From the Section President, 18.

Custodio, E., (1987). Salt-fresh water interrelationships under natural conditions. Groundwater Problems in Coastal Areas, UNESCO Studies and Reports in Hydrology, 45, 14-96.

Davis, J. H. (1996). Hydraulic investigation and simulation of ground-water flow in the Upper Floridan aquifer of north central Florida and southwestern Georgia and delineation of contributing areas for selected City of Tallahassee, Florida, Water-Supply Wells. Tallahassee, Florida, U.S. Geological Survey**:** 55.

Davis, J. H. and Katz, B. G. (2007). Hydrogeologic investigation, water chemistry analysis, and model delineation of contributing areas for City of Tallahassee public-supply wells, Tallahassee, Florida, Geological Survey (US).

Davis, J. H., Katz, B. G. and Griffin, D. W., (2010). Nitrate-N movement in groundwater from the land application of treated municipal wastewater and other sources in the Wakulla Springs Springshed, Leon and Wakulla counties, Florida, 1966–2018. US Geol Surv Sci Invest Rep, 5099, 90.

Davis, J. H. and Verdi, R., (2014). Groundwater Flow Cycling Between a Submarine Spring and an Inland Fresh Water Spring. Groundwater, 52 (5), 705-716.

Diersch, H., (2002). FEFLOW reference manual. Institute for Water Resources Planning and Systems Research Ltd, 278.

Diersch, H., (2005). FEFLOW finite element subsurface flow and transport simulation system. Reference manual. Berlin, Germany: WASY GmbH.(Cité aux pages 20 et 102.).

Dreybrodt, W., (1988). Processes in karst systems, physics, chemistry, and geology.

Dyer, S. B. (2015). Dye tracing confirms conduit connections from Lost Creek Swallet to Spring Creek Springs and the Leon Sinks - Wakulla cave system. Department of Earth, Ocean and Atmosphere. Tallahassee, FL, Florida State University. **Master**.

Farnsworth, R. K. and Thompson, E. S., (1983). Mean monthly, seasonal, and annual pan evaporation for the United States, US Department of Commerce, National Oceanic and Atmospheric Administration, National Weather Service,

Faulkner, J., Hu, B. X., Kish, S. and Hua, F., (2009). Laboratory analog and numerical study of groundwater flow and solute transport in a karst aquifer with conduit and matrix domains. Journal of contaminant hydrology, 110 (1), 34-44.

FGS (2004). Wakulla Springs Scientific Symposium, May 13, 2004. Special Publication. Tallahassee, Florida. **56**.

Fleury, P., Bakalowicz, M. and de Marsily, G., (2007). Submarine springs and coastal karst aquifers: a review. Journal of hydrology, 339 (1), 79-92.

Florea, L. J. and Vacher, H., (2006). Cave levels, marine terraces, paleoshorelines, and the water table in peninsular Florida. Archives of Climate Change in Karst, 188.

Ford, D., Lauritzen, S. and Ewers, R., (2000). Hardware and software modeling of initial conduit development in karst rocks. Speleogenesis: Evolution of Karst Aquifers. National Speleological Society, Huntsville, 175-183.

Ford, D. C. and Williams, P. W., (1989). Karst geomorphology and hydrology, Unwin Hyman London, Gallegos, J. J., Hu, B. X. and Davis, H., (2013). Simulating flow in karst aquifers at laboratory and sub-regional scales using MODFLOW-CFP. Hydrogeology journal, 21 (8), 1749-1760.

Green, R. T., Painter, S. L., Sun, A. and Worthington, S. R., (2006). Groundwater contamination in karst terranes. Water, Air, & Soil Pollution: Focus, 6 (1), 157-170.

Groves, C. G. and Howard, A. D., (1994). Early development of karst systems: 1. Preferential flow path enlargement under laminar flow. Water Resources Research, 30 (10), 2837-2846.

Guo, W. and Langevin, C., (2002). User's guide to SEWAT: a computer program for simulation of three-dimensional variable-density ground-water flow. Water Resources Investigations Report. United States Geological Survey, (6).

Harbaugh, A. W., (2005). MODFLOW-2005, the US Geological Survey modular ground-water model: the ground-water flow process, US Department of the Interior, US Geological Survey Reston, VA, USA,

Harbaugh, A. W., Banta, E. R., Hill, M. C. and McDonald, M. G., (2000). MODFLOW-2000, the US Geological Survey modular ground-water model: User guide to modularization concepts and the ground-water flow process, US Geological Survey Reston, VA,

Hill, M. C. and Tiedeman, C. R., (2006). Effective groundwater model calibration: with analysis of data, sensitivities, predictions, and uncertainty, John Wiley & Sons,

Hill, M. E., Stewart, M. T. and Martin, A., (2010). Evaluation of the MODFLOW ‐ 2005 Conduit Flow Process. Groundwater, 48 (4), 549-559.

Howard, A. D. and Groves, C. G., (1995). Early development of karst systems: 2. Turbulent flow. Water Resources Research, 31 (1), 19-26.

Hu, B. X., (2010). Examining a coupled continuum pipe-flow model for groundwater flow and solute transport in a karst aquifer. Acta carsologica, 39 (2).

Hubbert, M. K., (1940). The theory of ground-water motion. The Journal of Geology, 785-944.

Inouchi, K., Kishi, Y. and Kakinuma, T., (1990). The motion of coastal groundwater in response to the tide. Journal of hydrology, 115 (1), 165-191.

IPCC, (2007). Contribution of Working Groups I, II and III to the Fourth Assessment Report of the Intergovernmental Panel on Climate Change. Geneva, Switzerland, 104.

Katz, B. G., Chelette, A. R. and Pratt, T. R., (2004). Use of chemical and isotopic tracers to assess nitrate contamination and ground-water age, Woodville Karst Plain, USA. Journal of hydrology, 289 (1), 36-61.

Kaufmann, G. and Braun, J., (2000). Karst aquifer evolution in fractured, porous rocks. Water Resources Research, 36 (6), 1381-1391.

Kincaid, T. R. and Werner, C. L. (2008). Conduit Flow Paths and Conduit/Matrix Interactions Defined by Quantitative Groundwater Tracing in the Floridan Aquifer. Sinkholes and the Engineering and Environmental Impacts of Karst: Proceedings of the Eleventh Multidisciplinary Conference, Am. Soc. of Civ. Eng. Geotech. Spec. Publ.

Konikow, L. F. and Kendy, E., (2005). Groundwater depletion: a global problem. Hydrogeology journal, 13 (1), 317-320.

Kulakowski (2010). Chromophoric dissolved organic carbon loading of five intermittent streams recharging Wakulla Springs, Florida. Department of Earth, Ocean and Atmosphere Science. Tallahassee, FL, Florida State Universiy. **Master**.

Kuniansky, E. L. (2008). U.S. Geological Survey Karst Interest Group Proceedings, Bowling Green, Kentucky. Bowling Green, Kentucky, U.S. Geological Survey 142.

Lane, E., (2001). The Spring Creek submarine springs group, Wakulla County, Florida, Florida Geological Survey,

Langevin, C. D., Shoemaker, W. B. and Guo, W., (2003). MODFLOW-2000, the US Geological Survey Modular Ground-Water Model--Documentation of the SEAWAT-2000 Version with the Variable-Density Flow Process (VDF) and the Integrated MT3DMS Transport Process (IMT), US Department of the Interior, US Geological Survey,

Lauritzen, S.-E., Odling, N. and Petersen, J. (1992). Modeling the evolution of channel networks in carbonate rocks. ISRM Symposium: Eurock.

Li, G., (2004). Laboratory simulation of solute transport and retention in a karst aquifer.

Li, X., Hu, B. X., Burnett, W. C., Santos, I. R. and Chanton, J. P., (2009). Submarine ground water discharge driven by tidal pumping in a heterogeneous aquifer. Groundwater, 47 (4), 558-568.

Liedl, R., Sauter, M., Hückinghaus, D., Clemens, T. and Teutsch, G., (2003). Simulation of the development of karst aquifers using a coupled continuum pipe flow model. Water Resources Research, 39 (3).

Liu, G., Wang, P. and Zheng, C. (2001). An explicit and mass-conservative scheme without time-step limit for modeling advection-dominated contaminant transport. 2001 MODFLOW international conference in Golden, Colorado.

Loper, D. E., Werner, C. L., Chicken, E., Davies, G. and Kincaid, T., (2005). Coastal carbonate aquifer sensitivity to tides. Eos, Transactions American Geophysical Union, 86 (39), 353-357.

Martin, J. B. and Dean, R. W., (1999). Temperature as a natural tracer of short residence times for groundwater in karst aquifers. Karst Modeling. Karst Waters Institute Special Publication, 5, 236-242.

Martin, J. B. and Dean, R. W., (2001). Exchange of water between conduits and matrix in the Floridan aquifer. Chemical Geology, 179 (1), 145-165.

Maupin, M. A. and Barber, N. L., (2005). Estimated withdrawals from principal aquifers in the United States, 2000.

McDonald, M. G. and Harbaugh, A. W., (1988). Techniques of the Water-Resources Investigations of the United States Geological Survey. A Modular Three-Dimensional Finite-Difference Ground-Water Flow Model, Book, 6, 11-11.

Miller, J. A. (1986). Hydrologic framework of the Floridan aquifer system in Florida and in parts of Georgia, Alabama, and South Carolina, U.S. Geological Survey Professional Paper**:** 91.

Moore, W. S. and Wilson, A. M., (2005). Advective flow through the upper continental shelf driven by storms, buoyancy, and submarine groundwater discharge. Earth and Planetary Science Letters, 235 (3), 564-576.

Oude Essink, G., Van Baaren, E. and De Louw, P., (2010). Effects of climate change on coastal groundwater systems: a modeling study in the Netherlands. Water Resources Research, 46 (10).

Perry, E., Velazquez-Oliman, G. and Marin, L., (2002). The hydrogeochemistry of the karst aquifer system of the northern Yucatan Peninsula, Mexico. International Geology Review, 44 (3), 191-221.

Pilson, M. E., (2012). An Introduction to the Chemistry of the Sea, Cambridge University Press,

Poeter, E. P. and Hill, M. C., (1998). Documentation of UCODE, a computer code for universal inverse modeling, DIANE Publishing,

Reimann, T., Birk, S., Rehrl, C. and Shoemaker, W. B., (2012). Modifications to the Conduit Flow Process Mode 2 for MODFLOW‐2005. Groundwater, 50 (1), 144-148.

Reimann, T., Geyer, T., Shoemaker, W. B., Liedl, R. and Sauter, M., (2011a). Effects of dynamically variable saturation and matrix‐conduit coupling of flow in karst aquifers. Water Resources Research, 47 (11).

Reimann, T., Giese, M., Geyer, T., Liedl, R., Maréchal, J.-C. and Shoemaker, W. B., (2014). Representation of water abstraction from a karst conduit with numerical discrete-continuum models. Hydrology and Earth System Sciences, 18 (1), 227-241.

Reimann, T. and Hill, M. E., (2009). MODFLOW‐CFP: A New Conduit Flow Process for MODFLOW–2005. Groundwater, 47 (3), 321-325.

Reimann, T., Liedl, R., Giese, M., Geyer, T., Maréchal, J.-C., Dörfliger, N., Bauer, S. and Birk, S. (2013). Addition and Enhancement of Flow and Transport processes to the MODFLOW-2005 Conduit Flow Process. 2013 NGWA Summit—The National and International Conference on Groundwater, Ngwa.

Reimann, T., Rehrl, C., Shoemaker, W. B., Geyer, T. and Birk, S., (2011b). The significance of turbulent flow representation in single - continuum models. Water Resources Research, 47 (9).

Ritter, D. F., Kochel, C. R. and Miller, J. R., (2002). Process Geomorphology, McGraw-Hill, 576.

Rupert, F. and Spencer, S. M., (1988). Geology of Wakulla County, Florida, Florida Geological Survey,

Saller, S. P., Ronayne, M. J. and Long, A. J., (2013). Comparison of a karst groundwater model with and without discrete conduit flow. Hydrogeology journal, 21 (7), 1555-1566.

Saltelli, A., Tarantola, S., Campolongo, F. and Ratto, M., (2004). Sensitivity analysis in practice: a guide to assessing scientific models, John Wiley & Sons,

Saltelli, A., Tarantola, S. and Chan, K.-S., (1999). A quantitative model-independent method for global sensitivity analysis of model output. Technometrics, 41 (1), 39-56.

Scanlon, B. R., Mace, R. E., Barrett, M. E. and Smith, B., (2003). Can we simulate regional groundwater flow in a karst system using equivalent porous media models? Case study, Barton Springs Edwards aquifer, USA. Journal of hydrology, 276 (1), 137-158.

Schmidt, W., Lloyd, J. M. and Collier, C., Eds. (1998). The Wakulla Springs Woodville Karst Plain Symposium. Special Publication 46. Tallahassee, Florida, Florida Geological Survey.

Schmitter-Soto, J., Comín, F., Escobar-Briones, E., Herrera-Silveira, J., Alcocer, J., Suárez-Morales, E., Elías-Gutiérrez, M., Díaz-Arce, V., Marín, L. and Steinich, B., (2002). Hydrogeochemical and biological characteristics of cenotes in the Yucatan Peninsula (SE Mexico). Hydrobiologia, 467 (1-3), 215-228.

Scott, T. M., Means, G. H., Meegan, R. P., Means, R. C., Upchurch, S., Copeland, R., Jones, J., Roberts, T. and Willet, A., (2004). Springs of Florida.

Shoemaker, W. B., (2004). Important observations and parameters for a salt water intrusion model. Ground Water, 42 (6), 829-840.

Shoemaker, W. B., Cunningham, K. J., Kuniansky, E. L. and Dixon, J., (2008a). Effects of turbulence on hydraulic heads and parameter sensitivities in preferential groundwater flow layers. Water Resources Research, 44 (3).

Shoemaker, W. B., Kuniansky, E. L., Birk, S., Bauer, S. and Swain, E. D., (2008b). Documentation of a conduit flow process (CFP) for MODFLOW-2005.

Singh, A., (2006). Assessing coastal vulnerability: developing a global index for measuring risk, UNEP/Earthprint,

Spiessl, S. M. (2004). Development and evaluation of a reactive hybrid transport model (RUMT3D), Ph. D. Thesis, Georg-August-University of Goettingen. http://webdoc. sub. gwdg. de/diss/2004/spiessl/spiessl. pdf.

Spiessl, S. M., Prommer, H., Licha, T., Sauter, M. and Zheng, C., (2007). A process-based reactive hybrid transport model for coupled discrete conduit–continuum systems. Journal of hydrology, 347 (1), 23-34.

Stone, W. C., (1989). The Wakulla Springs Project, US Deep Caving Team,

Voss, C. I. and Provost, A. M., (1984). SUTRA. US Geological Survey Water Resources Investigation Reports, 84-4369.

Voss, C. I. and Souza, W. R., (1987). Variable density flow and solute transport simulation of regional aquifers containing a narrow freshwater ‐ saltwater transition zone. Water Resources Research, 23 (10), 1851-1866.

Werner, A. D., Bakker, M., Post, V. E., Vandenbohede, A., Lu, C., Ataie-Ashtiani, B., Simmons, C. T. and Barry, D. A., (2013). Seawater intrusion processes, investigation and management: recent advances and future challenges. Advances in Water Resources, 51, 3-26.

Werner, A. D. and Simmons, C. T., (2009). Impact of sea ‐ level rise on sea water intrusion in coastal aquifers. Groundwater, 47 (2), 197-204.

Werner, C. L. (2001). Preferential flow paths in soluble porous media and conduit system development in carbonates of the Woodville Karst Plain, Florida. Department of Earth, Ocean and Atmosphere Science. Tallahassee, FL, Florida State University. **Master of Science**.

WHO (2011). Guidelines for Drinking-water Quality. WHO chronicle. **38:** 104-108.

Wilson, A. M., Moore, W. S., Joye, S. B., Anderson, J. L. and Schutte, C. A., (2011). Storm ‐ driven groundwater flow in a salt marsh. Water Resources Research, 47 (2).

Winter, T., Harvey, J., Franke, O. and Alley, W., (1998). Natural processes of ground-water and surface-water interaction. Ground Water and Surface Water: A Single Resource, US Geological Survey Circular, 1139, 2-50.

Xu, Z., Hu, B. and Ye, M., (2016). Numerical modeling and sensitivity analysis of seawater intrusion in a dual-permeability coastal karst aquifer with conduits Journal of hydrology.

Xu, Z., Hu, B. X., Davis, H. and Cao, J., (2015a). Simulating long term nitrate-N contamination processes in the Woodville Karst Plain using CFPv2 with UMT3D. Journal of hydrology, 524, 72-88.

Xu, Z., Hu, B. X., Davis, H. and Kish, S., (2015b). Numerical study of groundwater flow cycling controlled by seawater/freshwater interaction in a coastal karst aquifer through conduit network using CFPv2. Journal of contaminant hydrology, in press.

Zervas, C., (2001). Sea level variations of the United States, 1854-1999, US Dept. of Commerce, National Oceanic and Atmospheric Administration, National Ocean Service,

Zheng, C. and Bennett, G. D., (2002). Applied contaminant transport modeling, Wiley-Interscience New York,

Zheng, C. and Wang, P. P. (1999). MT3DMS: a modular three-dimensional multispecies transport model for simulation of advection, dispersion, and chemical reactions of contaminants in groundwater systems; documentation and user's guide, DTIC Document.

Zötl, J. G., (2013). Karsthydrogeologie, Springer-Verlag,

BIOGRAPHICAL SKETCH

ZEXUAN XU

PROFESSION EXPERIENCE

05/2016 – present Postdoctoral Research Associate, Earth and Environment Division
Lawrence Berkeley National Laboratory, Berkeley, CA

EDUCATION EXPERIENCE

08/2012 – 05/2016 Ph.D in Geology, Florida State University (FSU), Tallahassee, FL
Major in Hydrogeology / Numerical Groundwater Modeling
Supervisor and Committee Chair: Dr. Bill X. Hu
Dissertation: Date analysis and numerical modeling of seawater through conduit network in a coastal karst aquifer

08/2008 – 06/2012 B. Sc in Geology, Zhejiang University (ZJU), Hangzhou, Zhejiang, China

INTERNSHIP EXPERIENCE

06/2015 – 08/2015 Intern, Florida Geological Survey (FGS), Tallahassee, FL

05/2014 – 08/2014 Intern, Idaho National Laboratory (INL), Idaho Falls, ID

SHORT-TERM EDUCATION

05/2013 – 07/2013 Visiting Student, China University of Geoscience, Beijing, China

08/2010 – 09/2010 Exchange Student, University of California, Los Angeles, CA

RESEARCH KNOWLEDGE AND INTEREST

- Numerical simulation of flow and solute transport in porous and fracture media, especially using discrete-continuum hybrid model.
- Numerical modeling of variable-density flow and salinity transport problems, such as submarine groundwater discharge (SGD) and seawater intrusion in heterogeneous karst aquifer
- Uncertainty analysis and risk analysis of numerical models and hydrologic parameters
- Numerical simulation of chemical reaction on solid-liquid interface, especially rock-water dissolution and precipitation chemistry process
- Groundwater contamination remediation
- Surface water and groundwater interaction coupled model

RESEARCH EXPERIENCE

09/2014 – present Numerical modeling of seawater intrusion in coastal karst aquifer with well-developed conduits: A development of VDFST-CFP (Variable Density Flow and Solute Transport – Conduit Flow Process) model.

06/2014 – 08/2014 Phase-field modeling of solute precipitation/dissolution chemical reaction using MOOSE: A finite element method (at INL)

01/2014 – 05/2015 Quantitatively study of a groundwater flow cycling controlled by seawater / freshwater interface in a coastal aquifer using CFPv2

01/2013 – 04/2014 Numerical simulations of nitrate-N and chloride transport processes through conduits in the Woodville Karst Plain using CFPv2 with UMT3D

TEACHING EXPERIENCE

01/2012 – 05/2016 Teaching Assistant, Dept. of EOAS, FSU

GLY1000 Dynamic Earth

GLY1000L Dynamic Earth Laboratory

GLY4751/5757 Introduction to Remote Sensing and GIS

ACADEMIC SKILLS

Computer Skills:

Fortran, C/C++, Python, Java, R, SQL

Linux/Unix, OpenMP, MPI

Codes:

MODFLOW, MODFLOW-CFP, MT3DMS, SEAWAT, UCODE

Software:

MATLAB, Mathematica, ArcGIS, CorelDraw, LaTeX, Groundwater Vistas

Graduate Courses:

Earth Sciences: Principle of Geochemistry / Principle of Hydrology / Applied Hydrogeology / Basin Analysis / Geohazards Assessment / Chemical Oceanography / Stable Isotope

Numerical Methods: Numerical Stochastic Methods of PDE / Scientific Programming / Numerical Groundwater Modeling / Numerical Methods for Differential Equations / Uncertainty Analysis

PEER-REVIEWED PUBLICATIONS

Zexuan Xu, Seth Bassett, Bill X. Hu and Scott Dyer, 2016. Seawater intrusion through conduit networks in the Woodville Karst Plain (WKP) by the attraction of Wakulla Springs, submitted to Scientific Report.

Zexuan Xu and Bill X. Hu, 2016. Development of a discrete-continuum VDFST-CFP numerical model for simulating seawater intrusion to a coastal karst aquifer with conduit network, submitted to Water Resource Research.

Zexuan Xu, Bill X. Hu and Ming Ye, 2016. Numerical modeling and sensitivity analysis of seawater intrusion in a dual-permeability coastal karst aquifer with conduits, submitted to Journal of Hydrology.

Zexuan Xu, Bill X. Hu, Hal Davis and Stephen Kish, 2015. Numerical study of groundwater flow cycling controlled by seawater/freshwater interaction in a coastal karst aquifer through conduit networks using CFPv2, Journal of Contaminant Hydrology, 182, 131-145.

Zexuan Xu, Bill X. Hu, Hal Davis and Jianhua Cao, 2015. Simulating long-term nitrate-N contamination processes in the Woodville Karst Plain using CFPv2 with UMT3D, Journal of Hydrology, 52(4), 72-88.

CONFERENCE PROCEEDINGS

Zexuan Xu and Bill X. Hu, Numerical simulation of freshwater/seawater interaction in a dual-permeability karst system with conduits: the development of a discrete-continuum VDFST-CFP model, European Geosciences Union (EGU) General Assembly 2016, Vienna, Austria, April 2016 (oral).

Zexuan Xu and Bill X. Hu, Variable density numerical modeling of seawater intrusion in coastal aquifer with well-developed conduits, American Geophysical Union (AGU) 2015 Fall Meeting, San Francisco, California, December 2015 (poster).

Zexuan Xu and Bill X. Hu, Simulating seawater intrusion using numerical variable-density SEAWAT model in coastal karst aquifer with well-developed conduits, Geological Society of America (GSA) Annual Meeting, Baltimore, Maryland, November 2015 (oral).

Bill X. Hu and **Zexuan Xu** (presenter), Numerical study on groundwater flow cycling in the Woodville Karst Plain controlled by seawater intrusion to a karst aquifer through conduit network using CFPv2, OMICS International Conference on Geology, Orlando, Florida, June 2015 (oral).

Zexuan Xu, Bill X. Hu, Hal Davis and Stephen Kish, Numerical study of a groundwater flow cycling controlled by seawater intrusion within karst conduit networks using MODFLOW-CFP, American Geophysics Union (AGU) 2014 Fall Meeting, San Francisco, California, December 2014 (poster).

Zexuan Xu, Bill X. Hu and Hal Davis, Using CFP numerical solute transport method to simulate nitrate-N and chloride contamination in Woodville Karst Plain, Geological Society of America (GSA) 125th Annual Meeting, Denver, Colorado, October 2013 (oral).

COLLOQUIUM PRESENTATION

Zexuan Xu and Bill X. Hu, Numerical modeling of seawater intrusion in a heterogeneous coastal karst aquifer with conduits. 5th UF Water Institute Symposium, University of Florida, Gainesville, Florida, February 2016.

Zexuan Xu and Bill X. Hu, Numerical modeling of groundwater and seawater intrusion in the Woodville Karst Plain. Workshop of study on groundwater and surface water in the Woodville Karst Plain, Florida State University, Tallahassee, Florida, September 2015 (organizer as well).

Zexuan Xu and Bill X. Hu**,** Numerical modeling of seawater intrusion in coastal karst aquifer with well-developed conduits: the development of VDFST-CFP (Variable Density Flow and Solute Transport – Conduit Flow Process), invited by NWFWMD (Northwest Florida Water Management District), Midway, Florida, June 2015.

Zexuan Xu, Bill X. Hu and Hal Davis, Numerical study of a groundwater flow cycling controlled by seawater intrusion within karst conduit networks using MODFLOW-CFP, Southwest Florida Water Resources Conferences, Fort Myers, Florida, February 2015.

Bill X. Hu, **Zexuan Xu** and Hal Davis, Using numerical model to simulate the interaction between submarine and inland spring driven by seawater intrusion in a well-developed karst aquifer. International Symposium of Sustainable Utilization of Water Resources in Developing Countries, Guilin, Guangxi, China, October 2014.

Bill X. Hu, Josue Gallegos, **Zexuan Xu** and Hal Davis, Simulating groundwater and solute transport in a Karst aquifer with conduits, 2014 International Conference of Mathematics, Information and Computational Sciences, Beijing, China, October 2014.

Zexuan Xu, Bill X. Hu and Hal Davis, A groundwater flow cycling controlled by seawater intrusion near Tallahassee and numerical simulation using MODFLOW-CFP. Natural Sciences Graduate Symposium, FSU, October 2014.

Zexuan Xu, Bill X. Hu and Hal Davis, Numerical study of nitrate-N and chloride transport in a well-developed karst aquifer, Thalassic Society EOAS Student Symposium, FSU, November 2013.

Bill X. Hu, Josue Gallegos, **Zexuan Xu** and Hal Davis, Numerical simulation of groundwater flow and solute transport in a karst aquifer with conduits, The International Symposium on Karst Water under Global Change Pressure, Guilin, Guangxi, China, April 2013.

REVIEWRS FOR JOURNALS

Stochastic Environment Research and Risk Assessment (SERRA)

Journal of Water Resource and Hydraulic Engineering (JWRHE)

HONORS AND AWARDS

J O'Brien Graduate Travel Grant, Dept. of EOAS, FSU (2016)

Lyman Toulmin Memorial Fund, FSU (2015-2016)

Robert Lamar Parker Endowed Memorial Fund, FSU (2014-2015)

COGS Travel Grant, FSU (2013, 2014, 2015)

Outstanding Undergraduate Student of Zhejiang, China (only 200 winner each year, 2012)

Panasonic Scholarship, ZJU (only 20 winner each year, 2011)

First-Class Scholarship for Outstanding Students, ZJU (3%, 2010)

Excellent Student Awards, ZJU (15%, triple, 2011, 2010 & 2009)